VALIDATION OF MARKERLESS MOTION CAPTURE FOR THE ASSESSMENT OF SOLDIER MOVEMENT PATTERNS UNDER VARYING BODY-BORNE LOADS

ISABEL COLL

Thesis submitted to the University of Ottawa
in partial Fulfillment of the requirements for the

Master of Applied Science in Biomedical Engineering

Ottawa-Carleton Institute of Biomedical Engineering (OCIBME)
Faculty of Engineering
University of Ottawa

ABSTRACT

Modern soldiers are burdened by an increase in body-borne load due to technological advancements related to their armour and equipment. Despite the potential increase in safety from carrying more protective equipment, a heavier load on the soldier might decrease field performance both cognitively and physically. Additionally, an increasing load on military personnel concurrently increases their risk of musculoskeletal injuries. Therefore, there is a necessity for research on the soldier's biomechanical outcomes under different loading conditions. When it comes to biomechanics research, marker-based technology is widely accepted as the gold standard in terms of motion capture. However, recent advancements in markerless motion capture could allow the quick collection of data in various training environments, while avoiding marker errors. In this research project, the Theia3D markerless motion capture system was compared to the marker-based gold standard for application on participants across varying body-borne load conditions. The aim was to estimate lower body joint kinematics, gastrocnemius lateralis and medialis muscle activation patterns, and lower body joint reaction forces from the two motion capture systems. Data were collected on 16 participants for three repetitions of both walking and running under four body-borne load conditions by both motion capture systems simultaneously. Electromyography (EMG) data of lower limb muscles were collected on the right leg and force plates measured ground reaction forces. A complete musculoskeletal analysis was completed in OpenSim using the Rajagopal full-body model and standard workflow: model scaling, inverse kinematics, residual reduction, static optimization, and joint reaction analysis. Estimations of joint kinematics and joint reaction forces were compared between the two systems using Pearson's correlation coefficient, root-mean-square errors, and Bland-Altman limits of agreement. Very strong correlations ($r = 0.960 \pm 0.038$) and acceptable differences ($RMSE = 7.8° \pm 2.6°$) were observed between the kinematics of the marker-based and markerless systems, with some angle biases due to joint centre differences between systems causing an offset. Because the marker-based motion capture system lost line of sight with markers more frequently in the heavier body-borne load conditions, differences generally increased with heavier body-borne loads. Timing of muscle activations of the gastrocnemius lateralis and medialis as estimated from both systems agreed with the ones measured by the EMG sensors. Joint reaction force results also showed a very strong correlation between the systems but the markerless model seemed to overestimate joint reaction

forces when compared to results from the marker-based model. Overall, this research highlighted the potential of markerless motion capture to track participants across all body-borne load conditions. However, more work is necessary on the determination of angle bias between the two systems to improve the use of markerless data with OpenSim models.

ACKNOWLEDGMENTS

I would like to start by thanking one of my co-supervisors, Dr. Allison Clouthier, for her continued support and advice during the last two years. I am immensely thankful for all the time she has put into assisting me on this research project. I would also like to thank my other co-supervisor, Dr. Ryan Graham for taking me into his laboratory, first as a coop student and then as a graduate student. He's given me the opportunity to evolve in his state-of-the-art laboratory and has made many resources available to ensure the project's continued progress. Also, I would like to thank all other Spine and Movement Biomechanics Lab members, especially Matthew Mavor, for his help and guidance in the laboratory.

A huge thank you goes to my thesis advising committee, Dr. Thomas Uchida and Dr. Thomas Karakolis for the time they spent reviewing my thesis and for their valuable comments. A special thank you goes to Dr. Thomas Uchida who taught me a lot during his Biomechanics of Movement class. He also introduced me to his "Biomechanics of Movement" textbook which was fundamental to the writing of my thesis. I would also like to thank the *Fonds de recherche du Québec – Nature et technologies* (FRQNT) and the University of Ottawa for their generous financial support.

I could not have completed this research project without my 16 loyal participants who took valuable time to accompany me into the lab for data collection. These few hours have been a real workout for some, running with more than 40 kg of weight on their back!

As most of these participants were volunteers from my close friends and family, this leads me to thank them for their never-ending encouragement and for always lending a compassionate ear. This research project and thesis would not have been possible without the time off spent with them. Special thanks to Thierno for his constant encouragement. Thanks to my parents for their precious guidance and endless support during my academic studies. Finally, a special thank you goes to the one and only Gianluca Marchese, my most caring and supportive half. Thanks for creating such a cozy nest with me, it's been an incredible asset in the completion of this research project.

TABLE OF CONTENTS

LIST OF FIGURES viii

LIST OF TABLES xii

ACRONYMS xv

1. INTRODUCTION 1

1.1. BACKGROUND 1

1.2. OBJECTIVES 3

1.3. EXPECTED RESULTS 4

1.4. OUTLINE 5

2. LITERATURE REVIEW 6

2.1. MILITARY LOAD CARRIAGE AND CORRESPONDING CHALLENGES 6

2.2. MARKER-BASED MOTION CAPTURE 9

2.3. LIMITATIONS OF MARKER-BASED MOTION CAPTURE 12

2.4. MARKERLESS MOTION CAPTURE 15

2.5. MUSCULOSKELETAL MODELS 20

3. EXPERIMENTAL METHOD 23

3.1. PARTICIPANTS 23

3.2. ETHICS APPROVAL 23

3.3. EXPERIMENTAL PROTOCOL 24

3.4. MARKER-BASED DATA PREPROCESSING 28

3.5. MARKERLESS DATA PREPROCESSING 29
3.6. EXCLUDED TRIALS 30
3.7. MUSCULOSKELETAL MODELLING ANALYSIS 30
3.8. STATISTICAL ANALYSIS 36
4. RESULTS AND DISCUSSION 38
4.1. RESULTS 38
4.1.1. Initial musculoskeletal analysis 38
4.1.2. Kinematics comparison – Static trials 39
4.1.3. Kinematics comparison – Dynamic trials 41
4.1.4. Muscle activation comparison 46
4.1.5. Joint loading comparison 48
4.2. DISCUSSION 53
4.2.1. Kinematics comparison – Static trials 55
4.2.2. Kinematics comparison – Dynamic trials 57
4.2.3. Muscle activation comparison 61
4.2.4. Joint loading comparison 62
4.3. LIMITATIONS 64
5. CONCLUSION 68
5.1. SUMMARY 68
5.2. FUTURE WORK 71

REFERENCES 73

Appendix A – Participant anthropometrics and sizing 84

Appendix B – Certificate of ethics approval..... 85

Appendix C – Research consent form 87

Appendix D – Equipment weight per loading condition 90

Appendix E – Experimental marker set 91

Appendix F – List of trials excluded from the analysis and reason 94

Appendix G – Results of the initial musculoskeletal analysis with initial angle bias 95

Appendix H – Participant angle bias per loading condition for the hip, knee, and ankle flexion 106

Appendix I – Plots of lower limb joint angles from the initial musculoskeletal analysis without angle bias applied..... 108

Appendix J – Plots of lower limb muscle activation 109

Appendix K – Summary of recommendations for using Theia3D data in OpenSim 112

LIST OF FIGURES

Figure 1: Steps to perform an inverse dynamics analysis in OpenSim..... 21

Figure 2: Participant during data collection in a) C1, b) C2, c) C3, and d) C4 24

Figure 3: Flowchart of preprocessing steps for the marker-based data 28

Figure 4: Flowchart of preprocessing steps for the markerless data..... 29

Figure 5: Flowchart of musculoskeletal modelling steps in OpenSim 31

Figure 6: Loaded model. a) Side view, b) Front view 32

Figure 7: Ground reaction forces (GRFs) from the right and left foot during gait and time ranges used for the musculoskeletal analysis of walking trials..... 34

Figure 8: Ground reaction forces (GRFs) from the right and left foot during gait and time ranges used for the musculoskeletal analysis of running trials 34

Figure 9: Marker-based (red) and markerless (blue) static poses of a representative participant for C1. a) Front view, b) Side view, c) Top view..... 40

Figure 10: Plots of lower limb joint angles for a full gait cycle under all loading conditions for walking trials. RMSEs computed as the difference between both curves through all timeframes. 41

Figure 11: Plots of lower limb joint angles for a full gait cycle under all loading conditions for running trials. RMSEs computed as the difference between both curves through all timeframes. 42

Figure 12: Plots of gastrocnemius lateralis and medialis muscle activity as measured by EMG sensors and estimated from the marker-based and markerless data through gait under all loading conditions for walking trials. RMSEs computed as the difference between the motion capture curves through all timeframes..... 47

Figure 13: Plots of gastrocnemius lateralis and medialis muscle activity as measured by EMG sensors and estimated from the marker-based and markerless data through gait under all loading conditions for running trials. RMSEs computed as the difference between the motion capture curves through all timeframes. 48

Figure 14: Plots of lower limb joint reaction forces through gait under all loading conditions for walking trials. RMSEs computed as the difference between both curves through all timeframes. 49

Figure 15: Plots of lower limb joint reaction forces through gait under all loading conditions for running trials. RMSEs computed as the difference between both curves through all timeframes. 50

Figure 16: Walking speed of all participants under all loading conditions as estimated from marker-based and markerless motion capture data..... 51

Figure 17: Running speed of all participants under all loading conditions as estimated from marker-based and markerless motion capture data..... 51

Figure G.1: Plots of lower limb joint angles for a full gait cycle under all loading conditions for walking trials with angle bias applied to the markerless results, from the initial musculoskeletal analysis. RMSEs computed as the difference between both curves through all timeframes. 96

Figure G.2: Plots of lower limb joint angles for a full gait cycle under all loading conditions for running trials with angle bias applied to the markerless results, from the initial musculoskeletal analysis. RMSEs computed as the difference between both curves through all timeframes. 97

Figure G.3: Plots of gastrocnemius lateralis and medialis muscle activity as measured by EMG sensors and estimated from the marker-based and markerless data through gait under all loading conditions for walking trials, from the initial musculoskeletal analysis. RMSEs computed as the difference between the motion capture curves through all timeframes. 101

Figure G.4: Plots of gastrocnemius lateralis and medialis muscle activity as measured by EMG sensors and estimated from the marker-based and markerless data through gait under all loading

conditions for running trials, from the initial musculoskeletal analysis. RMSEs computed as the difference between the motion capture curves through all timeframes. 102

Figure G.5: Plots of lower limb joint reaction forces through gait under all loading conditions for walking trials, from the initial musculoskeletal analysis. RMSEs computed as the difference between both curves through all timeframes. 103

Figure G.6: Plots of lower limb joint reaction forces through gait under all loading conditions for running trials, from the initial musculoskeletal analysis. RMSEs computed as the difference between both curves through all timeframes. 104

Figure I.1: Plots of lower limb joint angles for a full gait cycle under all loading conditions for walking trials without angle bias applied to the markerless results 108

Figure I.2: Plots of lower limb joint angles for a full gait cycle under all loading conditions for running trials without angle bias applied to the markerless results 108

Figure J.1: Plots of biceps and rectus femoris muscle activity as measured by EMG sensors and estimated from the marker-based and markerless data through gait under all loading conditions for walking trials. RMSEs computed as the difference between the motion capture curves through all timeframes..... 109

Figure J.2: Plots of biceps and rectus femoris muscle activity as measured by EMG sensors and estimated from the marker-based and markerless data through gait under all loading conditions for running trials. RMSEs computed as the difference between the motion capture curves through all timeframes..... 109

Figure J.3: Plots of tibialis anterior and semitendinosus muscle activity as measured by EMG sensors and estimated from the marker-based and markerless data through gait under all loading conditions for walking trials. RMSEs computed as the difference between the motion capture curves through all timeframes..... 110

Figure J.4: Plots of tibialis anterior and semitendinosus muscle activity as measured by EMG sensors and estimated from the marker-based and markerless data through gait under all loading

conditions for running trials. RMSEs computed as the difference between the motion capture curves through all timeframes. 110

Figure J.5: Plots of vastus lateralis and medialis muscle activity as measured by EMG sensors and estimated from the marker-based and markerless data through gait under all loading conditions for walking trials. RMSEs computed as the difference between the motion capture curves through all timeframes 111

Figure J.6: Plots of vastus lateralis and medialis muscle activity as measured by EMG sensors and estimated from the marker-based and markerless data through gait under all loading conditions for running trials. RMSEs computed as the difference between the motion capture curves through all timeframes 111

Figure K.1: Markerless scaling factors in OpenSim 120

LIST OF TABLES

Table 1: Motion capture systems and their limitations 19

Table 2: Angle bias between the marker-based and markerless models averaged over participants for hip, knee, and ankle flexion 40

Table 3: Pearson's correlation coefficient for the ankle, knee, and hip joint angles of marker-based and markerless data through all loading conditions for walking and running trials 43

Table 4: Bland-Altman limits of agreement for the ankle, knee, and hip joint angles of marker-based and markerless data through all loading conditions for walking and running trials 44

Table 5: Comparison of average maximum residuals between marker-based and markerless motion capture systems through all loading conditions for walking and running trials 45

Table 6: Average maximal ground reaction forces through all loading conditions for walking and running trials 46

Table 7: Pearson's correlation coefficient for the ankle, knee, and hip joint reaction forces of marker-based and markerless data through all loading conditions for walking and running trials 52

Table 8: Bland-Altman limits of agreement for the ankle, knee, and hip joint reaction forces of marker-based and markerless data through all loading conditions for walking and running trials 53

Table A.1: Participant anthropometrics and sizing 84

Table D.1: Equipment weight per loading condition 90

Table E.1: Individual anatomical marker set 91

Table E.2: Cluster marker set 92

Table E.3: Equipment marker set 93

Table F.1: List of trials excluded from the analysis and reason 94

Table G.1: Angle bias between the marker-based and markerless models averaged over participants for hip, knee, and ankle flexion, from the initial musculoskeletal analysis 95

Table G.2: Pearson's correlation coefficient for the ankle, knee, and hip joint angles of marker-based and markerless data through all loading conditions for walking and running trials, from the initial musculoskeletal analysis..... 98

Table G.3: Bland-Altman limits of agreement for the ankle, knee, and hip joint angles of marker-based and markerless data through all loading conditions for walking and running trials, from the initial musculoskeletal analysis..... 99

Table G.4: Comparison of average maximum residuals between marker-based and markerless motion capture systems through all loading conditions for walking and running trials, from the initial musculoskeletal analysis..... 100

Table G.5: Pearson's correlation coefficient for the ankle, knee, and hip joint reaction forces of marker-based and markerless data through all loading conditions for walking and running trials, from the initial musculoskeletal analysis..... 105

Table G.6: Bland-Altman limits of agreement for the ankle, knee, and hip joint reaction forces of marker-based and markerless data through all loading conditions for walking and running trials, from the initial musculoskeletal analysis..... 105

Table H.1: Participant angle bias per loading condition for the hip, knee, and ankle flexion.... 106

Table K.1: Methods used for the computation of OpenSim joint angles from Theia3D pose matrices..... 118

Table K.2: List of settings used for the scaling step in OpenSim..... 119

Table K.3: List of settings used for the inverse kinematics step in OpenSim 121

Table K.4: List of settings used for the residual reduction algorithm step in OpenSim..... 122

Table K.5: List of settings used for the static optimization step in OpenSim 124

Table K.6: List of settings used for the joint reaction analysis in OpenSim 125

ACRONYMS

2D	-	Two-dimensional
3D	-	Three-dimensional
CAF	-	Canadian Armed Forces
CoM	-	Center of mass
DND	-	Department of National Defence
EMG	-	Electromyography
FD	-	Forward dynamics
GRF	-	Ground reaction force
ID	-	Inverse dynamics
IK	-	Inverse kinematics
JA	-	Joint angle
JC	-	Joint centre
JRA	-	Joint reaction analysis
ICC	-	Intraclass correlation coefficients
LOA	-	Limits of agreement
MDC	-	Minimal detectable change
Mocap	-	Motion capture
.mot	-	Motion file
MSI	-	Musculoskeletal injury
OA	-	Osteoarthritis
RGB	-	Red-green-blue
RGB-D	-	Red-green-blue-depth

RMSD	-	Root-mean-square difference
RMSE	-	Root-mean-square error
ROM	-	Range of motion
RRA	-	Residual reduction algorithm
RSI	-	Repetitive strain injury
SO	-	Static optimization
.trc	-	Track row column file
xBW	-	Times bodyweight

1. INTRODUCTION

1.1. BACKGROUND

Constantly evolving protective and communication technologies and heavier weapons have made load carriage more challenging for soldiers. While infantry soldiers rarely carried more than 15 kg before the 18th century, body-borne loads have been constantly rising since then. More recently, since the Vietnam War, an even faster rise in load seems to be related to technological advancements in protection, firepower, communications, and mobility equipment. The exact load transported by foot soldiers might depend on their environment, training, and role as well as the terrain, goal, and duration of their mission [1].

An increase in body-borne load can significantly decrease situational awareness and operational performance at both cognitive and physical levels, thus compromising the safety of military personnel. Mobility and operational performance are significantly related to equipment bulk, stiffness, and weight. As equipment bulk, stiffness, and weight increase, mobility decreases. It is believed that impaired mobility in the field might lengthen exposure time and thus increase the likelihood of being targeted by the enemy. Hence, when enhancing a soldier's personal protective equipment (PPE), there exists a trade-off between the decreased vulnerability in response to ballistics and the increased susceptibility of being targeted by ballistics [2]. Vulnerability is defined as the "probability of kill given a hit" and is decreased by the addition of PPE. On the other side, susceptibility is defined as the "probability of hit" and is affected by the decrease in situational awareness from the additional PPE itself [3].

Heavily loaded backpacks require postural adjustments at the expense of movement ease [4], which can lead to joint injuries and muscle strain [5], and may increase joint contact forces, regardless of the backpack attachment configuration [6]. According to the Health and Lifestyle Information Survey of the Canadian Armed Forces (CAF) conducted by the Department of National Defence (DND), between 2008/2009 and 2013/2014, there was an increase from 22.6% to 32.3% in the annual rate of repetitive strain injuries (RSI). CAF personnel even cite musculoskeletal injuries (MSI) as the most common cause for the inability to deploy. The report notes that in the year preceding the survey, 44.4% of all Regular Force personnel experienced

either an acute injury or an RSI [7]. In addition to musculoskeletal injuries, soldiers with heavy loads frequently experience discomfort related to conditions such as metatarsalgia and blisters [1]. As a mission's success relies on its troop's ease and speed of travel, it is crucial to objectively evaluate a soldier's movement patterns and biomechanical stress under different loading conditions [8]. Mobility improvement can be achieved by reducing or redistributing load, modifying equipment, and ensuring proper training. With appropriate solutions, soldiers may save on energy costs and be more likely to complete their mission successfully and without injuries or discomfort [1].

To evaluate possible avenues for solutions, biomechanics research on soldiers is necessary. Motion capture systems that record a participant's movement are a valuable tool when it comes to the measurement of a participant's gait metrics such as stride length and rate as well as joint kinematics. Combined with force plates or electromyography (EMG) sensors, motion capture offers the possibility of estimating joint kinetics, which can give insight into load carriage injury mechanisms in military personnel. Optical marker-based motion capture, which uses reflective markers placed at key anatomical landmarks on the participant's body, is considered by the biomechanics research community as the gold standard in motion capture [9]. However, the placement of markers becomes very challenging when it comes to heavily equipped participants as markers cannot be placed directly onto the skin. Another drawback of optical systems is the limitation to a small capture volume in a laboratory context, preventing any on-the-field evaluation [10].

An emerging option is markerless motion capture technology, such as Theia3D (Theia Markerless Inc., Kingston, ON). This system uses a deep neural-network machine learning architecture to track the position of anatomical landmarks from an array of synchronized video cameras. When compared to a marker-based method, Theia3D displayed excellent agreement in kinematics measurements [11], [12]. This video-based technique has the advantage of having a faster collection time as well as being user friendly. Furthermore, with video cameras being the only equipment required, the markerless method also enables motion capture in a more diverse range of environments and for many participants at once. More importantly, it reduces the possibility of error and loss of accuracy from manual marker placement required from marker-based systems and has even been indicated as more reliable than the marker-based solution when

it comes to the impact of garments [11], [13]. Although the markerless method seems to be promising, it has not been tested on users with bulkier apparel [14] or for military-based movements. For military applications, this motion capture system could, however, have many advantages over marker-based motion capture such as the possibility to record participants in their training environment, avoiding marker errors, and allowing rapid set-up times.

1.2. OBJECTIVES

The overall aim of this project is to determine whether a markerless motion capture system can accurately capture the lower body motion and joint loading of heavily equipped participants, compared to marker-based technology. Ultimately, this would allow validation of whether the markerless technology could be used to assess the biomechanics of soldiers carrying heavy loads under different loading conditions. More specifically, the objectives can be divided into three consecutive goals as listed below.

1. To compare the kinematics of the lower limbs, i.e., the joint angles at the ankle, knee, and hip, during a static pose trial and dynamic trials using both the markerless and the marker-based motion capture systems.
2. To compare EMG activation patterns of the gastrocnemius medialis and lateralis muscles, which have been reported as active during the reported gait interval [15], with the muscle activations estimated from both marker-based and markerless data.
3. To compare lower body joint reaction forces between the two systems to evaluate how the motion capture technology might impact joint kinetics analysis results.

It is to note that the inertial measurement unit (IMU) option was not considered as part of this project. Even though it might allow in-the-field motion capture collection for military participants, this project focuses exclusively on the markerless motion capture option.

1.3. EXPECTED RESULTS

Expected results regarding the three consecutive goals listed above were researched before data collection. Expected findings related to the three objectives are listed below.

1. To properly compare the kinematics estimated from both motion capture systems, there is a need to first assess the differences between the models used by both systems. As such, an evaluation of the bias in joint kinematics between the standard Visual3D model used by the Theia3D software and a full-body OpenSim musculoskeletal model was performed on static trials. At present, no literature is available on research done in OpenSim using data from the Theia3D markerless system. Also, information on the model usually used to perform kinematics analyses on data from the Theia3D system is limited. As such, values expected for the bias in joint kinematics between the two models are unknown. It is however expected that values of bias are constant across loading conditions and not null.

   Using biases estimated from static trials, dynamic walking and running trials can be compared for lower limb joint kinematics estimated from both marker-based and markerless motion capture data. Regarding this comparison, recent research is available which presents results of root-mean-square difference (RMSD) between the two. Kanko and colleagues have presented results in the hip, knee, and ankle flexion RMSD of 3.4, 3.9, and 3.6°, respectively [11]. Assuming that an accurate value of bias between the Theia3D and OpenSim models can be determined, similar values are expected for the lightest loading condition. However, the Theia3D system has not been tested on participants wearing bulky military equipment and such equipment might obstruct the line of sight between markers and infrared cameras. As such, it is expected that the difference between kinematics from the two motion capture systems will become more pronounced as bulk is added to the participants.
2. It is believed that signals from the gastrocnemius lateralis and medialis EMG sensors will detect muscle activation at around 40–45% of the gait cycle [15]. Based on previous literature, lower limb joint centre differences between the marker-based and markerless systems are expected to be less than 1.5 cm, leading to kinematic differences of up to 17% including angle biases [11]. With such kinematic differences, it was estimated that peak joint moments can vary by up to approximately 12 N·m, which represents about 50% of the peak moment without marker registration uncertainty [16]. As activation timing is expected to be similar between

the systems, differences in magnitude are expected for the gastrocnemius medialis and lateralis. Still, muscle activation patterns of these muscles are expected to display strong correlation despite a possible offset in magnitude.

3. From the literature, it is believed that the peak magnitude of hip contact forces will range around 2–2.5 times bodyweight (xBW) for normal walking and be even larger for running trials [17]. Similarly, the peak magnitude of knee contact force is expected to be around 4–5 xBW [18]. Finally, the peak magnitude of ankle contact force has been reported around 8–9 xBW [19]. As these three values of peak lower limb joint contact forces from the literature are expected for minimal load bearing, it is expected that the lower limb's joint reaction forces will increase with additional load on the participant.

1.4. OUTLINE

This thesis is arranged into five chapters. In Chapter 2, research on load carriage is briefly reviewed, marker-based motion capture and its limitations are discussed, and a summary of current literature on markerless motion capture, more specifically the Theia3D Markerless Motion Capture System, is laid out.

Chapter 3 presents the experimental method used to collect data in the laboratory. It includes details on participant requirements and recruitment, ethics approval, data collection protocol, data preprocessing, and subsequent musculoskeletal analysis methods.

Chapter 4 offers a look at the project's results from the musculoskeletal analysis of markerless and marker-based motion capture data. It gives quantitative results on how well results from the two motion capture systems agree with one another. It also covers a discussion on the implications and limitations of these results.

Finally, Chapter 5 summarizes the thesis and discusses achievement of the objectives. It also offers an idea of what future directions this project might take.

2. LITERATURE REVIEW

2.1. MILITARY LOAD CARRIAGE AND CORRESPONDING CHALLENGES

Heavy occupational loads have put a burden on soldiers all around the world. Protective equipment, weapons, ammunition, and different kinds of provisions contribute to increasing this load. While mainly worn at the torso, equipment weight can also be applied on the head, feet, or thighs [20]. Load carriage takes up an important place in a soldier's military duties. Both during training and on the battlefield, military personnel are required to carry bulky, stiff, and heavy equipment [21]. Even though soldiers are greatly impacted by load carrying, other field officers can also face this challenge. Law enforcement personnel and firefighters are also at risk when it comes to heavy loads. While general duties officers can carry daily loads varying around 10 kg [22], Special Weapons and Tactics (SWAT) officers conduct operations while wearing about 40 kg of load [23]. As for firefighters, the equipment carried usually weighs about 20 kg [24]. Still, what sets soldiers apart from law enforcement officers and firefighters is the remote context in which they operate. Being deployed on missions far from any support system, soldiers are required to carry a larger quantity of equipment on their own [20]. Thus, there exists a trade-off between the decrease in performance from heavy loads and access to potentially lifesaving equipment [21].

Many factors will impact the load carried by soldiers. The Corps (e.g., artillery, armored, engineers, infantry, and signals [25]), role, and the task of soldiers within their unit will directly influence the amount of load carried. The amount of weight transported by modern soldiers from Australia, Great Britain, Spain, Germany, and the USA can range from 25 kg to beyond 45 kg [20]. While the load carried by soldiers appears to have stayed relatively unchanged for over 2000 years, there seems to have had an apparent increase after the Vietnam War [26]. However, it is to be noted that even though absolute loads have increased, relative loads have not significantly changed. While Romans used to carry about 55% of their body weight to the battlefield, the 82nd Airborne Division in Afghanistan also transported 55% of their body weight in their 'approach march loads' equipment configuration [26]. Still, this increase in absolute weight could be linked to advancements in technology which add to the soldiers' carriage requirements for defensive and offensive gear [27].

The heavy occupational loads carried by military personnel have a considerable physiological impact. It has been noted that an increase in the weight carried leads to a decrease in endurance time [28] and an increase in the energy cost of walking [29] and running [30]. Placing the load closer to the body is linked with lower energy consumption [31]. Other than the load itself, the context in which a soldier performs also has a physiological cost. A study even suggested that energy cost is more impacted by increases in the speed of travel than by increases in the load carried [32]. When carrying a load, energy expenditure is also affected by terrain gradient. While less energy is spent for downhill or level walking, more is required if walking uphill [33], [34]. Measurements have suggested that a 1% increase in terrain gradient has a greater impact on VO_2 than a 1% load increase [35]. Terrain surface also impacts energy expenditure whether a load is carried or not. Soldiers will spend energy differently whether the terrain is sandy, muddy, or snowy [36], [37]. Terrain surfaces can be classified by terrain coefficients (η) with the most energy-expensive being deep snow [38], followed by sand, and the most energy-inexpensive being sealed blacktop roads [39].

As load weight and distribution, speed of travel, terrain gradient, and surfaces all have an impact on the energy consumption of military personnel, they also influence some important gait variables. Some key biomechanical metrics can be measured to evaluate how soldiers adapt to different travel conditions. It has been shown that increasing the load carried causes a decrease in the range of motion of knee flexion/extension and pelvis rotation. It also leads to an increase in hip rotation, hip adduction/abduction, and pelvic tilt. As weight increases, the double support phase of gait gets longer while stride length decreases [40]. Participants tend to increase stride frequency to adapt to heavier load carriage [41]. Additionally, trunk flexion increases with increasing load [5]. The same applies to vertical and anteroposterior ground reaction forces (GRFs). The impact peak and mediolateral impulse of the GRF are larger with increasing load. This is a concern because greater vertical GRFs cause greater stress on the soldier's body and are often linked with an increased risk of injuries [42].

All these gait adjustments can be challenging on even a properly trained soldier's musculoskeletal system. When carrying heavy occupational loads, soldiers are faced with considerable injury risks. First and foremost, fatigue most probably will result from increased energy expenditure combined with large and repetitive muscle demands [20]. With fatigue can

come a decrease in performance and a higher risk of injuries [1]. As movement speed decreases with heavy loads and associated fatigue, exposure time can subsequently increase and put soldiers at great risk of being targeted by the enemy [21]. Injuries associated with load carriage include musculoskeletal injuries such as fractures or damage to ligaments, skin conditions such as blistering, and neurological injuries [20]. While foot blisters and back pain are most related to long-distance load carriage, most injuries occur in the lower limbs, followed closely by the back. Back strain has been stated as the leading cause of a soldier's inability to complete a march [43]. As for foot blisters usually caused by friction, even though they might seem like a minor injury at first, they can evolve into cellulitis or sepsis conditions. Stress fractures, also called "fatigue fractures" or "march fractures", are common for recruits as well as for well-trained soldiers when marching a long distance. These long marches can apply a sudden increase in repetitive stress on soldiers' bones. This imbalance puts them at a greater risk of rupture [44]. When reviewing risk factors for the development of lower-limb osteoarthritis (OA), military personnel were highlighted as vulnerable to hip and knee OA. The risk of knee OA increases with the individual's age and military rank or length of service. Individuals serving in the Army or Air Force are cited as being more at risk than the ones in the Marines [45].

Musculoskeletal injuries impose a strain on military forces around the world. In 2017, Canadian Armed Forces (CAF) lost about 65 years of training time to recruit injuries alone. Corresponding recovery time for these injuries varies largely and averages 86 ± 76 days. Without considering health care costs related to these injuries, their cost in recruit salaries is estimated to be about $2 M [46]. Increases in RSI, especially to the lower back, thighs, and knees, have affected the ability of military personnel to deploy. Reasons to justify this increase are unknown, but it has been observed that most of these injuries occur while practicing supervised activities such as sports and military or physical training [7]. This means that with the proper measurement systems, significant knowledge could be learned on the mechanisms behind these injuries and could be valuable in injury prevention and intervention. This could significantly contribute to reducing costs related to MSI in the CAF.

2.2. MARKER-BASED MOTION CAPTURE

To be able to study and learn about the impact of load carriage on a soldier's movement, different motion capture technologies are available. They allow one to record a participant's motion and model it for further analysis. Motion capture is a key tool when it comes to identifying pathological gait. It is interesting to note that military applications were among the early motivations of motion capture experiments such as those conducted by Wilhelm Braune and Otto Fisher during the late 19th century [47]. Nowadays, the technology has evolved into a variety of different motion capture systems and methods. It is notably used for the diagnosis of pathologies that are linked with gait changes and for rehabilitation and preventive interventions [47]. Among the numerous systems available on the market, marker-based motion capture is regarded as the gold standard for human motion research. Marker-based motion capture systems such as the passive Vicon system (Vicon, Oxford, UK) and the active OptoTrak system (NDI, Ontario, Canada) are known for their accuracy compared to other types of human motion capture systems [9].

Active or passive markers can be used to perform marker-based motion capture. Active markers emit infrared light [48], and passive markers are just spheres that reflect the infrared light sent by optical cameras. Passive marker-based motion capture uses passive reflective markers placed directly onto the skin to follow the movement of body segments. These markers are tracked by a set of infrared video cameras positioned over a specific capture volume where the participant's movement will be recorded. By sending pulsed infrared light signals into the capture volume, motion-blur artifacts are reduced and so is the effect of the laboratory's lighting system. The passive markers reflect the infrared light to the camera which can then detect the presence of a marker in the capture volume through time-of-flight triangulation [9]. This technology is widely used in biomechanical research and clinical diagnosis as well as in the entertainment industry to animate video games and movies [48].

When modelling a participant from marker-based motion capture data, each body segment is modelled as a rigid body, and each joint is assumed frictionless [49]. By evaluating the relative movement of two consecutive segments, joint angles can be deduced [47]. A minimum of three non-collinear markers is necessary to follow a segment's motion. Markers can be placed on a bony

landmark deemed immobile about both adjacent segments to reduce the number of markers necessary for the estimation of segment position and orientation. For example, this is the case when placing markers on the medial and lateral femoral condyles of the knee. These markers are assumed fixed relative to the participant's shank and thigh segments and thus account for both segments' motion. Even though modelling can help reduce the number of markers, estimations of segment position and orientation will be improved from a larger marker set [48]. Still, large marker sets tend to obstruct the participant's natural movements and might make the identification of marker trajectories more difficult [49].

To avoid marker position from being impacted by the movement of skin, fat, and muscles, markers are commonly placed on bony anatomical landmarks where the thickness of these soft tissues is normally smaller [48]. The placement of markers on the participant is usually performed by an experimenter who has anatomical knowledge. However, despite adequate training, the exact placement of markers on bony anatomical landmarks is not obvious for all participants and might suffer from experimenter and day-to-day variability. To reduce soft tissue artifacts and marker occlusions, marker clusters, i.e., groups of three to four markers mounted onto rigid plates, may be placed onto segments via strap bands. These marker clusters may be more practical to determine the six degrees of freedom, i.e., three translations and three orientations, of tracked segments [49]. By collecting a quick static trial where the participant stays immobile in a fixed position, the position of marker clusters relative to relevant anatomical markers can be known. This way, the position of anatomical landmarks can be determined at any timeframe from the marker clusters only. Thus, for the following dynamic trials, the anatomical markers may even be removed, keeping only marker clusters [11].

When using a marker-based motion capture system, each camera will record the position of each marker through a trial via consecutive 2D images. Upon calibration of the system with an object of known size on which markers are positioned at a known distance, the computer stores information on the relative position of all cameras in the camera array. Using this calibration and the 2D images recorded by each camera, it is possible to reconstruct a three-dimensional trial with a 3D estimation of the position of all markers through all timeframes of a trial and relative to the laboratory global reference frame. It is important to note that the position of a marker can only be

estimated if it is captured by at least two video cameras, otherwise not enough information is available for the system to perform its estimation [48].

Depending on research interest and laboratory protocol, the size of the required capture volume might differ. Still, for biomechanical analyses requiring 3D data and movements covering a larger surface, dozens of cameras might be required. In all cases, increasing the number of cameras and their distance from one another is always preferable if space and budget permit. Not only does it improve the accuracy of marker position, but it also helps prevent a marker from being visible to fewer than two cameras and creates a larger capture volume [48].

Before performing computations on the collected data, marker-based motion capture requires some processing. Gap filling must be completed to fill information in timeframes where some markers might have been occluded from multiple cameras. The occluded marker's position can normally be interpolated using different techniques, depending on the information available at the gap's timeframe. Labelling is also necessary to identify the landmarks which correspond to all markers. In fact, since the markers used in marker-based motion capture are usually passive, the cameras have no way of identifying the anatomical significance of markers. Either performed manually or automatically, this step is necessary to distinguish between marker trajectories and consists of giving a proper label to all markers of a trial. It is to be noted that active markers which emit infrared light exist and alleviate the requirement of a labelling step since they can be identified by the cameras. However, because of the need for the participant to carry the active markers' power supply and cables and because of frequency limitations, these are not as commonly used [48].

Clean and labelled marker-based data containing information on the position of markers through all timeframes of a trial can be used as input for a constructed model. Depending on the region of interest, e.g., the lower body, upper body, or full body, an appropriate multi-segment model combined with experimental data will allow for the computation of joint angles, or joint kinematics. If the marker-based data are collected simultaneously with a force plate system, results can be taken even further. By combining the kinematics from the modelled marker-based data and the kinetic data from the force plates, joint moments and powers can be determined through an inverse dynamics analysis, hence the importance of having accurate motion capture data [49].

2.3. LIMITATIONS OF MARKER-BASED MOTION CAPTURE

Even though marker-based motion capture is currently the most common method to capture three-dimensional trials of a participant's movements, it still has some downsides. When evaluating the accuracy of marker-based motion capture systems, many variables need to be considered. Among these variables are the relative positioning of cameras, the distance between markers placed on the participant and the camera array, and the placement, type, and quantity of markers tracked [9], [50]. There is also a trade-off between the camera resolution and the experimental sample rate [9].

Because it requires access to a laboratory environment, marker-based motion capture may be inaccessible to some researchers or health professionals. This laboratory constraint can also make marker-based motion capture more susceptible to experimental artifacts which are difficult to measure and quantify in a research protocol. In fact, one can define *ecological validity* as "the extent to which [the user experience] evaluation setup matches the user's real work context" [51]. When designing an experimental protocol using participants, it is essential to try and replicate the context in which the tasks are usually performed, as to not impair the ecological validity of the experiment. When performing data collection in a laboratory setting, this is not always easy, yet these artifacts can impact the ecological validity of the experimental results. For example, participants may alter their gait patterns due to unnatural laboratory conditions such as the strapping of Velcro bands at the shank, thigh, pelvis, and arms. It has also been pointed out that participants are also likely to modify their stride pattern when walking on a treadmill [47]. Also, research suggests that walking speed is affected when participants are aware that they are under analysis [52]. The precise impact of laboratory artifacts can be difficult to quantify, and some might even be unknown. Considering that motion capture is often used to diagnose pathological gait, slight changes in gait patterns resulting from the laboratory environment might affect results and ensuing patient outcomes [47]. The laboratory requirement thus makes it difficult to apply research findings to everyday applications or contexts such as sports and the military [53].

In a laboratory setup, cameras can be arranged to generate different sizes of capture volume, i.e., the laboratory volume where markers will be seen by at least two cameras at once. This volume can be modified by varying the number of cameras in the array or by changing their placement and

orientation. Different models of infrared cameras might also have different field-of-view specifications. Even though a wide capture surface might be attractive to applications in domains such as sports or military, the increased number of cameras required may generate concerns for cost and calibration and synchronization time. A large number of cameras also make the portability and set-up of the system more complex [9]. An ideal motion capture system would permit the recording of motion data in the participant's natural environment to reduce laboratory artifacts as much as possible. For example, athletes should be measured in their corresponding sports fields and soldiers should be analyzed in their training field, which is most likely outdoors. To do so, the ideal motion capture system would require a large capture volume, larger than the one offered by marker-based motion capture [47].

Sensitive infrared cameras mean that marker-based motion capture systems are more likely to be affected by surrounding disturbances. Errors in the data might result from very slight changes in the camera position or orientation following system calibration [9]. Even though well-informed researchers will not voluntarily change their experimental set-up after running calibration, these small alterations in camera position or orientation can come from elsewhere. The heavy footsteps of a participant running in the capture volume might disturb and move a camera placed on a tripod. A camera mounted to the ceiling might be shifted from movement in the room above. Also, because the cameras detect infrared light bouncing on the reflective markers, they are sensitive to the laboratory lighting system. Usually, marker-based motion capture systems are preferably used in darker indoor settings. Sunlight coming through windows should be blocked because its strong infrared content might interfere with the marker-based system [9], [49].

Since marker-based motion capture systems require a direct line of sight between every marker and at least two cameras at once, this can pose a problem for research participants required to wear bulkier equipment. This also limits the use of objects in motion capture trials such as boxes or sports equipment which might obstruct this marker-camera line of sight. A temporary marker occlusion could induce an increase in marker error [10]. To avoid marker interference, participants are also required to wear tight-fitting clothing which can be both socially and physically uncomfortable. This attire also permits researchers to perform their palpation protocol to identify bony anatomical landmarks and apply the corresponding markers directly onto the skin where possible [11]. While this can limit a participant comfort in performing certain movements, it

becomes quite a challenge when studying participants with bulkier apparel which might interfere with the marker-camera line of sight.

The use of markers itself is also an important limitation of marker-based motion capture. Since they are applied on top of the skin to estimate the motion of the underlying bony landmark, their position can be strongly affected by skin movement and muscle contraction [47]. Soft tissue artifact is regarded as the largest source of error when using a marker-based motion capture system as it contradicts the rigid body assumption [48]. As it can cause both systematic and random errors at a frequency often similar to the participant's motion, soft tissue artifact is difficult to eliminate [49]. In fact, for healthcare researchers relying on the position of these markers to identify pathological gait, very slight changes can have a great impact on the subsequent results [47].

Even though these markers should be placed on the patient's body by experienced and knowledgeable researchers, there is an unavoidable variability in marker placement. Inter-laboratory, inter-session, and inter-tester variability might affect the reliability of results [54]. When identifying anatomical landmarks, errors can arise from three principal factors: the anatomical landmark consists of an irregular and sometimes wide surface rather than a point, the anatomical landmark is covered by a thickness of soft tissue, and a variable palpation procedure is used to identify the anatomical landmark [55]. There is thus a need for better practice as well as standardization of marker placement [54]. Marker placement errors can lead to errors in the orientation of segment anatomical coordinate systems and corresponding joint axes. Even though this might only result in slight errors in joint rotations performed in the primary plane of motion, larger errors can occur for rotations out of this plane. These large errors can lead to misinterpretation of the data [55].

As previously explained, marker-based motion capture systems can rely on a combination of anatomical markers and cluster markers which tend to minimize skin artifacts. However, for a full-body trial, the number of markers to place on the participant puts an important time burden on the researcher. When used in a clinical setting, this time concern, combined with the cost of the technology and its limited applicability restricts its versatility [47]. The number of markers and the location of the participant's body might differ depending on the research questions and the model used to answer them. However, for full-body analyses, markers are necessary to track the

movement of both the lower and upper limbs as well as the pelvis and torso. For such studies, the number of markers required can amount up to 50 which can become time consuming for the researcher [10]. The marker placement step of data collection usually takes between 20 and 30 minutes, depending on the researcher's abilities and experience and on the number of markers to apply [11]. Not only do these markers need to be placed on the participant, but they also subsequently need to be labelled through all timeframes of a trial for marker-based motion capture systems using passive markers [10]. Both marker placement and marker labelling take a long time and can be challenging for the researcher.

Even though marker-based motion capture relying on the use of reflective markers has long been considered a gold standard when researching human movement, some considerable limitations restrict its use to a wider range of applications. Although some attention to the protocol and thorough analysis methods can somewhat alleviate some of these constraints, alternatives to marker-based motion capture are essential for time and money considerations and to widen the range of possible applications.

2.4. MARKERLESS MOTION CAPTURE

To face the applicability and time limitations of marker-based motion capture, researchers have spent many years developing different non-invasive markerless technologies which would eliminate the need for markers and the corresponding errors in motion data. Not only would these systems considerably reduce the time to prepare a participant for a motion capture trial, but they would also alleviate the manual processing time following collection [47]. They would also allow for participants to be analyzed in their normal working environments and thus, potentially resolve the trade-off between the accuracy provided by a laboratory setting and the ecological validity provided by a natural environment [49]. Thanks to this research work, markerless motion capture is gaining in popularity and accuracy [48]. A variety of machine learning algorithms based on computer vision use video or photo data and process images to track a participant's motion without the need for markers. This relatively new technology offers an interesting motion capture option for applications in domains such as sports, rehabilitation, and the military [9], [49]. When there is a need to assess the gait patterns or musculoskeletal motion of many participants efficiently,

markerless motion capture offers the advantage of being cheaper, faster, and independent of the research operator [56].

A classic gait trial can be collected by a markerless system in about ten minutes, compared to approximately 2 hours for the same trial using marker-based motion capture. This enables the possibility of very large studies with many participants. Most markerless systems allow for collections outside the traditional laboratory setting imposed by marker-based motion capture. With the markerless technology, systems can be taken outdoors on the sports field, in various clinical settings, and workplaces, thus allowing for ecological validity. As it does not require markers, the participant can wear their outfit of preference to perform comfortably. This notably includes loose sporting clothes, outerwear, and protective equipment. However, it has been suggested that the increased contrast offered by light coloured clothing gives better markerless motion capture results. Also, the markerless system requires legs to be visible for lower limb tracking and so, participants are restricted from wearing long coats or dresses and skirts during data collection. Another interesting use of markerless motion capture is the possibility to easily collect data from multiple participants at once and analyzing them both individually and in interaction, enabling the collection of activities such as sports events. Finally, as its name suggests, markerless motion capture eliminates the errors caused by soft tissue artifacts and variability in marker placement since it detects anatomical landmarks from machine learning algorithms [11].

Most markerless motion capture currently available for research can be divided into depth sensor-based systems and video-based systems. Depth sensing cameras, or RGB-D (red, green, blue, depth) cameras, obtain a depth map by using integrated infrared projectors. An example of an active, depth-sensing camera is the popular Kinect (Microsoft, New Mexico, USA) designed for entertainment purposes. However, this system lacks accuracy for biomechanics research [49]. RGB-D cameras also require the participant to stand within 3.5 m so that they can give an accurate depiction of their pose. On the other side, video-based systems impose very few constraints on the collection environment. By using an array of fixed cameras with different views of the capture volume, multiple 2D sequences of a trial can be recorded. By synchronizing and calibrating the cameras, these 2D sequences can be combined into a 3D pose. Computer vision techniques are then employed to identify and extract the position and orientation of the participant's segments through all timeframes of the trial. Either hull reconstruction, which reconstructs the participant's

outer shell, or feature recognition by neural networks or other deep learning approaches can be employed. This technique has successfully been used as the basis of multiple video-based markerless motion capture systems to estimate participant pose. However, few have been tested against the marker-based motion capture standard for validity. The video-based method also poses the need for powerful computers to run its algorithm. Some have also critiqued the ambiguity of neural network algorithms which make the identification of biases complex. When using video data to estimate human pose, many video setting factors come into play. It is still unclear how factors such as frame rate, environmental lighting, and background contrast affect video-based systems [11].

Recently, the Theia3D Markerless Motion Capture System has made its appearance in the research world. This video-based system relies on deep convolutional neural networks to estimate human pose from an array of a minimum of six video cameras. The algorithm was trained on more than 500,000 images of people in various clothing and environments on which anatomical landmarks were manually marked by competent annotators. A testing dataset was formed from exclusively new images collected in a laboratory setting. When processing video data from a trial, the algorithm estimates the 2D position of 51 features on the participants through all frames of a given trial. The camera array having been synchronized and calibrated beforehand, these 2D positions can be combined to give estimations of 3D positions for all features. From these positions, a multi-body model can be scaled adequately to the participant, and the model's pose through the trial can be estimated using an inverse kinematics approach. Since it relies only on video data to estimate human pose, the Theia3D system can be used in a wide range of settings and on multiple participants at once [11], [57].

The Theia3D system recommends using at least eight cameras for optimal results. These must be arranged with different orientations to track the participant in the designated capture volume. Depending on the number and model of the cameras used in the experimental setup which might have different depth focus specifications, the capture volume size might change. For better results, it is suggested to make sure all joints are visible by at least three cameras through a trial [11].

Theia3D's accuracy in collecting spatiotemporal gait parameters has been validated for healthy adults walking on a treadmill. It has also been compared to the traditional marker-based motion

capture technology for joint positions and angles, producing similar results [11]. When testing for inter-session variability, the markerless system has even outperformed marker-based motion capture on reliability [13].

Even though markerless motion capture offers a new avenue for motion capture, these systems still have some drawbacks. Depending on the application and processing power, real-time video tracking can be complex. Processing times can be long and require high-powered computers, limiting its use for real-time measurements. For better image quality and data, some systems might also require high-speed cameras which can be expensive. Similar to marker-based motion capture systems, accuracy is dependent on certain variables in the experimental setup. Among these, the number of cameras and their position and orientation relative to the participant impact data accuracy. Markerless motion capture does not remove possible errors coming from the quality of calibration of the system. Just like the marker-based motion capture systems, markerless motion capture still relies on mounted cameras to track movement and so, it is subject to errors caused by any slight changes in these cameras' position and orientation during collection. Cameras also pose a trade-off between video resolution and the sampling frequency for markerless systems [9]. To adequately track a participant's movement, the markerless motion capture system must have a line of sight with the participant's limbs. For example, with movements where the participant is on all fours, hiding some pelvis and torso landmarks from the cameras, markerless motion capture has more difficulty properly tracking the participant's motion. Finally, removing the use of markers does not completely remove the risk of systematic errors. The markerless system replaces markers with virtual anatomical landmarks estimated from machine learning. Even though these landmarks might not suffer from soft tissue artifact, errors can still come from landmark tracking and joint centre definitions. For reference, Table 1 summarizes the limitations affecting marker-based and markerless motion capture technologies. The limitations of IMUs are also included.

Table 1: Motion capture systems and their limitations

Limitation	Marker-based (Vicon)	Markerless (Theia3D)	IMUs
Laboratory requirement	X - The system is restricted to laboratory use and susceptible to experimental artifacts.	✓ - The system can be used in a wide range of environments.	✓ - The system is the most mobile and can be used in a wide range of environments [9].
Limited capture volume	X - Depends on the configuration and specifications of the cameras.	X - Depends on the configuration and specifications of the cameras.	✓ - The system is not limited by a capture volume.
Sensitive equipment	X - Cameras can be affected by surrounding disturbances.	X - Cameras can be affected by surrounding disturbances.	X - The system can be sensitive to nearby metals [9].
Line-of-sight requirement	X - Markers need to be visible by at least two cameras at once, complicating the use of bulky equipment.	✓ - The algorithm can track participants despite partial occlusions but some line of sight is still required for the cameras to identify the necessary keypoints.	✓ - The system does not require cameras.
Soft tissue artifact	X - Marker position is affected by skin and muscle movement.	✓ - Because no markers are required, the system is not affected by soft tissue artifact.	X - IMUs are mounted on the skin and can be affected by soft tissue artifact. It can also cause discomfort if equipment is applied on top of it.
Marker placement variability	X - Inter-laboratory, inter-session, and inter-tester variability is possible.	✓ - Because no markers are required, the system is not affected by marker placement variability.	X - Depending on their use, location and orientation of the IMUs can affect the results.
Time required	X - Marker placement and labelling can be tedious.	✓ - Data collection can be performed quickly, but computation times can be long.	X - Placement of IMUs can require some time.
Expensive	X - Full marker-based systems are expensive.	X - Full markerless systems are expensive.	X - Full IMU systems are expensive.
Operator experience	X - The system requires experienced operators to affix markers.	✓ - Little to no experience is required to collect data.	✓ - Little to no experience is required to collect data.
Position tracking	✓ - The system can estimate the participant's pose (orientation and position).	✓ - The system can estimate the participant's pose (orientation and position).	X - The system is unable to determine global position on its own [9].
Calibration	✓ - Calibration is required and straightforward.	✓ - Calibration is required and straightforward.	X - Calibration is required but can be complex.

2.5. MUSCULOSKELETAL MODELS

Muscle-driven simulations serve as a powerful analytical tool that gives motion capture data additional meaning. Human musculoskeletal actions are intricately tied to the neuromuscular system. The way these two systems interact with each other is complex. Research on this matter is required for the design of treatment interventions or devices that might assist the injured. This research might also assist in the training of athletes towards better performance [58]. To predict movement and compute quantities that cannot be measured directly in the laboratory, computer simulations are valuable in musculoskeletal research. Such quantities can include muscle forces or joint loading during a particular motion. These estimates can become crucial when researching injury mechanisms [48]. To perform such simulations, different software are available such as AnyBody (AnyBody Technologies, Aalborg, Denmark), Visual3D (C-Motion, Boyds, MD, USA), and OpenSim. OpenSim is an open-source software available online. It can be used for biomechanical modelling, simulation, control, and analysis of data related to the musculoskeletal system. It also offers a powerful tool for motor control science research. Examples of applications are gait dynamics, sports performance research, and surgery simulation [59].

Computational simulations can be divided into forward dynamic and inverse dynamic types of analysis. When using a forward dynamics (FD) simulation, the model's movements can come from measured muscle activations or its own neural command which activates the muscles required to generate enough force to perform the said movement. When reversing the process of forward dynamics, an inverse dynamics (ID) simulation is obtained. In an inverse dynamics analysis, the starting point of the analysis resides in the participant's measured motion. From there, the simulation gives an estimate of the muscle forces necessary to create that movement. In fact, to perform such an analysis, both experimental motion capture data and a biomechanical model are required. As illustrated in Figure 1, the very first step in the process to obtain muscle forces from inverse dynamics in OpenSim is to estimate joint angles from the experimental data using an inverse kinematics analysis. From there, the joint angles can be differentiated once to obtain joint velocities or twice to obtain joint accelerations. These estimations, combined with force plate kinetic data and the biomechanical model, can serve to compute muscle forces during the inverse dynamics analysis [48].

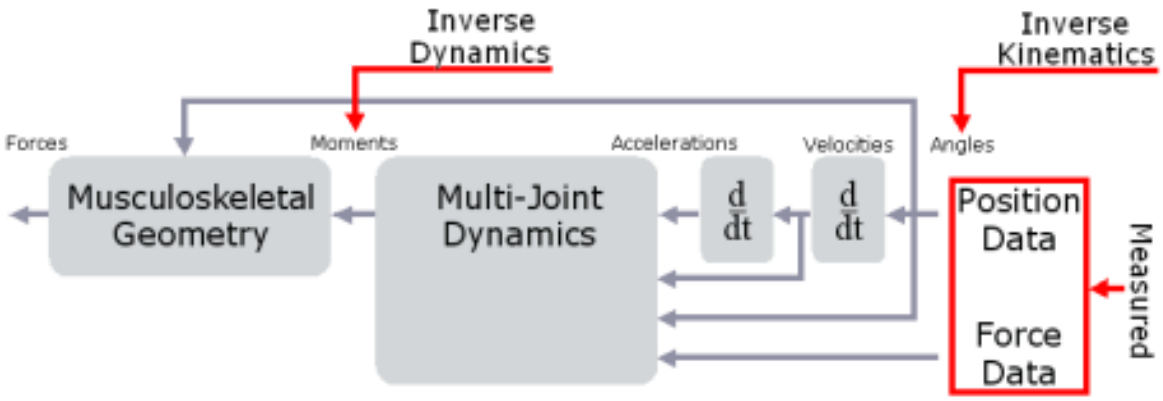

Figure 1: Steps to perform an inverse dynamics analysis in OpenSim

Biomechanical models are at the centre of these simulations. The use of musculoskeletal models is non-invasive and gives valuable insight into human movement and the effect of certain interventions on gait [58]. They are developed from equations of muscle activation dynamics, muscle-tendon contraction dynamics, musculoskeletal geometry, and skeletal dynamics which will all impact the response of the musculoskeletal system to muscle activation. For valid muscle force estimations, an accurate model which conforms to the motion studied is necessary. However, the human musculoskeletal system is complex. It is made up of many joints to allow complex movements. This inevitably creates many degrees of freedom. Due to dynamic coupling, the activation of muscles about a joint is likely to affect multiple body segments by creating induced forces. When researching musculoskeletal systems comprising multiple body segments, joints, and muscles, estimating muscle forces is a challenging task [48].

To simplify, assumptions must be made to operate muscle-driven simulations, depending on the research objectives. For different complexity levels in the motion analyzed, the musculoskeletal model chosen may be either 2D or 3D. It may also comprise a different number of muscles that actuate the model to generate the motion observed. Still, a larger number of degrees of freedom makes the model more complex and requires considerably more effort put into the simulation. Even though complexity is sometimes necessary, it is often better to opt for the simpler model if it is sufficient to answer the research objectives [48].

Before running a simulation using the chosen generic musculoskeletal model, it is necessary to scale it to the participant's size. Multiple tests can be performed in the laboratory to give insight into a participant's range of motion and joints' location and orientation. These will help make the

scaled model more representative of the participant's real musculoskeletal system. In OpenSim, the Scale tool adjusts the generic model by minimizing the position error between the model and experimental data [48].

Traditionally, marker-based motion capture data have been used to drive musculoskeletal models from measurements of marker position. However, as stated in Section 2.3, marker-based motion capture has limitations, especially regarding participant setup time and the tracking of bulky equipment. Researchers have been investigating a way to run these simulations without the need to collect marker-based data. For mobility purposes, IMUs have been used widely for estimating joint kinematics using musculoskeletal models [60]. The process of evaluating a participant's pose from IMUs has even been integrated into OpenSim as the OpenSense workflow [61]. However, putting on IMUs can still be time-consuming and expensive. It can also interfere with the participants' movement when worn under heavy and bulky equipment by causing discomfort. The corresponding calibration may also be ambiguous. Another option is markerless motion capture systems such as OpenCap (Stanford University, USA), an open-source and web-based software. The software can be used freely without the need for specialized hardware or software. From two iOS devices and a laptop, data can be collected and visualized, and the inverse kinematics (IK) process is run via OpenSim [62]. Still, limited research has been completed on the use of markerless motion capture to drive muscle-driven simulations. As markerless motion capture might present an interesting option to efficiently track military personnel in their full equipment, running these muscle-driven simulations from markerless data would be valuable. This research project explores this avenue by collecting both marker-based and markerless motion capture data on participants equipped with different military body-borne load conditions.

3. EXPERIMENTAL METHOD

3.1. PARTICIPANTS

Sixteen participants took part in this project – eight males and eight females. The average participant mass was 72.8 ± 10.0 kg, the average participant height was 1.7 ± 0.1 m, and the average participant age was 30 ± 12 years old. Appendix A presents a detailed overview of participants' height, mass, and equipment sizing. Participants were recruited among healthy adults over the age of 18. Healthy was defined as no musculoskeletal disorder that would limit the participant's ability to safely perform each of the tasks required by the experimental protocol. Specifically, participants who were suffering from a sprained joint, broken bone, muscle tear or pull, or any injury that would limit their ability to use the full range of motion of any joint at the time of recruitment were excluded from the participant pool. At this stage of research on the agreement between the marker-based and markerless motion capture systems, untrained civilians were deemed sufficient as participants. Real-life military personnel were not recruited for this validation experiment. A total of 16 participants – 8 females and 8 males – were recruited for this study based on previous load carriage literature and on the results of a 10-participant pilot study. These participants were recruited on a first-come, first-served basis. Potential participants were informed of the study via email, word of mouth, and Microsoft Teams. Supplementary participants were informed through email or word of mouth that their participation was appreciated but not needed.

3.2. ETHICS APPROVAL

The research project was ethically approved by the University of Ottawa Research Ethics Board, (ethics file number: H-06-18-721, modification request ID: MOD6-72). Appendix B presents a copy of the ethics approval received for this research project.

Before starting the data collection, every participant gave informed consent by signing the consent form presented in Appendix C. They also consented to have their trial's video recorded. Raw video data was stored in a password-protected folder only accessible by the research team. Once processed, data in text files were used for the rest of the analysis. Such text files only contain

joint coordinate data and so, the participant can't be identified from them. Raw video data was not and will not be used in any presentations discussing this research project.

3.3. EXPERIMENTAL PROTOCOL

To perform data collection, participants were invited to the University of Ottawa Spine and Movement Biomechanics Laboratory (200 Lees Avenue, E020) for a session of approximately two hours. The study protocol included a static trial and a series of two dynamic movements: walking and running over a 6-meter distance. Both dynamic tasks were performed three times each under four loading conditions: 5 kg (C1), 21 kg (C2), 35 kg (C3), and 41 kg (C4) for a total of 28 dynamic trials per participant (2 movements x 3 repetitions x 4 loading conditions + 4 static trials = 28 trials).

The loading conditions were accomplished through backpacks and protective equipment similar to what the Canadian Armed Forces (CAF) wear [63]. The first loading condition (C1) corresponded to the slick conditions in which the participants wear only military boots and a military helmet while carrying a mock rifle. In the second condition (C2), or the medium condition, both tactical and fragmentation vests were added to C1. In the third condition (C3), additional weight was added to C2 through a daypack. Finally, in the fourth and last condition (C4) the daypack was replaced by a larger rucksack. Figure 2 presents a participant wearing all four loading conditions during data collection. A breakdown of loading conditions and associated equipment weight is presented in Appendix D.

a) 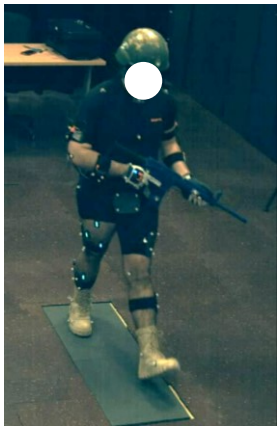 b) 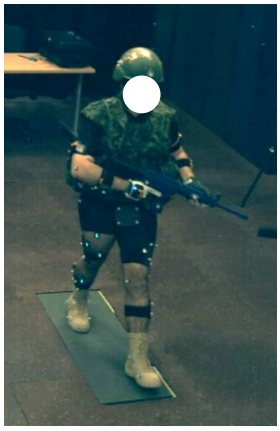 c) 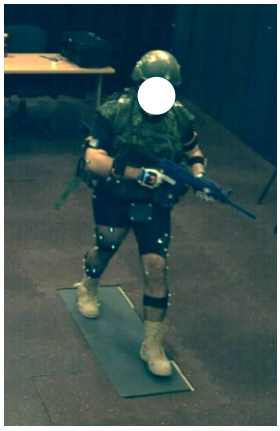 d) 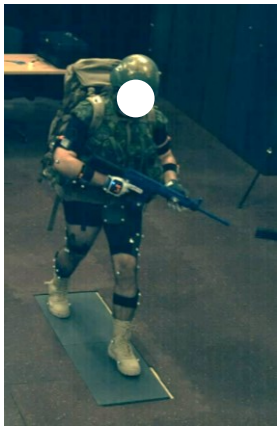

Figure 2: Participant during data collection in a) C1, b) C2, c) C3, and d) C4

For every trial collected, a total of five systems simultaneously recorded different types of data on the participant. The first one was the marker-based motion capture system including 11 infrared optical motion capture cameras recording at 120 Hz (Vantage V5, Vicon, Oxford, UK). It recorded the position of 37 individual reflective markers placed on the participant's upper and lower limbs, trunk, pelvis, and head as well as 10 clusters of four markers. A complete list of the marker set can be found in Appendix E. Then, the markerless motion capture system also collected video data of the participant's trial through 7 red-green-blue (RGB) video cameras recording at 60 Hz (Vue, Vicon, Oxford, UK). Both the marker-based and markerless systems were synchronously controlled via Vicon's Nexus software (Nexus, Vicon, Oxford, UK). Kinetic data were also recorded from both force plates and electromyography (EMG) sensors. The two in-ground force plates (Bertec FP4060, Bertec, Colombus, OH, USA) were aligned back-to-back to allow for the collection of one foot strike for both the right and left foot. Thus, they collected anteroposterior, mediolateral, and vertical ground reaction forces for one stance phase on each side. As for the EMG sensors (Delsys Trigno Avanti, Delsys, Natick, MA, USA), they were applied on eight of the participant's right leg muscles: the tibialis anterior, the gastrocnemius lateralis, the gastrocnemius medialis, the biceps femoris, the semitendinosus, the vastus lateralis, the vastus medialis, and the rectus femoris. They recorded the muscles' signals, also through Vicon's Nexus software. Here, it must be noted that the marker-based and markerless motion capture systems, force plates, and EMG sensors all collected data synchronously through Vicon's Lock Sync Box and Nexus software. Finally, the upper body of the participants was also equipped with one half of the Xsens inertial measurement unit (IMU) suit (MVNBIOMECH Link, Xsens, Enschede, the Netherlands) as well as the Xsens gloves by Manus (Manus, Eindhoven, the Netherlands). The idea was to record the participant's finger position via the gloves. Since the gloves can only record data if it is paired with the Xsens IMU suit, both were used simultaneously. Even though these data were collected, they were not analyzed in the scope of this research project. The data might, however, be relevant for future applications.

Before the participant arrived at the laboratory, both the marker-based and markerless motion capture systems were started, and drive storage space was cleared on the laboratory computer. For the marker-based system, small areas in the cameras' field of view were masked to avoid reflective objects in the laboratory to cause errors in the data. For both the marker-based and markerless systems, the cameras were calibrated, and the volume origin was set as a corner of a force plate on

the ground for all trials. The force plates were zeroed from the "Auto Zero" button on the analog amplifiers. A new session and participant were created in Nexus following a naming convention.

Upon arrival at the laboratory, the experimental procedure and the different equipment systems used were explained to the participant. Time was provided to answer the participant's questions and concerns, if necessary. The participant was then given some more time to thoroughly read and sign the consent form. Thereafter, anthropometrics, i.e., height and mass, were measured and noted. It is to be noted that upon confirmation of the session time, the participants were all instructed to wear comfortable sports shorts to the laboratory session as well as a sports bra for the females. Once in the laboratory, participants were asked to change into the Xsens IMU suit upper body shirt. Flexible Velcro bands were applied around the participant's shanks, thighs, pelvis, and upper and lower arms, on top of clothing.

Then, participants were first equipped with the EMG sensors on their right leg. After the appropriate area on the leg was shaved and sterilized, EMG sensors were placed following SENIAM recommendations [64]. The Xsens IMUs were then attached at the provided locations in the upper body shirt. At the same time, participants were asked to put on the Xsens gloves. The Xsens IMU suit was calibrated following the corresponding protocol using the MVN Animate software (MVN Animate, Xsens, Enschede, the Netherlands). As for the gloves, they were calibrated following the corresponding protocol using the Manus Core software (Manus Core, Manus, Eindhoven, the Netherlands). Finally, participants were equipped with 37 reflective individual markers and 10 clusters of four markers at the appropriate anatomical landmark position as presented in the marker set located in Appendix E.

Before starting the collection, participants were shown two video tutorials which showed how to hold the mock rifle when walking, i.e., pointing down, and when running, i.e., pointing up. Instructions were also given as to what auditive cues would mark the start and end of a trial. They were instructed to follow the beat of a metronome when walking (90 bpm) and running (140 bpm) so that their heel would strike the ground on each beat of the metronome. Lastly, they were asked to always land with their right foot on the first force plate and left foot on the second one to standardize the data.

Once participants were set up with the appropriate equipment and understood the experimental protocol, the data collection could start. For all four loading conditions, participants were asked to first perform a static trial doing a "biker pose" for a few seconds, without the mock rifle. Then, a few minutes were allowed for participants to practice the instructions previously given for the dynamic trial. When the participants were comfortable with the metronome, the rifle hold, and the force plate spacing, three walking trials, followed by three running trials were recorded for all loading conditions. A rest period of 30–60 seconds was allowed after each trial to reduce fatigue. After the static trial and all six dynamic trials were properly recorded, equipment corresponding to the next loading condition was added to the participants. It is to be noted that with additional equipment, some reflective markers sometimes needed to be moved or removed from the participants because they would lose line of sight with the cameras, hence the new static trial for each loading condition. To track equipment, reflective markers were also applied to the helmet (3), mock rifle (3), daypack (4), and rucksack (4).

After all loading conditions were completed, equipment was removed from the participants. They were asked to change into their regular clothing and were then free to leave the laboratory. All equipment and clothing were sanitized for safety purposes. In Nexus, all video data from the trials were transferred to the appropriate codec for the Theia3D software (Theia Markerless, Kingston, ON, Canada). Then, this data could be processed via the Theia3D software to obtain markerless human pose estimations. As for the marker-based data, before exporting any information from the trials, it was necessary to go through the lengthy process of gap filling and labelling the trials. Gap filling allowed interpolation of marker position when jumps in timeframes occurred from the temporary occlusion of the marker-camera line of sight. Labelling gives each marker an anatomically significant name through all timeframes of a trial. Using the same marker naming convention in all trials, the marker-based data could be analyzed using a musculoskeletal model in OpenSim (SimTK, USA) as will be presented in the following sections. For reference, the complete marker set with the corresponding marker naming convention was included in Appendix E. Overall, a total of 768 dynamic trials were analyzed (2 motion capture systems x 16 participants x 4 loading conditions x 2 movements x 3 repetitions = 768 trials).

3.4. MARKER-BASED DATA PREPROCESSING

The dynamic trials were cropped according to force plate signals directly into Vicon Nexus using the "Detect events from forceplate" pipeline. Only the portion of the trials between the first heel strike, i.e., right foot heel strike, and the second toe off, i.e., left foot toe off, was kept. This is the only portion of the trials for which force plate data is available and should also be the clearest part of the trials as the force plates are located in the middle of both the marker-based and markerless control volumes. The steps taken to preprocess the marker-based motion capture data so that they would be ready to input into OpenSim for analysis are illustrated in Figure 3. Once the dynamic trials were adequately cropped, both static and dynamic trials were gap filled and labelled to obtain continuous and anatomically labelled data for all markers. Once satisfied with this step, the marker coordinate data for all trials were exported as track row column files (*.trc*). At the same time, GRF data were also exported for all trials as motion text files (*.mot*).

To standardize the orientation of all trials with regard to a 3D axis system, all trials were rotated to the same orientation system using a custom Matlab script. This standard coordinate system was defined as an *x*-axis pointing in the direction of the movement, i.e., in the direction the participant is looking, a *y*-axis pointing upwards, and a *z*-axis pointing to the right side of the participant. As stated previously, the origin was selected as a corner of the second force plate, on the ground. Once both the marker coordinates and GRF were rotated to this standard coordinate system, they were then ready to serve as inputs for the musculoskeletal modelling part of the analysis.

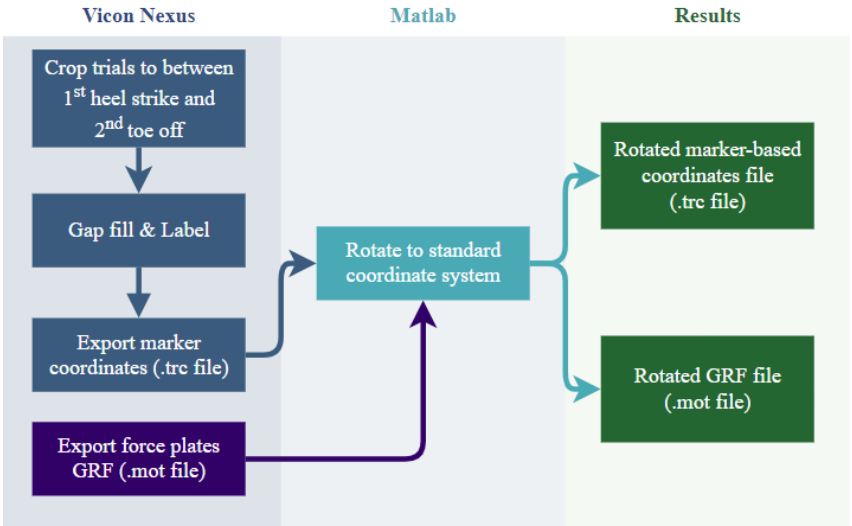

Figure 3: Flowchart of preprocessing steps for the marker-based data

3.5. MARKERLESS DATA PREPROCESSING

Similarly, for the markerless data, trials were also cropped from the first heel strike to the second toe off directly into Vicon Nexus. Figure 4 presents the steps taken to obtain the files required as inputs for the musculoskeletal modelling part of the analysis in OpenSim. Details from these steps have also been included in Appendix K. Once cropped, the markerless trials were first batch transferred and batch processed using the Theia3D software run from Vicon Nexus. The resulting *c3d* files could then be loaded into Visual3D (Visual3D, C-Motion, Boyds, MD, USA) to extract the necessary data. First, the rotation matrices for all segments of the Visual3D model were exported as Matlab files (*.mat*). These would serve to compute joint angles (JA). Coordinates for joint centres (JC) were also exported from Visual3D as Matlab files (*.mat*). Once all required information was exported from Visual3D for all trials, this information was imported into Matlab. First, the rotation matrices files were used to compute corresponding JA which were then exported from Matlab as motion text files (*.mot*). JC coordinates were also converted into trace text files (*.trc*) using Matlab. These coordinates also had to be rotated to properly match the previously established standard coordinate system (*x*: front, *y*: up, *z*: right) using a similar Matlab script as for the marker-based motion capture data. Once these preprocessing steps were completed, appropriate JA files (*.mot*) and rotated JC coordinate files (*.trc*) were ready to serve as input in OpenSim.

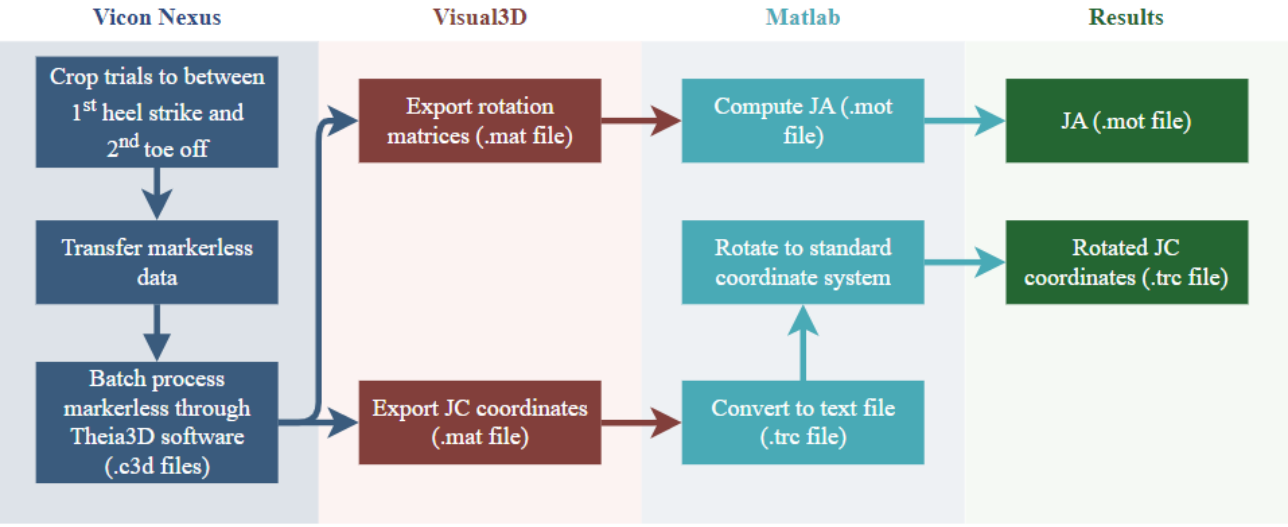

Figure 4: Flowchart of preprocessing steps for the markerless data

3.6. EXCLUDED TRIALS

Overall, 384 dynamic trials were collected simultaneously by the marker-based and markerless systems. Data from both systems were analyzed separately, resulting in a total of 768 dynamic trials to process and analyze (384 dynamic trials * 2 motion capture systems). During the musculoskeletal modelling analysis, certain trials were deemed unfit for analysis for multiple reasons. When this was the case, no matter which system was the cause, the dynamic trials from both systems were not considered for analysis. In total, 23 dynamic trials were considered inadequate (6% of the trials recorded during data collection), resulting in 46 trials excluded from the analysis. Most of these trials were excluded due to errors in the marker-based motion capture data related to a lack of marker visibility at the pelvis or marker clusters dangling from the participant during collection. Only six trials were excluded due to errors in the markerless motion capture data. Two of them were related to gaps in the markerless data when Theia3D could not recognize the participant for a portion of the trial. Two more were excluded because the Theia3D system did not track the participant correctly. Some other trials were excluded because the static optimization (SO) analysis failed on the markerless or marker-based trials. This is most probably due to modelling errors in the selection of SO settings which were inadequate for some of the dynamic trials, as the raw tracking data did not show signs of inadequate tracking. A list of the excluded trials and the reason for exclusion is included in Appendix F. It is to be noted that most excluded trials occurred for the heaviest loading condition (C4) where it was most difficult for the optical cameras to maintain a line of sight with the reflective markers.

3.7. MUSCULOSKELETAL MODELLING ANALYSIS

Figure 5 presents the steps taken for the musculoskeletal modelling analysis performed in OpenSim, from the inputs resulting from preprocessing, up to the joint reaction analysis (JRA). It is to be noted that the OpenSim process was completely run from Matlab using OpenSim's Matlab Scripting Environment. Supplementary Matlab functions were created to deal with the data as will be described in this section. Both marker-based and markerless data went through the same processing steps in OpenSim.

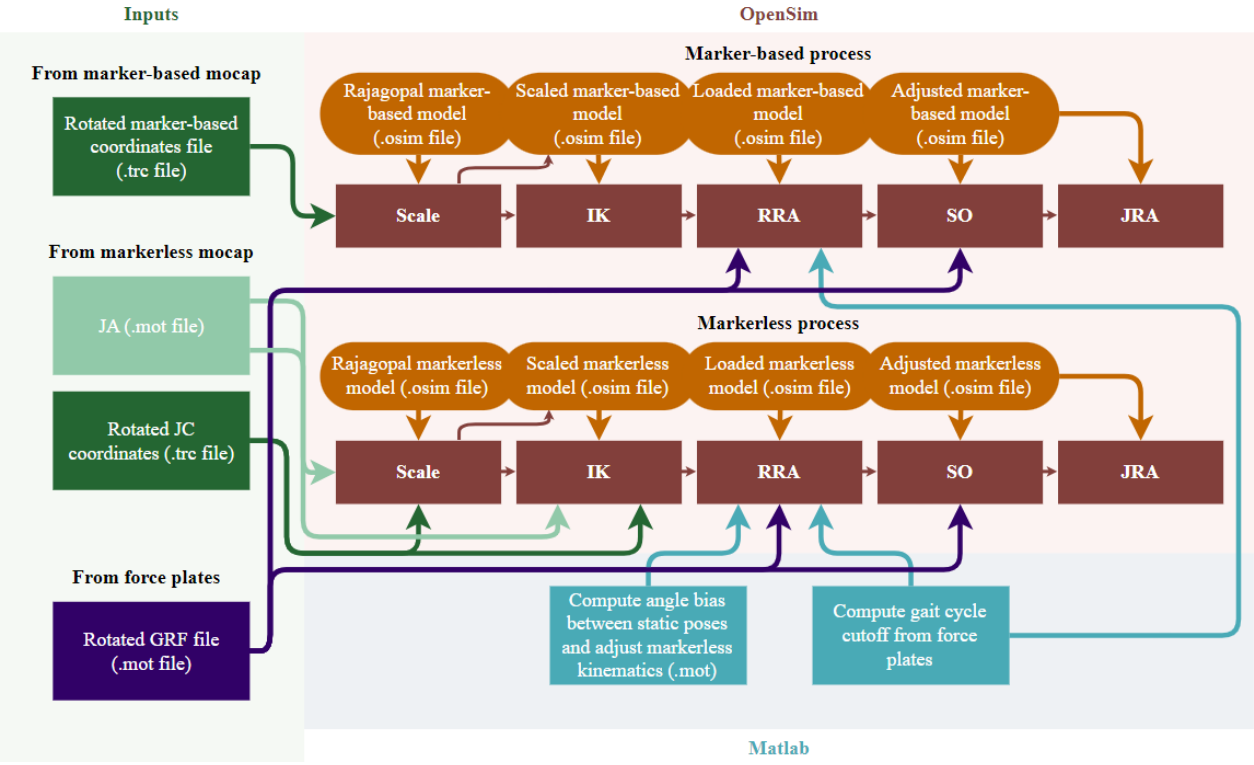

Figure 5: Flowchart of musculoskeletal modelling steps in OpenSim

The first step of the musculoskeletal modelling analysis was to scale the model specific to each participant using OpenSim's Scale tool [65]. Here, Rajagopal's full-body musculoskeletal model was used to model both the marker-based and markerless data. The model includes 37 degrees of freedom (20 at the lower body), 80 muscle-tendon units in the lower limbs, and 17 ideal torque actuators at the upper limbs [58]. The marker set of the Rajagopal model was adjusted for the marker-based and markerless data to reflect (i) the experimental marker set and (ii) Theia's available joint centres, respectively. Equipment was also added to the model to reflect the loading conditions evaluated in the laboratory as illustrated in Figure 6. Here, it is to note that the helmet, backpack, mock rifle and both vests' geometries pictured in Figure 6 only served aesthetics purposes as the corresponding weight was added to the Rajagopal model's musculoskeletal geometries.

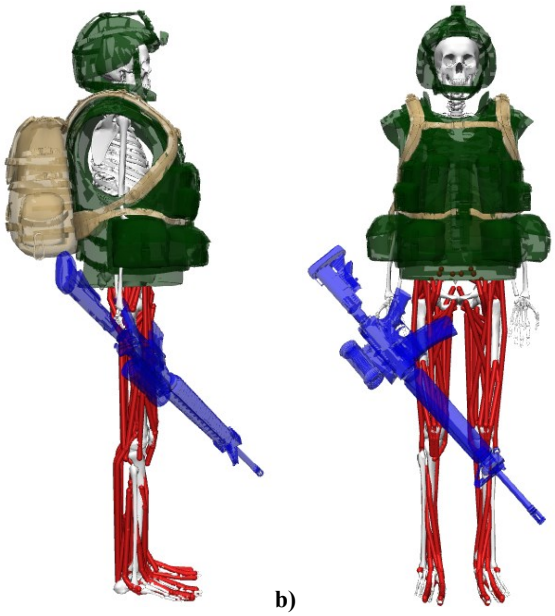

Figure 6: Loaded model. a) Side view, b) Front view

For the marker-based processing, the participant's marker coordinates when performing the static bikerpose in the slick loading condition (C1) were used to scale the model's anthropometry. It is to be noted that only the bikerpose in C1 was used to compute the scale factors necessary to resize the model as the most markers and the least amount of equipment were present for this loading condition. For the following conditions, the scaled model from C1 was also used, but an adjustment of the marker placement was performed using again the Scale tool [65], to account for any marker movement or change. For the markerless processing, the model was scaled using the joint centre coordinates extracted from the markerless data of the static bikerpose in C1, and the static pose was estimated from the joint angles, also extracted from the markerless data. Again, complete scaling was not redone for the three following conditions. To be consistent, the same scaled model, i.e., the one scaled using C1's bikerpose, was used for all loading conditions. Only a readjustment of the "marker placement" was performed using the Scale tool to account for any change in joint centre coordinates through the loading conditions. Theoretically, joint centres should keep the same position no matter the loading condition. However, in the event that additional weight impacts markerless tracking of the joint centres, a readjustment of their position at each new loading condition allows analysis of what the markerless system has collected for each specific loading condition.

Once both the marker-based and markerless data each had a properly scaled model, those models could be fed to OpenSim's Inverse Kinematics (IK) tool. Using that tool, an estimate of the participant's pose is given for each timeframe of the dynamic trials to match the given data as best as possible. This best estimate corresponds to the one which minimizes the sum of weighted squared errors between the data, either marker positions or joint coordinates, and the IK results [66]. For the marker-based data, the rotated coordinates files (*.trc*) of the dynamic trials were used as input data, along with the scaled marker-based model. For the markerless data, both the joint angles (*.mot*) and the rotated joint centre coordinates (*.trc*) were used to estimate the kinematics of the dynamic trials. In doing so, the kinematics of all trials were estimated according to both the marker-based and markerless data. To evaluate differences in the Rajagopal model compared to the Visual3D model used by the Theia3D software to define joint angles, angle biases were computed for all participants in all four static bikerpose trials. These values of biases were calculated as the difference between the marker-based scaled model placed in the bikerpose and the scaled markerless model placed in the same pose. If these values were consistent, the initial idea was to add them to the computed markerless kinematics values to mitigate errors due to the differences in biomechanical model definitions for the two systems. However, as detailed in Section 4.1.1, values of angle bias were inadequate and it was decided to keep the markerless kinematics unadjusted for the rest of the musculoskeletal analysis. This way, the conclusions drawn from the results would not be affected by incorrect application of angle bias on the results.

Once estimates of kinematics were known for both systems, OpenSim's Residual Reduction Algorithm (RRA) was used to minimize errors in the model that might have come from modelling itself and marker processing. These errors might have resulted in large nonphysical forces, called residual forces. To mitigate their impact on the model's results, the RRA can slightly modify the position of the torso centre of mass. Since the torso is the heaviest segment of the model, changing the location of its centre of mass can help reduce residual forces. The RRA also allows slight changes in kinematic results to be more consistent with the GRFs measured by the force plates [67]. Since the RRA uses the GRFs to perform its adjustments, it is necessary to only look at the portion of the trial where all the participant's weight is on the force plates. Otherwise, in the case of double support where one of the participant's feet is not on the force plate, for example, the RRA might think there are GRFs missing to balance the participant's weight and thus, make the wrong adjustments. To consider this in the analysis, the time range used to perform the RRA went

from the first peak in GRFs on the first force plate, to the second peak in GRFs on the second force plate. In other words, the time range considered started just after the first right foot strike, when the left back foot lost touch with the ground, covered the left foot strike and ended just before the right foot touched the ground. This small analysis of gait cut-off time was performed as a separate function in Matlab. The same time ranges were used for both the marker-based and markerless data. For reference, these time ranges are illustrated in Figure 7 and Figure 8 for walking and running trials, respectively. The complete gait cycle (0–100%) had to be cut after the IK step to start at the end of double support for walking trials for the subsequent RRA, SO, and JRA steps. This was not the case for running trials, where no double support is present and the complete gait cycle was kept.

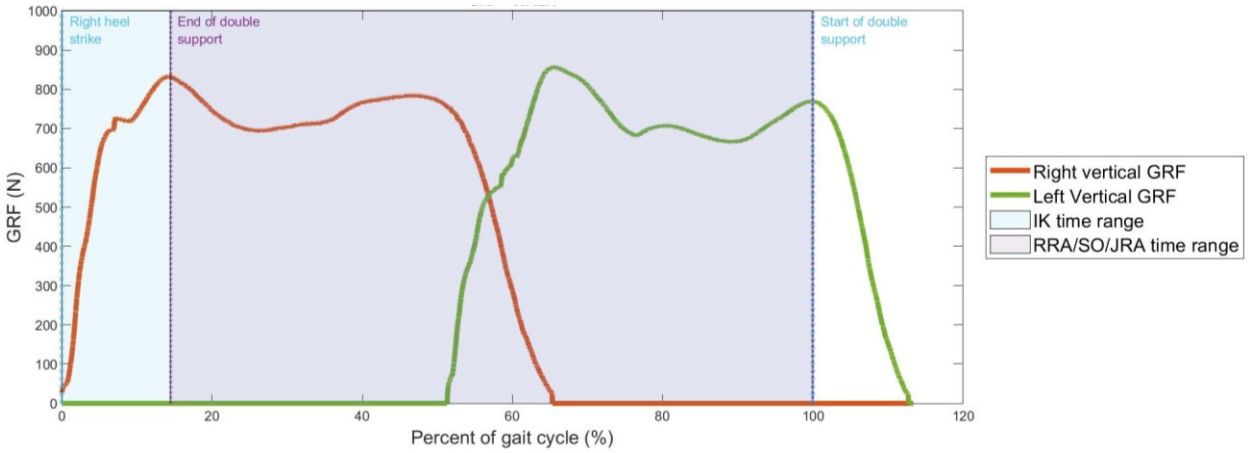

Figure 7: Ground reaction forces (GRFs) from the right and left foot during gait and time ranges used for the musculoskeletal analysis of walking trials

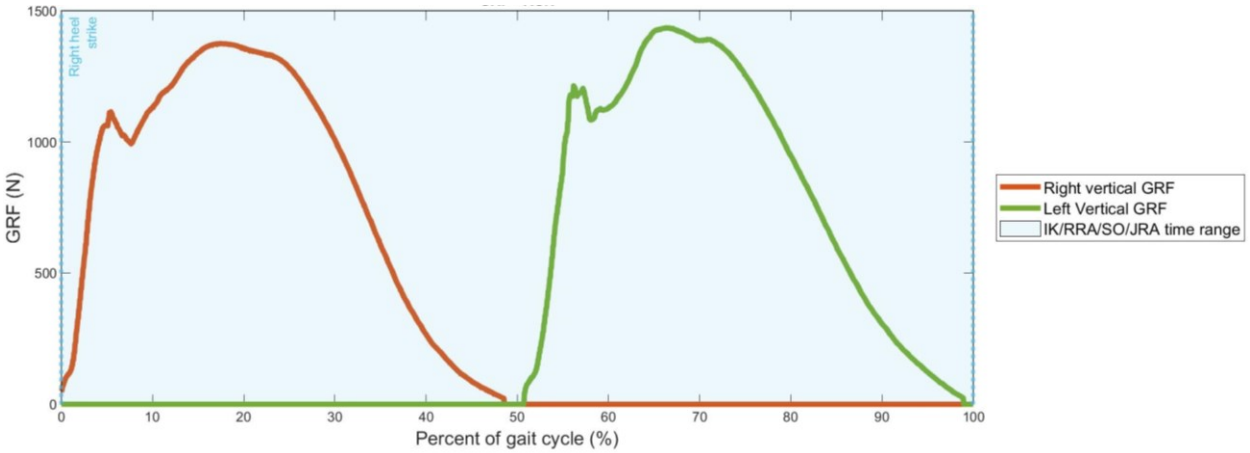

Figure 8: Ground reaction forces (GRFs) from the right and left foot during gait and time ranges used for the musculoskeletal analysis of running trials

Since the RRA performs computations using the model's mass to estimate residual forces, it was necessary to "load" the model with adequate equipment weights at this point. Here, it must be noted that changes in the participant's inertia resulting from the additional equipment were not considered as part of this project. Thus, only the mass of the model segments was adjusted when equipment was added. In the slick loading conditions (C1), only the rifle's weight was added as a supplementary mass at the model's right wrist. In the medium condition (C2), both the tactical and fragmentation vests were put on by the participant. They were modelled as additional weight located at the torso centre of mass. The same goes for the first heavy condition (C3) where the daypack was added. It was also modelled as additional weight at the torso centre of mass. In the heaviest condition (C4), the daypack was replaced by a heavier rucksack which was also modelled as more weight at the torso centre of mass. These scaled models with adequate equipment weight are referred to as "loaded models". They are the ones used to perform the RRA and evaluate residual forces.

This way, both marker-based and markerless loaded models were used to perform the RRA, respectively. The kinematics resulting from the IK step were used as input for the RRA. To achieve an optimal solution, two mass iterations were performed on the loaded models using the RRA recommendations. For each RRA iteration, the mass adjustments were applied to the loaded model's segments using the Scale tool without marker movement [68]. Adjusted models and kinematics resulting from the second iteration of the RRA were used for the upcoming steps of the musculoskeletal modelling analysis.

The next step was to use OpenSim's Static Optimization (SO) tool to estimate muscle forces through the same time range as used for the RRA. SO uses inverse dynamics, i.e., it uses a biomechanical model combined with estimations of kinematics and an optimization algorithm to give the best guess regarding the muscle forces necessary by the model to obtain those kinematics. The optimization minimizes the sum of squared muscle activations at each timeframe to obtain the best estimation of muscle forces [69]. Here, the models adjusted through the RRA as well as the adjusted kinematics were used to perform SO for both the marker-based and markerless data. Combined with the GRFs, estimates of muscle forces through the time range were obtained for both motion capture systems.

Finally, using the muscle forces found through SO, OpenSim's Joint Reaction Analysis (JRA) was performed to compute contact forces and moments at the ankle, knee, and hip joints for all dynamic trials. To sum up the forces operating at each joint of the lower limbs, the JRA requires the muscle forces found through SO [70]. These forces were filtered using a dual pass 2nd order Butterworth filter with a cut-off frequency of 7 Hz before serving as input to the JRA [71]. Again, the adjusted models were used as well as the adjusted kinematics for both motion capture systems.

3.8. STATISTICAL ANALYSIS

Several statistical metrics were computed from the IK and JRA results to evaluate their agreement, differences, and correlation. First, root-mean-square error (RMSE) was computed on all trials of a same loading condition and movement for the hip, knee, and ankle joints. It was first computed on results of IK and then on results of JRA. This metric gives insight on the average difference between the marker-based and markerless motion capture results along each trial. Values of RMSE are equivalent to values of RMSD (root-mean-square difference) which is the metric reported by Kanko and colleagues [11]. These values help to evaluate the systems' agreement with one another for IK and JRA results and allow kinematics RMSE to be compared with values found in the literature. Thus, RMSE allows to answer the first and third objectives as listed in Section 1.2.

Then, Pearson's correlation coefficient was evaluated on the results of joint kinematics and kinetics to assess the correlation between the two measurement methods. To use this coefficient, it was assumed that the selected sample of participants is representative of the population on which conclusions are drawn. In fact, at this stage of research on agreement between the marker-based and markerless motion capture systems, real-life military personnel were not recruited. Healthy participants were deemed sufficient for the current research. The variables on which Pearson's coefficient were calculated were also assumed to be continuous, jointly normally distributed, and random. Coefficients can be classified for interpretation using their magnitude. This way, coefficients between 0.40 and 0.69 indicate moderate correlation, between 0.70 and 0.89 strong correlation, and between 0.90 and 1.00 very strong correlation [72]. Pearson's correlation coefficient also allows to answer the first and third objectives as listed in Section 1.2.

Finally, Bland-Altman limits of agreement (LOA) were also computed for both IK and JRA results to estimate the agreement of the two measurement methods. The Bland-Altman LOA evaluates the mean difference between measurements from the two systems and suggests LOA within which 95% of the markerless measurements compared to the marker-based ones [73]. In the use of Bland-Altman LOA, it was assumed that both measurement methods have similar precisions and that this precision is constant. Also, it was assumed that the bias between the two measurement methods is constant along all trials [74]. Finally, to validate the normality assumption, results of differences from both IK and JRA will be tested for kurtosis, i.e., the measure of the peaks and tails of the probability curve. If these differences correspond to a standard normal distribution, they will display a kurtosis of 3, corresponding to a mesokurtic distribution [75]. Bland-Altman LOA also give information to answer the first and third objectives as listed in Section 1.2.

4. RESULTS AND DISCUSSION

4.1. RESULTS

4.1.1. Initial musculoskeletal analysis

Before presenting the most current results, a note must be made regarding results of the initial musculoskeletal analysis. For reference, results of that analysis have been included in Appendix G. In fact, the musculoskeletal analysis process detailed in Section 3.7 was used a first time on the collected data to obtain an initial set of results. However, further investigation into these results highlighted some ambiguities regarding results from both the marker-based and markerless datasets. Concerning marker-based kinematics results, visual representation of the marker-based dynamic trials in OpenSim showed a model exaggeratedly bent forward in the heavier loading conditions compared to video footage of the same trials. As the number of dynamic trials analyzed is quite large, each individual trial was not visually assessed in OpenSim. Still, the marker-based kinematic results presented in Appendix G suggested a considerable increase in hip flexion with increased load, which is not consistent with literature [4], [40]. In the initial kinematic results, a visible shift of the marker-based hip flexion curves upward in heavier conditions was observed and is inconsistent with literature suggesting that hip flexion does not significantly change with increased load [40]. Only hip flexion range of motion (ROM) can be expected to increase slightly [4]. This resulted in the models walking exaggeratedly bent forward along the entire gait cycle.

To correct this fault in marker-based results, the scaling weights were modified at the scaling step of the musculoskeletal analysis in OpenSim to minimize the overall root-mean-square marker error. Once a satisfying corrected scaled model was obtained, the new corrected weights were used to rerun the scaling step for all static trials and these newly scaled models served as the starting point for the musculoskeletal analysis. Results from this analysis are the ones presented as marker-based results in this section.

Concerning the markerless results, the initial idea was to adjust markerless kinematics from Theia3D using the computed angle bias, i.e., the difference between marker-based and markerless static pose kinematics. This was done in the initial musculoskeletal analysis. However, results of angle bias from that analysis presented in Appendix G are not consistent and display considerable

variations between loading conditions. For the musculoskeletal analysis presented in this section, the idea was to try and get a better look at how marker-based results compare with raw markerless results, without the impact of potentially incorrect values of angle bias. It was thus decided to only compare the corrected marker-based results to raw or unadjusted markerless results.

In fact, further research in the literature has also highlighted that "joint angles are not vectors. This means that they cannot be added or subtracted. Therefore, a normalized joint angle is not computed simply by subtracting the joint angle in the reference posture from the computed joint angle at a given frame of data" [76]. The method used to compute and apply angle bias might have been incorrect. While the computed values of angle bias might serve as a good indicator of how well the static poses match between the motion capture system, applying them on all timeframes of dynamic trials should not be done. That is why, for now, only the unadjusted markerless results are presented in this section. Avenues for solutions will be suggested later in Section 5.2.

4.1.2. Kinematics comparison – Static trials

During the first step of the musculoskeletal analysis, the Rajagopal model was scaled using static trials as measured by both the marker-based and markerless motion capture systems. The resulting scaled model placed in its static pose as indicated by static trial measurements differed between the two motion capture technologies. To quantify these differences, angle biases were computed as the difference between the marker-based scaled model and the markerless scaled model placed in the same static pose (i.e., bias = marker-based – markerless). These values of angle bias are presented in Table 2 for joints of the lower limbs in all four loading conditions. While ankle angle biases seem relatively constant, the knee and hip angle biases appear to be increasing with increasing equipment weight and bulkiness. At the hip flexion coordinate, biases go from 1.17° in C1 up to 12.51° in C4. When looking at individual coordinate values per motion capture system, the hip flexion angle measured by the marker-based system is also considerably increasing through loading condition, varying between -0.50° and 13.01°, which might be linked to the participants leaning forward during their static trial from the heavier load on their back in C3 and C4. However, this is not observed when looking at the same coordinate measured by the markerless system. According to the markerless system, hip flexion stays approximately constant around a value of 0° through loading conditions. A similar pattern is observed at the knee flexion

coordinate which shows a variation from 5.10° to 7.61° according to the marker-based motion capture system but stays relatively close to 0° according to the markerless one.

Table 2: Angle bias between the marker-based and markerless models averaged over participants for hip, knee, and ankle flexion

		Hip flexion (°)			Knee flexion (°)			Ankle flexion (°)		
Motion capture system		Marker-based	Markerless	Bias	Marker-based	Markerless	Bias	Marker-based	Markerless	Bias
Loading condition	C1	-0.50	-1.67	**1.17**	5.10	0.09	**5.01**	-3.19	5.13	**-8.32**
	C2	-0.10	-1.65	**1.55**	6.14	0.67	**5.47**	-2.50	4.86	**-7.36**
	C3	9.86	1.04	**8.82**	5.43	-1.39	**6.82**	-1.82	3.73	**-5.54**
	C4	13.01	0.50	**12.51**	7.61	-1.61	**9.21**	0.55	6.27	**-5.71**

For reference, the scaled OpenSim model of a participant loaded in the C1 condition is illustrated in Figure 9, where the red and blue skeletons represent marker-based and markerless models, respectively. In this figure, the skeleton can be seen from the front, side, and top view for visualization purposes. Angle biases of the upper body are not covered in the scope of this research project. A list of all participants' angle biases per loading condition has also been included for reference in Appendix H.

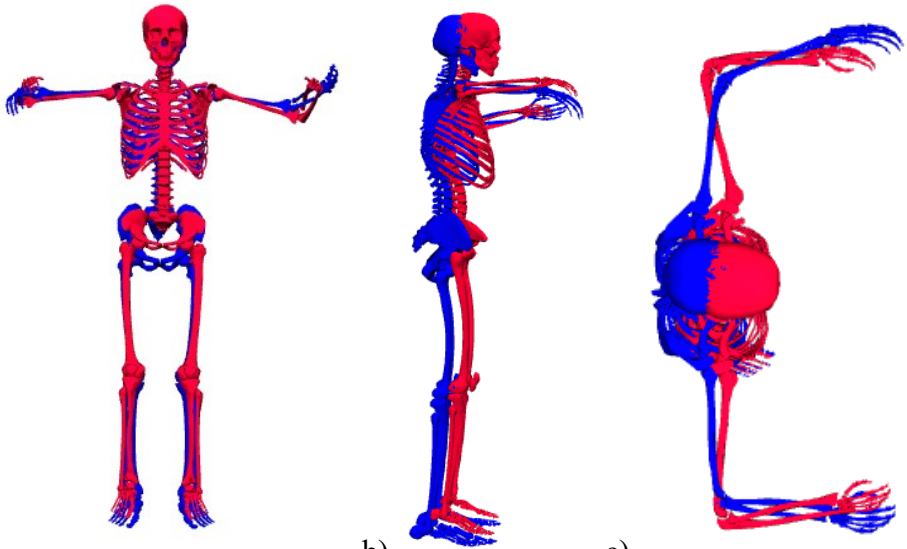

a) b) c)

Figure 9: Marker-based (red) and markerless (blue) static poses of a representative participant for C1. a) Front view, b) Side view, c) Top view

4.1.3. Kinematics comparison – Dynamic trials

The second step of the musculoskeletal analysis involved performing an IK analysis to estimate joint angles from motion capture measurements, using the previously scaled model. As discussed previously, biases were not deemed satisfactory enough for them to be applied to the markerless kinematic results. Instead, the markerless kinematic results were left unadjusted, i.e., the raw results from Theia3D were used to compare to marker-based kinematic results. Results for the walking trials are represented in Figure 10. In this figure, the subplots are arranged so that subplots from the same column reference the same loading condition and subplots from the same row reference the same lower body joint. This way, each curve represents the average of a joint angle for all three repetitions of all participants in a particular loading condition and the shaded area represents the standard deviation. Data from the marker-based motion capture system are displayed in red and data from the markerless motion capture system are in blue. Note that only the right leg is considered in this plot. Since the right foot was the first one to strike the force plates during the walking trials, 0 to 60% of the gait cycle represents the right stance phase. Lumbar extension was also included for reference.

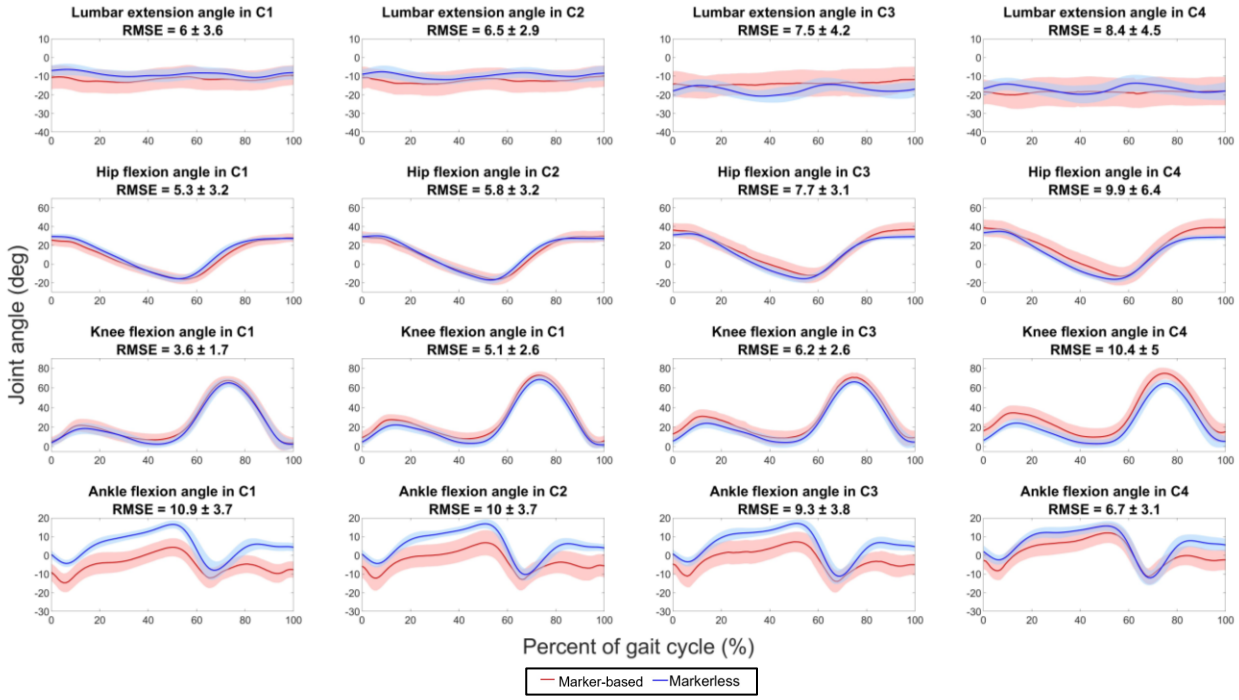

Figure 10: Plots of lower limb joint angles for a full gait cycle under all loading conditions for walking trials. RMSEs computed as the difference between both curves through all timeframes.

The curves are compared using values of root-mean-square error (RMSE) where smaller values of RMSEs indicate better agreement between the motion capture systems through the trials. Looking at RMSE values in C1, it seems that markerless data best matches marker-based data for the knee joint and does worst for the ankle joint. Through loading conditions, RMSEs are increasing with additional weight for the knee and hip flexion angles. However, they are decreasing for the ankle flexion angle. When looking at knee and hip flexion angle RMSEs, they increase from 3.6° to 10.4°, and 5.3° to 9.9°, from C1 to C4, respectively. On the other side, ankle flexion RMSEs decrease from 10.9° to 6.7° from C1 to C4.

Similarly, lower limb joint angles for a full gait cycle under all loading conditions for running trials are presented in Figure 11 using the same organization, i.e., columns represent loading conditions and rows, joint angles. Again, for the first loading condition, knee flexion seems to match the best between the two motion capture systems, with an RMSE value of 3.6°. Ankle flexion is again the worst joint angle for running trials. Its peak RMSE value of 12° in C1 is comparable to the 10.9° observed for walking trials in the same loading condition. Results of RMSEs do not seem considerably affected by whether the participant is walking or running.

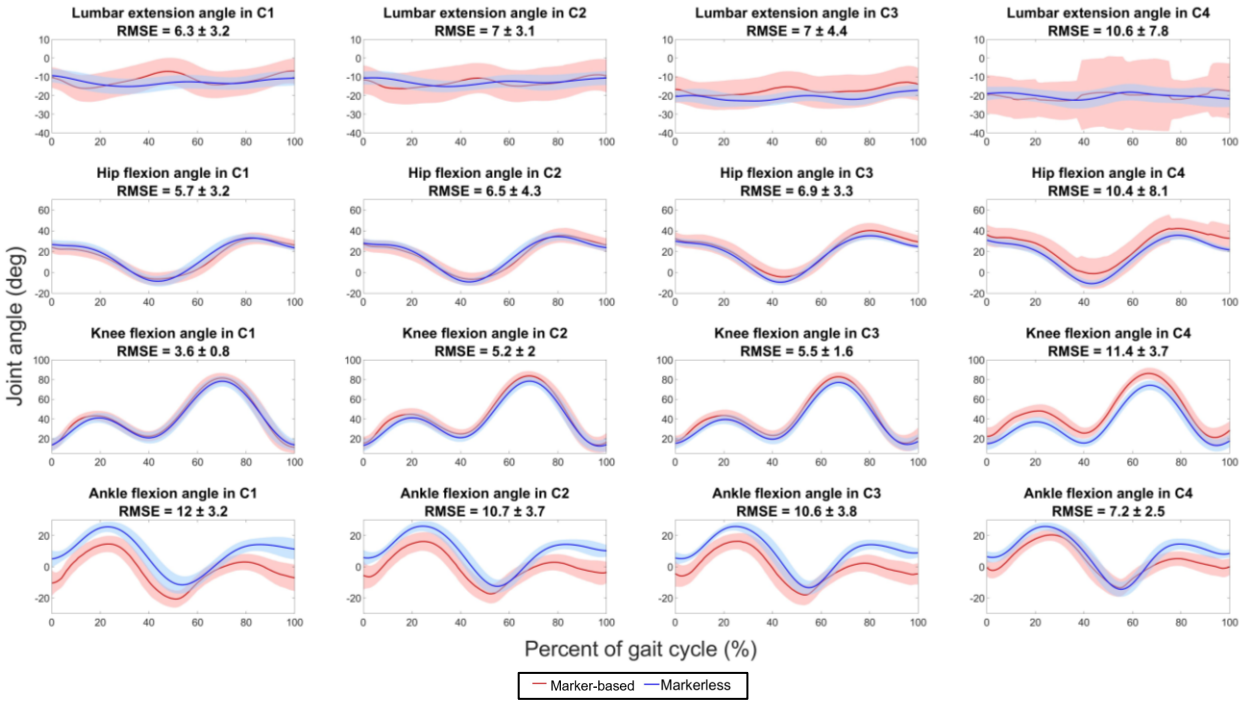

Figure 11: Plots of lower limb joint angles for a full gait cycle under all loading conditions for running trials. RMSEs computed as the difference between both curves through all timeframes.

In addition to RMSEs, the results of joint angles were also compared using Pearson's correlation coefficient. Before computing Pearson's correlation coefficient, a kurtosis test was performed to verify that the difference data was normal. Average kurtosis results of 2.5, 2.7, and 2.9 were found at the hip, knee, and ankle respectively for walking and running trials. These values were deemed sufficiently close to a mesokurtic distribution to assume normality in kinematics differences. Table 3 displays the correlation coefficient results for the ankle, knee, and hip joint angles of marker-based and markerless data through all loading conditions for walking and running trials. Values displayed in the table represent averages across all trials of the same movement and loading condition. While values between 0.70 and 0.89 indicate a strong correlation between the systems, values between 0.90 and 1.00 suggest a very strong correlation between them [72]. Looking at the values presented in Table 3, results of hip and knee flexion in all loading conditions suggest a very strong correlation between the motion capture systems. Knee flexion results show the best correlation with correlation coefficients reaching 0.996 for both walking and running trials in C2. Hip flexion results also show very strong correlations with minimal correlation coefficients of 0.977 for walking trials and 0.955 for running trials. The correlation coefficients for ankle flexion in loading condition C1 of the walking and running trials are the only ones that display a strong correlation instead of a very strong one, with values of 0.861 and 0.899, respectively.

Table 3: Pearson's correlation coefficient for the ankle, knee, and hip joint angles of marker-based and markerless data through all loading conditions for walking and running trials

			Joint		
			Hip	Knee	Ankle
Walking trials	Loading condition	C1	0.985	0.995	0.861
		C2	0.985	0.996	0.917
		C3	0.977	0.989	0.913
		C4	0.977	0.978	0.902
Running trials		C1	0.974	0.994	0.899
		C2	0.979	0.996	0.924
		C3	0.983	0.994	0.938
		C4	0.955	0.989	0.937

Finally, Bland-Altman limits of agreement (LOA) were also computed to quantify the agreement between the motion capture systems. Table 4 presents means of the Bland-Altman limits of agreement for the ankle, knee, and hip joint angles of marker-based and markerless data through all loading conditions for walking and running trials. Here, results are presented as "Bias ± LOA" or, in other words, "Mean difference ± 1.96 * Standard deviation of differences". Thus, a smaller mean difference value indicates a smaller bias and better agreement between the motion capture systems. Narrower LOA also indicates a smaller standard deviation and better agreement between the systems [73]. All values in Table 4 are in units of degrees (°), the same unit used to measure the joint angles previously. Results look best at the hip level with low mean difference between the systems. Walking trials experienced a maximal 5.52° of mean difference for hip flexion in C4, while running trials displayed a maximal mean difference of 7.34° for hip flexion in C4. The largest mean differences were observed for the ankle flexion, where maximal values of 10.27° and 10.88° of mean difference were computed for walking and running trials in loading condition C1, respectively.

Table 4: Bland-Altman limits of agreement for the ankle, knee, and hip joint angles of marker-based and markerless data through all loading conditions for walking and running trials

			Joint		
			Hip (°)	Knee (°)	Ankle (°)
Walking trials	Loading condition	C1	2.78 ± 5.85	-2.31 ± 4.54	10.27 ± 7.25
		C2	1.03 ± 6.11	-4.30 ± 4.51	8.35 ± 6.61
		C3	-3.51 ± 7.94	-4.99 ± 5.89	8.02 ± 6.86
		C4	-5.52 ± 8.06	-9.50 ± 5.66	4.60 ± 6.77
Running trials		C1	1.52 ± 6.81	-1.74 ± 5.69	10.88 ± 9.55
		C2	0.54 ± 6.15	-4.01 ± 4.98	9.41 ± 8.42
		C3	-3.08 ± 5.78	-4.21 ± 5.25	9.42 ± 7.87
		C4	-7.34 ± 7.35	-10.77 ± 6.00	5.25 ± 8.23

Once the joint angles were obtained from IK, an RRA was performed to optimize the model. Table 5 presents a comparison of average maximum residuals between marker-based and markerless motion capture systems through all loading conditions for walking and running trials. Values of residuals have been normalized as percentage of maximal GRFs. The residual forces are divided between the 3D axis into anteroposterior (*x*-axis), vertical (*y*-axis), and mediolateral (*z*-axis) residual forces. Lower values of residual forces indicate better agreement between the model

and the measured ground reaction forces data. From the results presented in Table 5, the marker-based motion capture model seems to almost constantly have lower residual forces than the markerless. Marker-based average maximum residuals vary between 1.5 and 31.1% of maximal anteroposterior GRFs, 1.3 and 2.7% of maximal vertical GRFs and 6.8 and 41.7% of maximal mediolateral GRFs. However, markerless has lower residuals than marker-based in three instances which are highlighted in yellow in Table 5 and all occur in loading condition C3. The highest value of residual force is observed during running trials in loading condition C4 in the *z*-direction for the markerless system. This value of 53.9% is highlighted in red in Table 5.

Table 5: Comparison of average maximum residuals between marker-based and markerless motion capture systems through all loading conditions for walking and running trials

		Motion capture system	Marker-based	Markerless	Marker-based	Markerless	Marker-based	Markerless
			Anteroposterior residual F_x (% of max. GRF)		Vertical residual F_y (% of max. GRF)		Mediolateral residual F_z (% of max. GRF)	
Walking trials	Loading condition	C1	1.5	2.3	1.3	2.1	7.5	17.5
		C2	2.7	5.9	1.6	3.0	6.8	25.3
		C3	10.0	8.8	2.3	3.0	41.7	47.3
		C4	7.2	16.0	1.8	2.3	29.2	40.7
Running trials		C1	2.8	2.8	1.5	2.3	6.9	16.0
		C2	8.1	8.7	1.7	2.8	14.4	24.2
		C3	31.1	15.8	2.7	2.2	40.9	44.5
		C4	15.8	18.4	1.5	2.0	36.3	53.9

To give context to the values of residual forces presented in the previous table, the averages of maximal GRF in all three directions are presented in Table 6. Values of average maximal GRF were normalized as factors of each participant's bodyweight (xBW). For walking trials, GRFs in all directions increase with additional weight. For the vertical direction, this means an increase in average maximal GRF from 1.154 xBW in C1 to 1.646 xBW in C4. For running trials, while vertical GRFs also increase with weight, anteroposterior and mediolateral GRFs seem fairly constant. The increase is still noted in the vertical direction where the average maximal GRF goes from 1.829 xBW in C1 up to 2.257 xBW in C4. It must be noted that the same GRFs data from the in-ground force plates were used for both the marker-based and markerless musculoskeletal analyses.

Table 6: Average maximal ground reaction forces through all loading conditions for walking and running trials

			Average maximal anteroposterior GRF (xBW)	Average maximal vertical GRF (xBW)	Average maximal mediolateral GRF (xBW)
Walking trials	Loading condition	C1	0.223	1.154	0.081
		C2	0.279	1.390	0.092
		C3	0.320	1.559	0.103
		C4	0.331	1.646	0.116
Running trials		C1	0.238	1.829	0.122
		C2	0.246	1.951	0.126
		C3	0.253	2.153	0.122
		C4	0.246	2.257	0.124

4.1.4. Muscle activation comparison

After performing the RRA, the adjusted model was used to run SO, following an ID process. Figure 12 presents the results of the muscle activation for the gastrocnemius lateralis and medialis when estimated from marker-based motion capture data (red) and markerless motion capture data (blue) for walking trials. Muscle activation measured by EMG sensors placed on the participants during the trials is also displayed in these plots (green). It is to be noted that the activity of a total of eight muscles was recorded via EMG sensors. Because they were among the most active during the reported gait interval which excludes double support, the gastrocnemius lateralis and medialis are the only ones presented in this section [15]. The reader is referred to Appendix J for plots presenting the muscle activity of the biceps femoris, rectus femoris, tibialis anterior, semitendinosus, vastus lateralis, and vastus medialis, in the same format. Since the maximal contraction of the muscles was not measured as part of the experimental protocol, data from all three curves were normalized using the maximum muscle activation of each trial individually. Similar to the plots previously presented, Figure 12 displays values of RMSE between the marker-based and markerless curves and is organized so that subplots from the same row correspond to the same lower body muscle and subplots from the same column correspond to the same loading condition. Here, for walking trials, the double support phase could not be included in the ID analysis as part of the participant's weight was not on the force plate. Therefore, the presented data starts at 17% of the gait cycle, up to 100%. From, it can be observed that all curves peak around 40–50% of the gait cycle. RMSEs between the muscle activation estimated from the marker-based

and markerless data increase with loading condition. While a minimal gastrocnemius lateralis RMSE value of 0.097 is observed for walking trials in C1, a maximal value of 0.124 is observed for walking trials in C4. The same goes for the gastrocnemius medialis where minimal and maximal values of 0.09 and 0.117 are observed in C1 and C4, respectively.

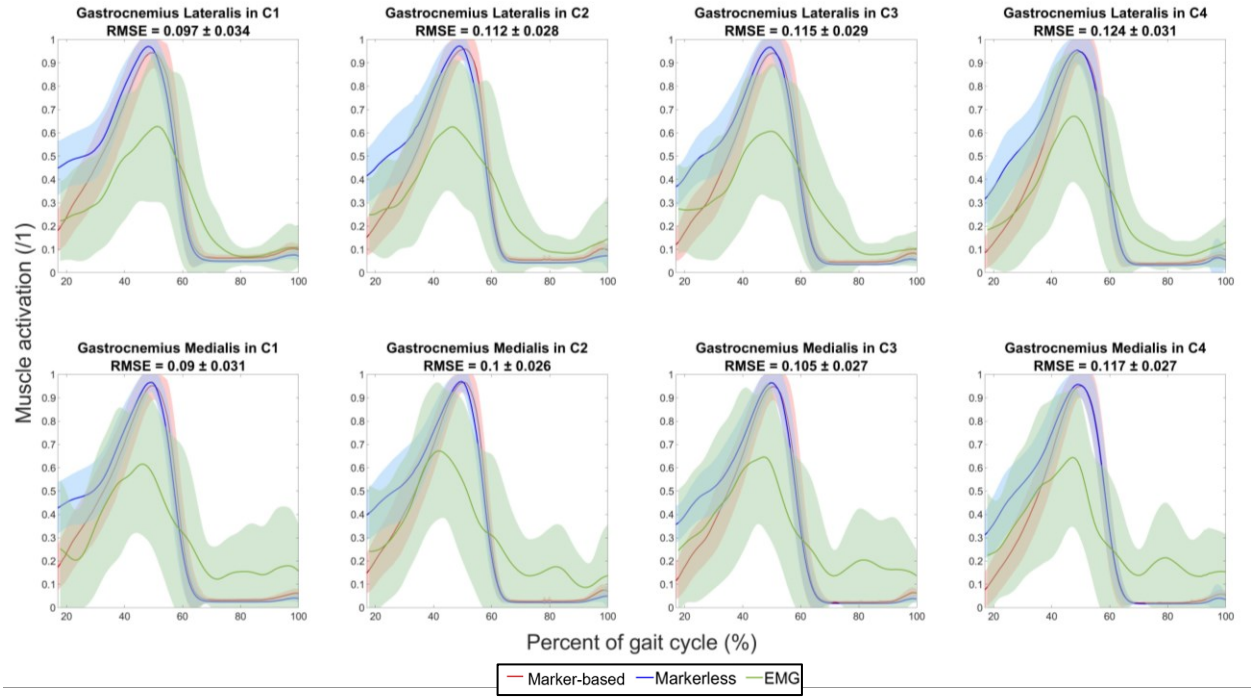

Figure 12: Plots of gastrocnemius lateralis and medialis muscle activity as measured by EMG sensors and estimated from the marker-based and markerless data through gait under all loading conditions for walking trials. RMSEs computed as the difference between the motion capture curves through all timeframes.

Muscle activation from running trials is also presented in Figure 13 which presents data from marker-based and markerless motion capture, as well as EMG sensors. Here, because the participants were running, the double support phase was not present and so, the entirety of the gait cycle could be kept in the ID analysis. Again, all curves appear to peak around 30–40% of gait cycle. RMSE values between the marker-based and markerless data still increase with additional load. Gastrocnemius lateralis RMSE values vary between 0.109 and 0.134. As for gastrocnemius medialis RMSE values, they vary between 0.118 and 0.157.

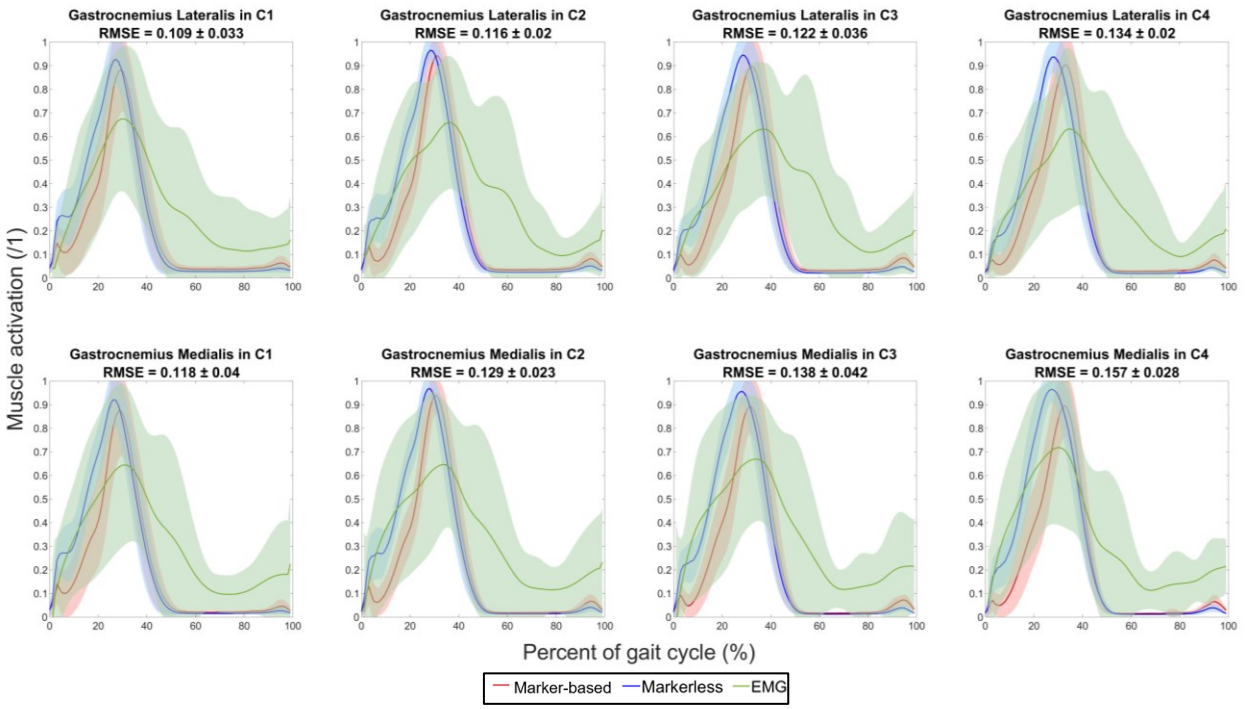

Figure 13: Plots of gastrocnemius lateralis and medialis muscle activity as measured by EMG sensors and estimated from the marker-based and markerless data through gait under all loading conditions for running trials. RMSEs computed as the difference between the motion capture curves through all timeframes.

4.1.5. Joint loading comparison

Using the resulting muscle forces obtained from SO, the JRA allowed estimation of the reaction forces applied at the ankle, knee, and hip. Figure 14 presents a plot of the magnitude of lower limbs' joint reaction forces through gait under all loading conditions for walking trials. Again, the subplots are organized so that subplots from the same column all correspond to the same loading condition, and subplots from the same row all correspond to the same lower body joint. Data between 60% and 100% were taken during the swing phase of the gait cycle, where the participant's right foot was in the air. Thus, the magnitude of joint reaction force for this part of the trials is very low. The difference between the marker-based and markerless motion capture curves is evaluated using RMSEs. Looking at those values, the motion capture systems still seem in best agreement for the knee joint reaction force where RMSEs vary between 0.340 xBW and 0.442 xBW. The knee and ankle RMSEs seem to be increasing with increasing load. RMSE values for the ankle joint reaction forces go from 0.337 xBW in C1 up to 0.529 xBW in C4. As for the hip reaction force, RMSE values vary between 0.462 xBW and 0.604 xBW.

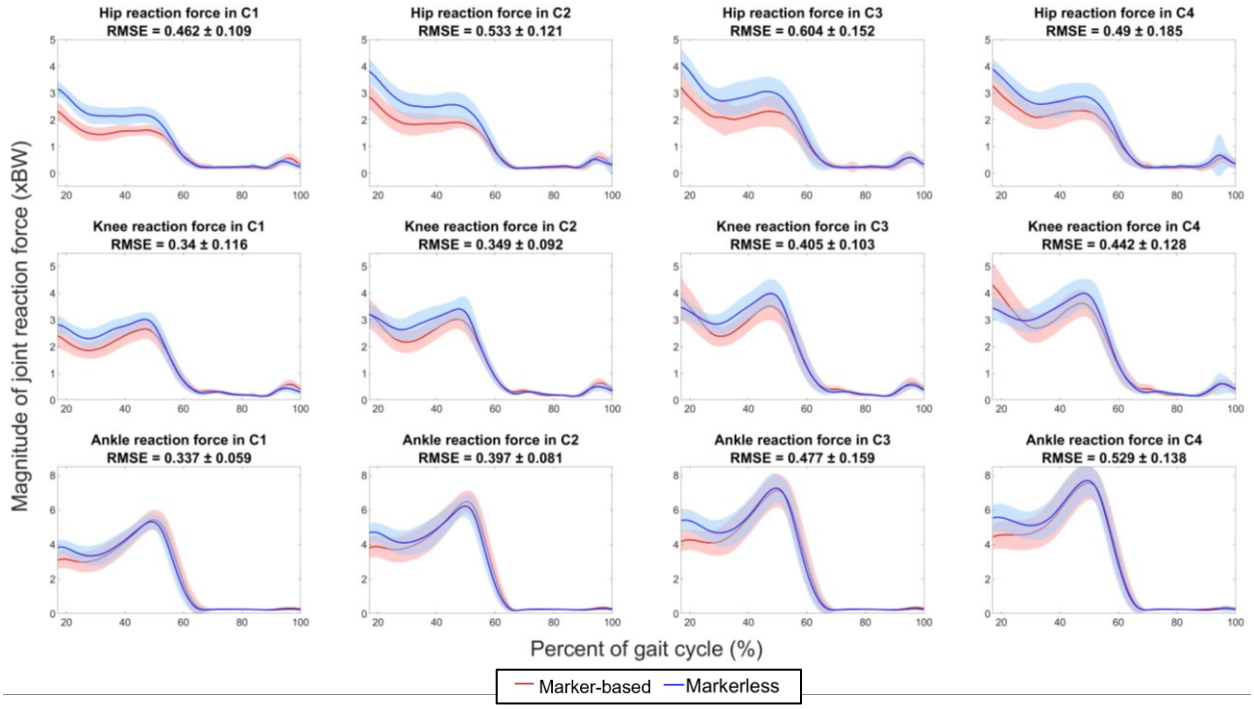

Figure 14: Plots of lower limb joint reaction forces through gait under all loading conditions for walking trials. RMSEs computed as the difference between both curves through all timeframes.

A similar plot was created for the running trials. All 12 subplots of lower limbs' joint reaction forces through gait under all loading conditions are illustrated in Figure 15. Like the results for walking trials, knee and ankle joint reaction forces are increasing with weight. While values of knee joint reaction forces go from 0.493 xBW to 0.993 xBW, those for ankle joint reaction forces range between 0.411 xBW and 0.703 xBW. These values of ankle and knee reaction force RMSE are larger than the ones found for walking trials. RMSEs for hip reaction forces vary between 0.422 xBW and 0.618 xBW.

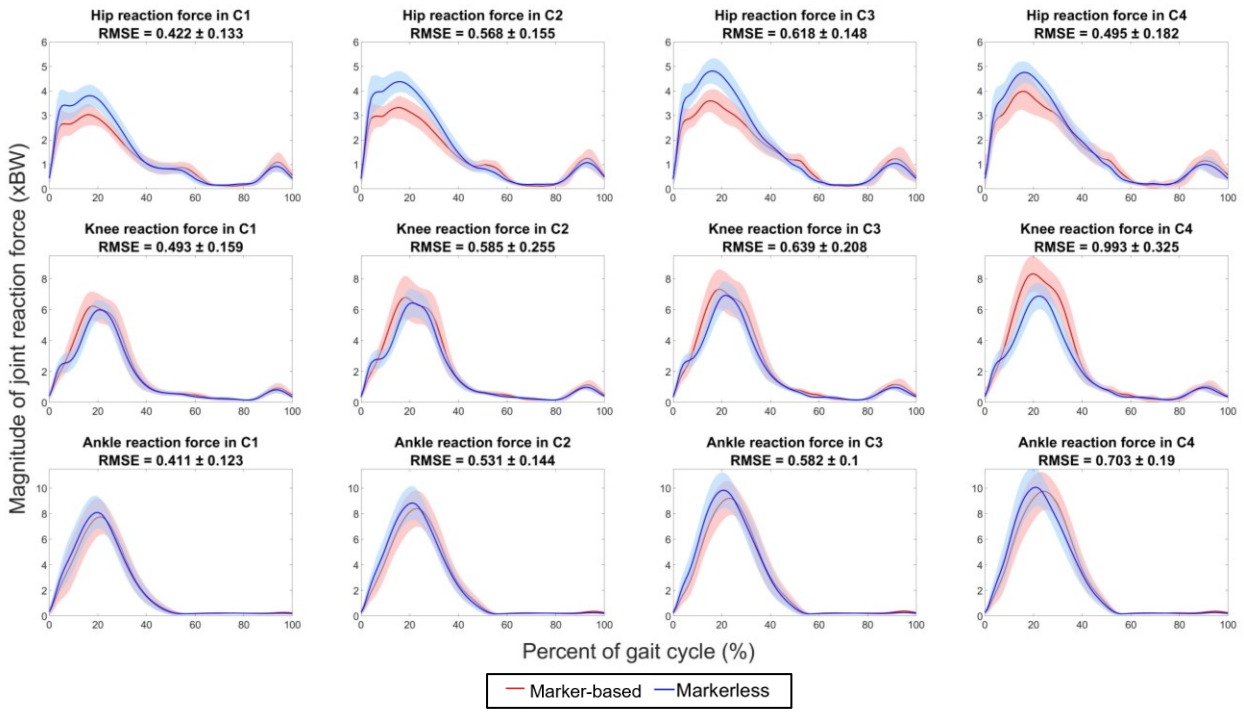

Figure 15: Plots of lower limb joint reaction forces through gait under all loading conditions for running trials. RMSEs computed as the difference between both curves through all timeframes.

As joint reaction forces can vary with traveling speed, walking and running speeds for all trials are represented in Figure 16 and Figure 17 below. In these figures, "Mean ± Standard Deviation" are displayed at the bottom of the corresponding boxplot. These boxplots indicate that walking speeds were mostly lower than running speeds, as dictated to the participants by the metronome. Speed was computed using the FPVLL marker, on the front pelvis cluster, when estimated from the marker-based data. Using the displacement of the pelvis centre of gravity estimated from the markerless data, speed could also be computed. The following figures suggest that both motion capture systems estimated similar walking and running speeds on dynamic trials. However, they also suggest that participants were not all walking and running at the same speeds during the trials. For walking trials, even though whiskers indicate that walking speeds sometimes varied by as much as 0.55 m/s, the average walking speeds do not differ considerably between loading conditions. In fact, they were all estimated to be around 1.07 m/s by both motion capture systems. This is not the case for running trials where running speeds decreased from an average of 1.89 m/s in C1 down to 1.73 m/s in C4 as measured from the markerless motion capture data. This would indicate that participants have run slower under increasing loads. Again, whiskers indicate that running speeds varied by as much as 1.25 m/s for the same loading condition.

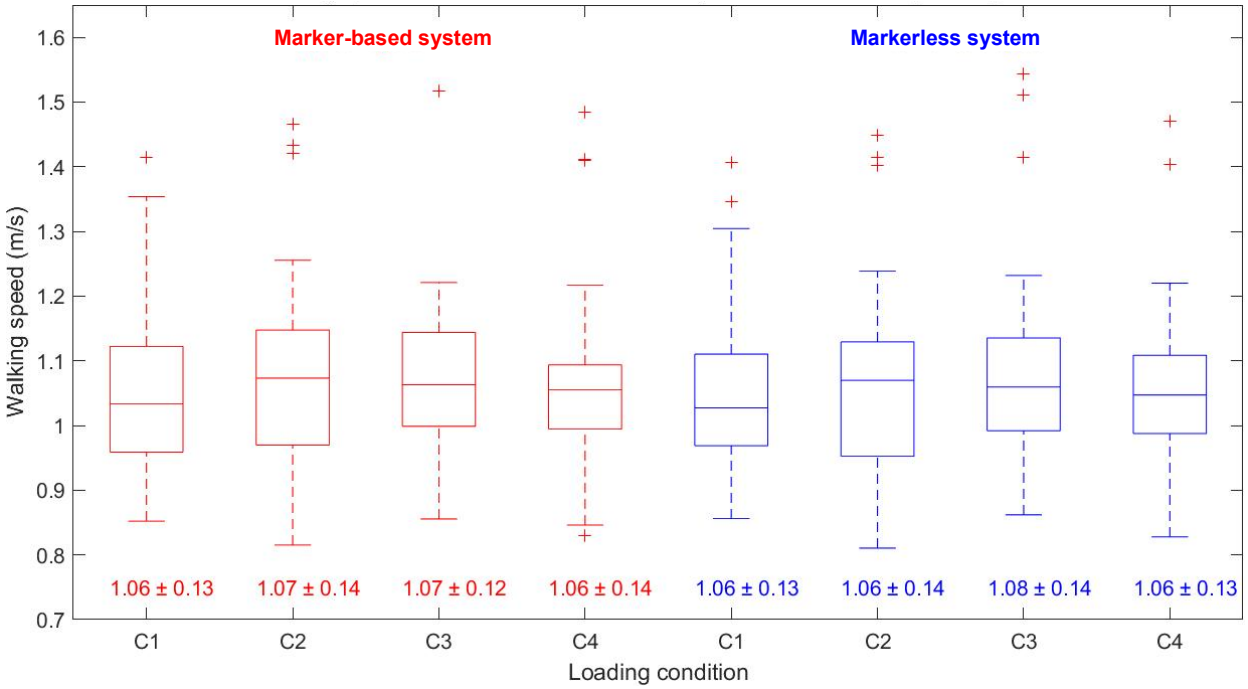

Figure 16: Walking speed of all participants under all loading conditions as estimated from marker-based and markerless motion capture data

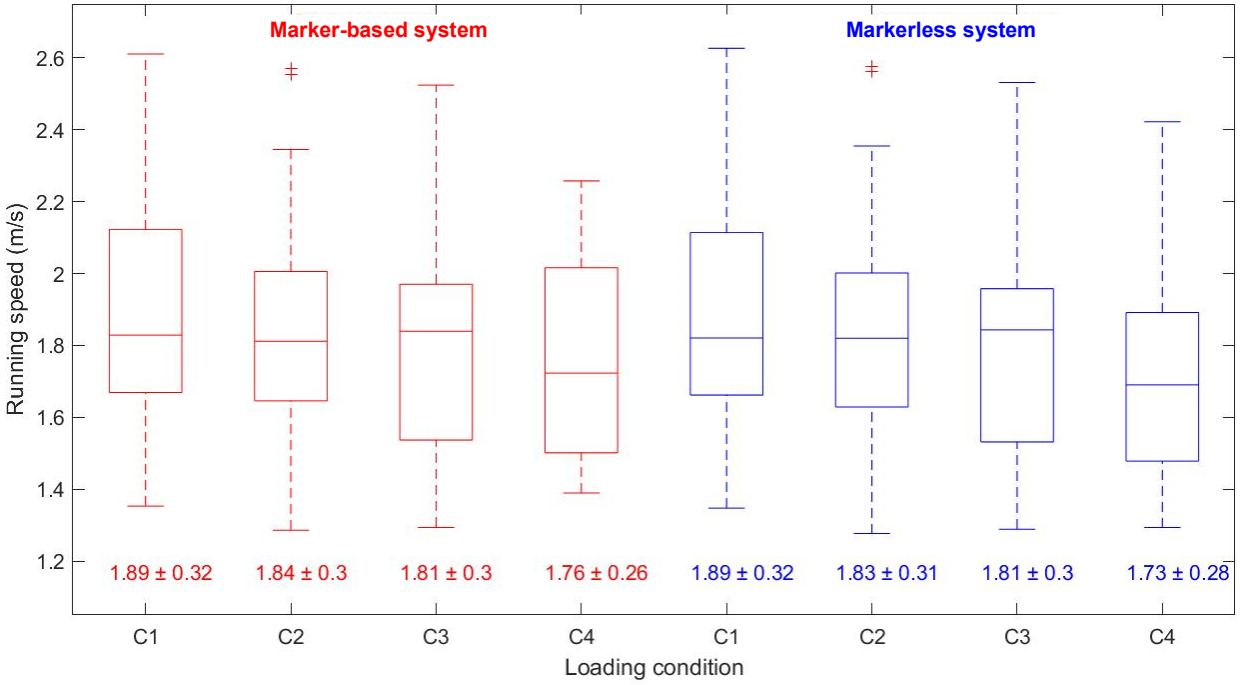

Figure 17: Running speed of all participants under all loading conditions as estimated from marker-based and markerless motion capture data

Pearson's correlation coefficient was computed between joint reaction forces from the marker-based and markerless motion capture systems to test their correlation. Again, kurtosis was estimated on the differences in joint loading to verify the normality assumption. Average kurtosis results of 2.4, 3.9, and 3.4 were found at the hip, knee, and ankle, respectively for all trials. From these values, it was supposed that the differences could be assumed as normally distributed. Table 7 presents the resulting coefficients for the ankle, knee, and hip joint angles of marker-based and markerless data through all loading conditions for walking and running trials. Values displayed in the table represent averages across all trials of the same movement and loading condition. Again, all of them indicate a very strong correlation between the curves, i.e., values above 0.90.

Table 7: Pearson's correlation coefficient for the ankle, knee, and hip joint reaction forces of marker-based and markerless data through all loading conditions for walking and running trials

			Joint		
			Hip	Knee	Ankle
Walking trials	Loading condition	C1	0.980	0.981	0.988
		C2	0.980	0.982	0.988
		C3	0.978	0.978	0.987
		C4	0.970	0.969	0.990
Running trials		C1	0.980	0.982	0.993
		C2	0.980	0.979	0.989
		C3	0.972	0.979	0.988
		C4	0.974	0.980	0.984

Finally, as Pearson's correlation coefficient indicates a correlation between the joint reaction forces results between the two motion capture systems, the JRA results were also tested for agreement using the Bland-Altman LOA. Table 8 presents the results of the mean difference with corresponding LOA for the ankle, knee, and hip joint angles of marker-based and markerless data through all loading conditions for walking and running trials. The ankle joint reaction forces displayed the lowest mean difference with values ranging between 0.03 xBW and 0.15 xBW for walking trials and between 0.01 xBW and 0.14 xBW for running trials. Mean differences were the largest for hip joint reaction forces with values ranging between 0.28 xBW and 0.36 xBW for walking trials and between 0.16 xBW and 0.27 xBW for running trials.

Table 8: Bland-Altman limits of agreement for the ankle, knee, and hip joint reaction forces of marker-based and markerless data through all loading conditions for walking and running trials

			Joint		
			Hip (xBW)	Knee (xBW)	Ankle (xBW)
Walking trials	Loading condition	C1	0.29 ± 0.71	0.16 ± 0.57	0.04 ± 0.62
		C2	0.34 ± 0.80	0.15 ± 0.60	0.03 ± 0.74
		C3	0.36 ± 0.89	0.14 ± 0.70	0.14 ± 0.88
		C4	0.28 ± 0.75	0.07 ± 0.81	0.15 ± 0.91
Running trials		C1	0.18 ± 0.74	-0.16 ± 0.89	0.08 ± 0.74
		C2	0.27 ± 0.97	-0.20 ± 1.05	0.08 ± 0.99
		C3	0.27 ± 1.07	-0.25 ± 1.14	0.14 ± 1.10
		C4	0.16 ± 0.88	-0.49 ± 1.69	0.01 ± 1.32

4.2. DISCUSSION

This research project is composed of three distinct objectives related to comparisons between the marker-based and markerless motion capture systems. The first objective is to compare their estimations of kinematics at the ankle, knee, and hip. To do so, static trials of the participants performing a bikerpose were first compared between the systems. This resulted in a nearly constant ankle angle bias between the standard Visual3D model used by the Theia3D software and the Rajagopal OpenSim musculoskeletal model, while knee and hip angle biases seemed to be increasing with load. This is especially obvious for the hip flexion coordinate where marker-based results suggest an increasing hip flexion with increasing load, while markerless results suggest an almost constant value of 0° of hip flexion. This increasing hip flexion measured by the marker-based system created an increasing gap between the two systems' measurements, resulting in angle biases increasing with load. This contradicts the expectation that angle biases would be constant across loading conditions. It also hints at the possible difficulty of the marker-based system to track participants wearing bulky equipment.

Then, also as part of the first objective, dynamic walking and running trials were compared. When looking at IK results, the lowest RMSE values are found at the knee coordinate in loading condition C1 for both walking and running trials with values of 3.6° in both cases. Obtained kinematic RMSEs are higher than the 3.4, 3.9, and 3.6° at the hip, knee, and ankle reported by Kanko and colleagues [11]. RMSE values for knee and hip flexion are increasing with additional

load. Such an increase in RMSE through loading conditions might suggest that one or both motion capture systems might have more difficulty to track participants with additional equipment. However, ankle flexion RMSEs decrease with increasing load for both walking and running trials. Still, curves of kinematic results for the ankle, knee, and hip displayed strong or very strong correlations between the two systems according to Pearson's correlation coefficient.

The second objective was to compare the gastrocnemius medialis and lateralis' activation patterns as estimated from the marker-based and markerless motion capture systems, as well as from EMG sensors. Results of muscle activation from both motion capture systems and EMG sensors peaked around the same time for both walking and running trials. Results from both motion capture systems were compared using RMSEs which increased with additional load on the participants. For walking trials, maximal RMSE values of 12.4% and 11.7% are found in loading condition C4 for the gastrocnemius lateralis and medialis, respectively. During running trials, the gastrocnemius lateralis had a maximal RMSE of 13.4%, while the gastrocnemius medialis had a maximal RMSE of 15.7%, both in loading condition C4. These RMSE values are considered low when compared to the expected 50% differences in peak joint moment reported in the literature [16].

The third objective was to compare the ankle, knee, and hip joint loading between the marker-based and markerless systems. The knee and ankle joints showed the best agreement between the two systems for walking trials with the lowest RMSE values and lowest mean difference according to the Bland-Altman analysis. Both knee and ankle joint reaction force RMSEs increased with an increased load for both walking and running trials. Hip joint reaction forces RMSEs were the largest for walking trials with values varying between 0.462 xBW and 0.604 xBW. Larger RMSE values are found for running trials than for walking trials for the knee and ankle joints. Still, all joint coordinates showed very strong correlation between the two systems along both walking and running trials, according to Pearson's correlation coefficient.

4.2.1. Kinematics comparison – Static trials

When evaluating the Rajagopal OpenSim model and the Theia3D Visual3D kinematic model, there are differences between the two. The Rajagopal model has 20 degrees of freedom at the lower body – six at the pelvis and seven per leg. The pelvis degrees of freedom include pelvis tilt, list, and rotation as well as three translations (in *x, y,* and *z*). At the hip, hip flexion, adduction, and rotation are considered. The knee can only flex and the foot contains degrees of freedom for ankle flexion, subtalar inversion, and metatarsophalangeal flexion, even though subtalar inversion and metatarsophalangeal flexion are most often locked into a fixed and neutral position (0°). It is also the case for wrist flexion and ulnar deviation as the experimental data used to test the model and generate sample simulations was not collected with a fine enough motion capture system [58]. The Rajagopal open-source model has been validated and is well-detailed in the 2016 article by Rajagopal and colleagues. For example, from that article, Rajagopal describes the orientation of the pelvis as zero when it is oriented so that the right and left anterior-superior iliac spines and the pelvic tubercles are aligned in the frontal plane [58]. On the other side, the Theia3D standard model is divided into the upper and lower body kinematic chains, with an extra six degrees of freedom at the head. When looking at the lower body kinematic chain only, the pelvis serves as the root segment and has the same six degrees of freedom as the Rajagopal model. However, it is unclear what the Theia3D standard model describes as a null orientation for the pelvis [77]. This unclarity regarding the alignment of the pelvis coordinate system is also a problem for other joint coordinate systems of the model. Without this key information, the use of markerless data from the Theia3D software with another musculoskeletal model, the OpenSim Rajagopal model in this case, becomes quite challenging. Without knowing how markerless data translates to the Rajagopal model, it is difficult to say whether joint angle differences between the marker-based and markerless results come from coordinate system misalignment or from motion capture errors in the tracking of the participant. Another important difference between the models is that the Theia3D standard model contains more degrees of freedom than the Rajagopal one. For example, the Theia3D standard model considers knee adduction and internal rotation as well as ankle adduction which are not modelled by Rajagopal [77].

Still, to try and understand the error caused by coordinate system misalignment, angle biases between the two systems were computed as presented in Table 2. These values were found from the static poses measured synchronously by the two motion capture systems as the difference between marker-based and markerless joint angles. As previously pointed out, participants had to perform static and dynamic trials while loads of up to approximately 41 kg were applied mainly on their torso. From the static trials, it appears that only the marker-based motion capture system noted an increase in hip flexion with increasing load, while the markerless motion capture system reported an almost constant hip flexion angle. Since participants were instructed to stand still in the bikerpose position, hip, knee, and ankle coordinates are expected to be relatively similar through loading conditions. Still, a slight leaning forward of the trunk can be expected as load is increased on the participants' back. However, increases of more than 10° between C1 and C4 as estimated from marker-based motion capture might seem exaggerated. In fact, research suggests that increases in body borne load does not have a significant impact on hip flexion but does increase trunk flexion [78]. Forward lean can be expected in heavier conditions to adjust the center of mass (CoM) location as load is applied on the participants' back [4]. There is a possibility that the markerless system has more difficulty tracking the pelvis segment than the lower limbs because pelvis landmarks might be more complex for the algorithm to identify, resulting in the system not tracking slight changes in pelvis orientation. However, because marker-based hip flexion varies so much in C3 and C4 for static poses, there is also a possibility that the marker-based motion capture system exaggerates hip flexion kinematics because it has difficulty tracking the pelvis segment which is obstructed by equipment. By looking at modelling results compared with video data of the static trials, the possibility of the marker-based system lacking accuracy in heavier loading conditions is more likely. This resulted in an increasing angle bias through loading conditions for the hip and the knee coordinates. To avoid these increasing biases causing an inadequate adjustment of the offset between the models' coordinate systems or forcing markerless hip flexion results to considerably increase through loading conditions during dynamic trials, it was decided not to use angle biases to adjust markerless kinematics results. Therefore, in the following steps of the musculoskeletal analysis and the corresponding results, markerless kinematics correspond to raw or unadjusted markerless kinematics resulting from Theia3D's estimations.

In future research concerning angle biases, it would be logical to have constant values of biases no matter the loading condition or movement performed by the participant since the same models

will be compared, regardless. For example, no matter the experimental protocol, if markerless data from the Theia3D system needs to be adapted from their standard model to the OpenSim Rajagopal one, the hip, knee, and ankle would always need the same value of angle bias to translate between the two models.

4.2.2. Kinematics comparison – Dynamic trials

As previously stated, the markerless data were not "adjusted" by adding angle bias to the markerless kinematics obtained from IK. It is to be noted that considering this angle bias when plotting IK results would not have altered the shape of the lower limbs' markerless kinematics curve, but rather would have translated it vertically as the same angle bias would have been applied throughout the same trial. From Figure 10 and Figure 11, joint angle results seem to compare well for the knee flexion angle, as almost no gap is observed between the two curves. This is also expressed in the RMSE values quantifying the difference between results from the two systems. Similarly for hip flexion, kinematic curves also compare well, especially in the lightest loading conditions. Even though RMSEs are higher for the ankle flexion angle, there doesn't seem to be such a large offset between the maximum ankle flexion angle representing toe-off at around 65% of the gait cycle.

In addition to the RMSE values indicated in Figure 10 and Figure 11 which account for the difference between the joint angle values of the marker-based and markerless data, the same curves were also tested for correlation using Pearson's correlation coefficient. Without confirming the agreement between the motion capture systems, a correlation between the two curves would indicate that there is a relationship between the two. In other words, correlation captures the degree of interrelation between the two sets of results, or how well their curves' shape matches each other. Therefore, an offset in kinematic curves would not impact correlation results. In fact, when looking at Table 3, all correlation coefficients suggest a very strong correlation for all loading conditions in both walking and running trials, except for ankle flexion in loading condition C1 where correlation is strong. A more accurate value of angle bias could potentially help the kinematic curves to align better and reduce values of RMSE between the motion capture systems.

When looking at the Bland-Altman limits of agreement (LOA) results, the same trend that was observed for the RMSEs can be observed for values of mean difference reported in Table 4 through

loading conditions and movements. In fact, Bland-Altman mean differences are increasing through loading condition for the knee coordinate and decreasing for the ankle coordinate. Hip flexion mean differences start positive in loading condition C1 and become negative for loading conditions C3 and C4 most probably because of the marker-based system having trouble to properly track participants in the heavier loading conditions. There is still an offset between the kinematic results of both motion capture systems which could be addressed with proper angle bias investigation. Still, Bland-Altman LOA do not appear to be dependent on whether the participant is running or walking. Both hip and knee flexion LOA range between 4.51° and 8.06°, while ankle flexion displays farther agreement with LOA between 6.61° and 9.55°.

Previous literature on the Theia3D markerless motion capture system has already evaluated root-mean-square differences (RMSD) between the marker-based and markerless motion capture systems. However, data from both systems were analyzed using similar Visual3D models. Even though this does not remove the possibility of offsets between the two models, which depend on the landmarks used to create them, Kanko and colleagues were aware of how the models were constructed in Visual3D. It was therefore possible for them to obtain better alignment between the coordinate systems of the models and compute accurate values of angle bias. This resulted in the hip, knee, and ankle flexion RMSD of 3.4, 3.9, and 3.6°, respectively [11]. The obtained values of RMSE for the knee flexion angle in loading condition 1 displayed in Figure 10 for walking trials and Figure 11 for running trials are very close to the ones found by Kanko and colleagues with values of 3.6° for both. Results suggest that with the appropriate angle bias value, the RMSE of the hip flexion angle could be reduced to potentially be closer to the value obtained by Kanko and colleagues. The same might be true for the ankle flexion angle, but this is still unclear as the curves seem to reach a similar maximum at toe-off while suffering from a considerable offset for the rest of the trials. Kanko and colleagues also noted that the ankle position estimated by the markerless system seemed to better match the marker-based one at heel strike (0% of the gait cycle) and toe-off (60% of the gait cycle) [11]. This might be related to other ankle modelling differences. In fact, Visual3D, in which the Theia3D standard model was constructed, offers three methods to build the foot and corresponding ankle joint. The “Heel to Toe” method defines the proximal and distal ends of the foot from the heel and toe landmarks. The second method is the “Normalize to Proximal Segment” method which normalizes the ankle angle to the posture of the participant in the standing trial. Finally, the “Projected landmarks” method assumes that participants have their feet parallel

to the laboratory floor in the static trial. Depending on the application of the Visual3D model, one of these methods might be used depending on clinical relevancy. However, the choice of foot-building method will impact the corresponding ankle angles as some bias is present between the methods [79]. Here, it is important to note that the Theia3D team has not disclosed information on how their Visual3D standard model was built with regard to the ankle joint.

Regarding the results of ankle flexion kinematics, it must be noted that the participants in this research project wore large ankle-high military boots. Markers of the medial and lateral malleolus, heel, and first and fifth metatarsals had to be placed on top of these boots. It was assumed during the musculoskeletal analysis that all participants' boots were fitted properly so that the ankle movement of the participant was entirely translated to the boots. On the other hand, it is important to note that participants in the comparison research conducted by Kanko and colleagues wore tight and coloured minimal apparel and were allowed to put on their own running shoes for the data collection [11]. This undoubtedly resulted in better markerless and marker-based tracking of the participant's movements, especially for the ankle. Tang and colleagues also suggested that foot tracking errors might be related to the Theia3D system potentially estimating the segment's centre of mass from footwear contour, while the marker-based system uses markers placed on the first and fifth metatarsal heads. These differences in joint centres might lead to errors further in the ID analysis when computing moment arms. The same goes for differences in segment centre of mass positions which might cause errors later in the estimation of moments of inertia. Errors in moment arms and moments of inertia can considerably affect the forces and moments obtained from the ID results [80].

Other than the values obtained by Kanko and colleagues, the results of RMSE can also be compared to values of minimal detectable change (MDC) of kinematic data for the lower limbs. When assessing the test-retest reliability of kinematic data on healthy individuals, it was found that the hip, knee, and ankle peak flexion angles had an MDC of 8.6, 3.8, and 3.9°, respectively [81]. This places most hip flexion RMSEs below the reported MDC. While knee flexion RMSEs are also below MDC in loading condition C1, this is definitively not the case for ankle flexion RMSEs.

It is also interesting to note that from a quick look at some of the visual data produced by the Theia3D software where one can see an overlay of the participant's skeletal system on top of video data from the trials, the system seemed to track the participant with ease, despite bulky equipment. At first, it was thought that additional bulky equipment might result in inaccurate tracking of the participant using Theia3D, mostly because it is improbable that the algorithm was trained with data of participants wearing bulky military equipment. However, except for a few exceptions out of the 768 dynamic trials run in Theia3D, this was not the case. On the other hand, the marker-based motion capture had a hard time tracking the entire marker set when additional equipment was loaded onto the participant. Markers' lines of sight were lost in the bulkiest loading conditions. It was not rare to lose many pelvis markers at once from line-of-sight obstruction by the large rucksack and the placement of the rifle in front of some pelvis markers. Even though marker clusters at the pelvis were intentionally put lower and cameras were detached from their usual position on the ceiling to be placed lower on tripods, the marker-based motion capture was a real challenge to operate with so much equipment on the participants. Therefore, the difference between the motion capture systems in the heavier loading conditions might be due to inaccuracies in the marker-based motion capture tracking of the participant rather than to the capability of the markerless motion capture system to track the participant's motion.

Following research from Kanko and colleagues, recent research by Tang and colleagues has detailed the difference in lower limb joint centres and centres of mass between the Theia markerless and a marker-based motion capture system. They found the hip joint centres to be about 2 cm posterior in the markerless system when compared to their marker-based results [80]. As kinetic analyses are sensitive to changes in the inertial properties of the musculoskeletal segments, such small differences can propagate in the next step of the musculoskeletal analysis. These differences in the hip joint centre can thus potentially impact kinetic results at all joints.

Using a combination of joint accelerations found from the IK analysis and the GRFs measured by force plates, dynamic inconsistencies were estimated from an RRA. Through RRA, residual forces in the anteroposterior (F_x), vertical (F_y), and mediolateral (F_z) directions were computed as presented in Table 5. Recommendations suggest that researchers should make sure residual forces in their model are low enough so that they do not contribute significantly to the model's accelerations. As a guideline, it is suggested that force residuals should be less than 5% of the

ground reaction forces [82]. Comparing values from Table 5 and Table 6, vertical residual forces are below 5% of vertical GRFs for all loading conditions in both walking and running trials. As vertical GRFs are the largest, having large residuals in that direction would have compromised the model, but results show that it is not the case. For the anteroposterior direction, the direction in which the participant was traveling, residual forces go a little beyond the 5% limit, especially for heavier loading conditions. In fact, for the markerless model, the anteroposterior residual forces increased with loading conditions up to 18.4% for running in the C4 loading condition. This might be related to the extra weight and stiffness coming from the larger rucksack. The participant-backpack interface was simply modelled as additional weight at the torso, implying that the backpack was not allowed any movement from the participant's torso. However, this was most probably not the case, and both the backpack and rucksack swung a little from the participant's torso, especially when running, leading to additional residual forces. Finally, in the mediolateral direction, the 5% limit was also exceeded, and residual forces also increased with additional weight on the participant, probably for similar reasons. Residual forces in this direction were worse for markerless than marker-based modelling. As the marker-based model reached a maximum for walking in loading condition C3 with a value of 41.7%, markerless residual forces represented about 53.9% of GRFs for running in loading condition C4. As stated before, this considerable dynamic inconsistency in markerless modelling might derive from errors when adapting data from the Theia3D software to fit the Rajagopal OpenSim model. Differences in joint centres and centres of mass positions and errors in IK results might cause an increase in dynamic inconsistencies in the RRA.

4.2.3. Muscle activation comparison

Once the RRA was performed, a new "adjusted" model was used to run the following SO step and estimate muscle forces. Figure 12 and Figure 13 compare the results of this analysis as well as EMG measurement of muscle activation for the gastrocnemius lateralis and medialis. Here, as the maximal muscle contraction of these muscles was not measured during data collection, EMG muscle activation is normalized to the maximal activation of each trial. The same thing was done for marker-based and markerless estimations of muscle activation which are both normalized to their measurement of maximal activation during the trial. This way, it is not possible to compare the amplitude of muscle forces between the three curves. However, it can be easily remarked that

all three activate and reach their peak at around the same time, which is more meaningful. Other muscles measured by EMG include the tibialis anterior, the biceps femoris, the semitendinosus, the vastus lateralis, the vastus medialis, and the rectus femoris and their results are presented in Appendix J.

4.2.4. Joint loading comparison

The last step of the musculoskeletal analysis was to perform JRA to estimate the magnitude of JRF at all joints of the lower limbs. These results, presented in Figure 14 and Figure 15, show curves following roughly the same trajectory. Results of JRF estimated from the markerless data seem to almost always be higher than the ones estimated from the marker-based data. For the knee and ankle joints, RMSEs are increasing with loading conditions, meaning that additional equipment weight and bulkiness impact the estimation of JRFs. For the ankle joint however, RMSEs were decreasing with load when looking at kinematic comparisons between the motion capture systems. This could be linked to the increase in markerless residual force in heavier conditions.

Regarding the amplitude of these JRFs, one might expect an increase in JRFs with additional weight. From the average peak values of GRFs presented in Table 6, results of vertical GRFs indeed show an increase when a heavier loading condition was applied to the participant. However, research on whether larger vertical GRFs are related to larger knee JRFs in participants walking with body-borne loads has concluded that larger vertical GRFs are not strongly related to increases in tibial compression. In fact, it seems that participants tend to decrease their maximal tibial compression force and impulse to slow the transmission of large GRFs to their musculoskeletal system when walking [83]. The fact that increases in GRFs are not a direct indicator of an increase in tibial load has also been noted for running trials [84]. This could explain why plots of JRFs through loading conditions do not display a clear increase with additional weight.

Another important consideration when looking at the results of JRFs is the speed at which the participants were walking and running. Walking and running step frequency was controlled using an auditive cue to the participants via a metronome. The metronome was set at 90 bpm for walking trials and 140 bpm for running trials so that the participants would time their heel strike with the beeping sound they heard. However, even though this meant all participants had a similar stride

frequency, they still could increase their stride length to accelerate the trial and decrease it to facilitate load bearing. Because $speed = stride\ length * stride\ frequency$, this resulted in variations of walking and running speeds over all trials and participants, as presented in Figure 16 and Figure 17 [48]. As average walking speeds were fairly constant through loading conditions, the difference between minimal and maximal speeds could vary by as much as 0.55 m/s in the same loading conditions. A decrease in average running speed was also noticed through loading condition. In addition, variations as large as 1.25 m/s were identified for trials of the same loading condition. Research on the relationship between walking speeds and JRFs has concluded that faster walking speeds are linked with increased anteroposterior and vertical JRFs [85]. This has also been researched in a military population, where musculoskeletal injuries (MSI) are more common. Increases in walking speed for constant external loads have been linked with an increase in the magnitude of knee joint contact forces [18]. Thus, because walking and running speeds have not been normalized for all participants and loading conditions, an increase in JRFs through loading conditions is not evident.

In the last few years, more research on how measurement errors and modelling assumptions influence joint dynamics has emerged. Uncertainty in the measurement and modelling of joint kinematics has been highlighted as the principal source of error in ID results [86]. In fact, when using a marker-based motion capture system, it has been demonstrated that 2 cm of marker registration uncertainty can lead to variability in ankle flexion angle of about 15.9° and variability in ankle flexion moment of about 26.6 N·m. The same idea applies to other joints – Small marker and scaling uncertainty can create considerable variability in joint angle, moment, and power [16]. In the case of the current research project, the challenge of adapting markerless motion capture data to the OpenSim Rajagopal model has previously been detailed. Marker registration errors might have emerged when adapting the Rajagopal model's marker set to match the joint centers exported from Theia3D. This translated to uncertainty in the scaling step of the analysis as well as when performing IK to estimate lower limb joint angles. Undoubtedly, this led to further uncertainty in the estimation of JRFs and corresponding RMSEs.

Finally, the JRFs were further tested for correlation using, again, Pearson's correlation coefficient. The results, detailed in Table 7, were all above 0.9, indicating a very strong correlation between the markerless and marker-based motion capture results of JRFs. Similar to the results of

joint kinematics, the gap between the two curves might be reduced by determining and applying an accurate value of angle bias between the two models. Concerning the Bland-Altman LOA presented in Table 8, the interval of agreement is wider with increasing weight for the knee and ankle joints. This is due to a larger standard deviation of the mean difference between the two methods for heavier loading conditions. Again, as discussed previously, it is hard to tell whether this difference increases because of the difficulty of the markerless system to track participants with bulkier equipment or because of the marker-based motion capture system losing line of sight with several markers when putting on more equipment.

4.3. LIMITATIONS

The current research project came with its share of limitations. During the data collection part of this research project, typical sources or errors linked with the use of the marker-based motion capture system might have interfered with the data. The first one is errors in marker placement between subjects and sessions. In fact, for all participants, the same researcher applied each marker and marker cluster to the participant. However, there might have been some variability in marker placement between the different sessions of data collection. It has been well-researched that small differences in marker registration during data collection can impact the joint kinematics results [16], [80]. It must also be noted that the researcher who applied all the markers during data collection did not have much experience in performing this step. Even though, training sessions were completed, this might be linked to even greater variability in marker placement.

Another source of error linked with the collection of data from the marker-based motion capture system is the soft tissue artifact. Here, it must be noted that all participants wore minimal clothing, i.e., their own sports shorts and the Xsens suit upper body shirt. The use of marker clusters and the placement of individual markers on bony anatomical landmarks might have also helped in mitigating the impact of soft tissue artifacts on the marker-based data. However, as soft tissue artifact is often regarded as the most important limitation of the marker-based motion capture system [48], the movement of muscle, skin, and body fat might still have impacted the marker-based data. Furthermore, the use of a tactical vest, a fragmentation vest, a backpack, and a rucksack made the use of markers on the participant's torso very challenging. The left and right acromion markers had to be repositioned on top of equipment in heavier loading conditions. This new marker

position was impacted by the movement of equipment during dynamic trials. During motions with larger amplitudes such as running, joint motion becomes greater. Greater joint motion has been associated with larger errors in joint angle from soft tissue artifacts [80]. Also, as discussed previously, for heavier loading conditions, it was not rare for the optical cameras to lose line of sight with some of the markers on the participant. This created a gap in the marker-based data which had to be filled using different interpolation methods in the Nexus software. These gap-filling events lead to uncertainty in the marker-based data used for musculoskeletal analysis.

Because most military equipment is worn at the upper body, the lack of visibility of that part of the participant is inevitable. This comes as a limitation for optical motion capture systems relying on cameras to track a participant in a control volume, i.e., both marker-based and markerless technologies. Still, the risk of musculoskeletal injuries is higher at the lower limbs for military personnel. Thus, because the research project focused on lower limb movement, the impact of upper body markers losing line of sight with the cameras was not critical.

The challenge of defining an appropriate angle bias has previously been detailed. Further research will be needed to evaluate more accurate values of angle bias between the Theia3D standard model and the Rajagopal model for all joints of the Rajagopal model. Once these values are determined and properly researched, the collection of markerless data and subsequent kinematic and kinetic analysis in OpenSim will be possible without having to rely on simultaneous marker-based tracking. This will enable the full potential of markerless motion capture and allow for rapid data collection outside of the laboratory setting.

When adapting the marker set of the Rajagopal model to match markerless joint centres coming from the Theia3D model, assumptions were made regarding their position. In fact, little has been disclosed on how the Theia3D model is constructed in Visual3D. Therefore, it was challenging to match the joint centres and segment centres of mass exported from Visual3D to a specific location on the Rajagopal model. Visual interpretation of the markerless data on the Theia3D model in Visual3D was used to try and identify the most accurate location of these landmarks. However, inaccuracies in marker registration might have resulted in further errors in the scaling of the markerless model.

Also concerning the scaling process of the musculoskeletal analysis, it is important to note that 128 static trials (16 participants x 4 loading conditions x 2 motion capture systems) underwent the scaling step. As this step was run in Matlab using OpenSim's Matlab Scripting Environment, only a limited number of the resulting scaled models were opened in OpenSim's visualizer for a look at the results. From a few different sets of scaling weights, the one which minimized the overall root-mean-square marker error was used to scale the models. However, all possibilities of sets of scaling weights were not tested, and a better one might exist. This is also the case for the IK step of the musculoskeletal analysis where a total of 768 dynamic trials had to be individually processed to estimate joint kinematics. Because it would have taken an enormous amount of time to optimize each of the 768 trials individually and subsequently visualize them in OpenSim, this entire step was also run in Matlab. Again, the same generic scaling weights were used to minimize the difference in kinematics between the two motion capture systems. It should be noted that during the scaling and IK steps of the musculoskeletal analysis, different marker weights can lead to different scaling and kinematics results.

As mentioned previously, when adapting markerless data from the Theia3D model to fit the Rajagopal model, some degrees of freedom were lost in the process. This is the case for the knee adduction and internal rotation as well as the ankle adduction degrees of freedom which are not modelled by Rajagopal. Results of lower-limb kinematics found in OpenSim are therefore limited to the degrees of freedom of the Rajagopal model and do not allow to use the entire set of markerless data.

Finally, another limitation of this research project is the fact that even though marker-based motion capture currently acts as the gold standard for motion capture in the biomechanics community, it has received many critiques as detailed in Section 2.3. These many limitations of the marker-based system mean that there is room for amelioration. In fact, even though the markerless system evaluated in the context of this research project is quite new compared to its marker-based counterpart, it does not mean that it cannot perform better. When it comes to comparing the two systems, both have their limitations, and it becomes complex to establish which one is the most accurate. The marker-based system has been well researched in optimal laboratory settings on participants in tight and dark clothing who do not carry objects or equipment. However, it is evident that the system will not perform as well on a subject with bulky equipment because of

the intrinsic use of markers. In this situation, the markerless motion capture system might in fact perform better than the marker-based one but judging of which system is the “correct” one in different situations becomes quite complex.

5. CONCLUSION

5.1. SUMMARY

With the constant evolution of technologies designed to enhance the modern soldier, there is a considerable increase in the body-borne load that military personnel must carry in the field. Even though this new protective, firepower, communications, and mobility equipment aims at increasing their safety when out on a mission, the additional load puts soldiers at risk of musculoskeletal injuries and a decrease in performance from loss of mobility. This research project was conducted to respond to the need to assess soldier's biomechanical stress under different loading conditions. To do so, a reliable motion capture technology which can track a participant's movement despite the presence of bulky and heavy equipment is necessary. Therefore, two motion capture systems were compared as part of this research project – a traditional marker-based motion capture system and the new Theia3D markerless motion capture system. The objectives were to compare the kinematics of the lower limb joints between the systems, to compare EMG gastrocnemius lateralis and medialis muscle activation with estimations from the marker-based and markerless modelling, and finally, to compare lower body joint reaction forces between the two motion capture systems.

To answer these three questions, a data collection was conducted with 16 participants, performing walking and running trials, under four loading conditions, for three consecutive repetitions, and simultaneously tracked by both the marker-based and markerless motion capture systems. During all trials, the participants stepped on ground force plates which collected GRF data. Eight EMG sensors were also applied on their right leg to measure the muscle activation from eight muscles during gait. The data collected was preprocessed so that marker data, force plate data, and kinematic data from the markerless system were all oriented in the same manner. Using this data, a musculoskeletal analysis was performed on data from the marker-based and markerless motion capture systems. This analysis was done in OpenSim and included the scaling of models, an IK process to estimate lower limb joint kinematics, an RRA to minimize the impact of residual forces on the models, a SO step to estimate muscle activity, and a JRA to estimate lower limb JRFs. Kinematics and kinetics data from both systems were compared using RMSEs, Pearson's correlation coefficient, and Bland-Altman LOA.

The first objective aimed at comparing the kinematics of the lower limbs' joints between the motion capture systems. To compare kinematics, the initial plan was to adjust markerless motion capture data first using the angle biases between the standard Visual3D model used by the Theia3D software and the OpenSim model. To compute these biases, the kinematic differences between the models in static pose were used. However, ambiguity around the obtained values through loading conditions lead to the decision of not adding the values of angle biases to the computed kinematics of the markerless data. Also, research in the literature highlighted that adding or subtracting angle biases at each timeframe of a dynamic trial is not the correct way to align coordinate systems. Other solutions exist to reduce the offset between coordinate system orientation, and in the future, more efforts should be put into determining and applying values of angle bias. Further research is needed on the Theia3D standard model of which little information has been disclosed. A better knowledge of angle bias between the models could potentially enable the full potential of the markerless system by allowing its use without the simultaneous tracking of marker-based motion capture. This could facilitate data collections outside of the laboratory and with different kinds of equipment.

The IK step of the musculoskeletal analysis allowed the estimations of joint kinematics for the two systems and the subsequent comparison via RMSEs. Results of RMSEs suggest that hip and knee flexion angles match very well between the two systems in loading condition C1, with RMSE values of 5.3° and 3.6° for walking trials, respectively. These values are below the marker-based MDC target of 8.6° for hip flexion and 3.8° for knee flexion [81] and close to Kanko and colleague's RMSD of 3.4° for hip flexion and 3.9° for knee flexion [11]. fAs hip flexion and knee flexion RMSE values are low in loading condition C1 where no equipment is applied on the participant, they increase with increasing equipment weight. This might be due to one or both motion capture systems having difficulty tracking participants wearing bulky equipment. Finally, ankle flexion RMSEs start at 10.9° for walking trials in loading condition C1 and decrease down to 6.7° for walking trials in loading condition C4, going opposite to the trend affecting both hip and knee flexion. Those values are above the reported MDC of 3.9° [81], probably due to the ambiguity around how Theia3D models evaluate ankle flexion. These values are also larger than the 3.6° found by Kanko and colleagues [11]. Even though results still suffer from bias from not correcting for coordinate system alignment, results of Pearson's correlation coefficient suggest strong and very strong correlations between their kinematics results.

The second objective was to compare EMG muscle activation of the gastrocnemius medialis and lateralis with the muscle activation estimated from both marker-based and markerless data. As the maximal contraction of these muscles was not measured as part of the data collection, it was not possible to compare EMG data with marker-based and markerless estimations of muscle force magnitude. However, muscle activation patterns were still compared with regards to their timing during the gait cycle. Results showed very good agreement in synchronization between data from EMG and estimations from the marker-based and markerless motion capture systems. This shows that markerless motion capture has the potential to be used for the estimation of muscle activation.

Finally, the last objective was to compare lower body JRFs between the two systems. Results show an overestimation of JRFs by the markerless system when compared to the marker-based one. As RMSEs increase through loading conditions for knee and ankle JRFs, both coordinate system alignment and the difficulty of marker-based motion capture to maintain line of sight with the marker set when more equipment is applied may be at cause. Because stride frequency was normalized, but not walking speed, results of JRFs do not display an evident increase from lighter to heavier loading conditions. Kinematics errors, especially related to not adjusting markerless kinematics with an appropriate angle bias, might have played a considerable role in increasing errors in the results found after the IK step. Thus, RRA, SO, and JRA results could potentially benefit from a better knowledge of angle bias between the systems, as discussed earlier. Despite differences in results highlighted by RMSE values, results of Pearson's correlation coefficient for JRFs found from the marker-based and markerless systems all suggest a very strong correlation.

In conclusion, this research project highlights the potential of the Theia3D markerless motion capture system when it comes to assessment of the biomechanics of soldiers. Notably, it has proven to be a time-saving method in the laboratory because of how it mitigates the work needed from the researcher. As opposed to the marker-based system, the markerless system does not require the application of individual markers and marker clusters on the participant which allows to save about 20 to 30 minutes per data collection session. Furthermore, it alleviates the need for subsequent labelling and gap filling of the data which, in the case of this research project where more than 700 trials were collected, took a few weeks of full-time work. It is also important to note that in the heavier loading conditions, the marker-based motion capture system had difficulty keeping track of some markers because of the presence of bulky equipment getting in the way of the camera-

marker line of sight. Not only did this make it difficult to measure acceptable data during data collection, but some trials also ended up needing to be excluded from the analysis because of the lack of markers at the pelvis.

5.2. FUTURE WORK

In the future, next steps include performing more research on angle bias and the differences that exist between the Theia3D standard model in Visual3D and the Rajagopal model in OpenSim. Better knowledge on values of biases between the system might potentially decrease offsets in the results found as part of this research project. This will enable further exploration of the agreement of markerless and marker-based motion capture. By knowing values of angle bias between the models, markerless motion capture could be used on its own, without the need for simultaneous tracking of marker-based motion capture. This means that the system could be brought into the field to assess the biomechanics of soldiers during training in their own environment and with different kinds of equipment. A possible avenue to refine the process of including angle bias to the data from the markerless system could lie in the way the pose matrices processed by the Theia3D software are treated. These matrices could be transformed to match a given OpenSim model so that offset between the models would be mitigated. Another way could be to modify an OpenSim-borne model to match these matrices data and get a similar result. In any way, it is certain that knowledge on the way the Theia3D software creates its model is essential to a better understanding and estimation of the angle biases.

The OpenSim model used for the musculoskeletal analysis could also be improved by considering changes in the inertia of the participants as equipment is added. When it comes to marker-based kinematic results, uncertainty arises due to marker registration issues and modelling decisions. In fact, for both systems, marker positions on the models' bone meshes were assumed for the entire musculoskeletal analysis. Similarly, weights for the scaling and IK steps of the analysis were kept the same for all participants. More work into the decisions surrounding these variables could contribute to getting more accurate results. To further validate how the model is affected by different variables such as scaling weights, IK weights, and values of inertia, a sensitivity analysis could be performed.

Future work also includes extending these conclusions to other joints in the model, notably for upper body joints. Because back strain has been identified as the leading cause of a soldier's inability to complete a march, research could also be extended to the evaluation of spine loading using markerless motion capture. The impact of participant speed on markerless tracking could also be further investigated by collecting data on a trained military population. As Theia3D are constantly expanding their dataset to better their algorithm, markerless data from the upper body seem to have improved since the beginning of the Theia3D software. Also, future Theia3D updates might improve results obtained when performing analyses similar to the one done as part of this research project. Another avenue would be to test other movements, especially operationally relevant military movements such as transitions between running, walking, the kneel position, and the prone position [21]. In order for future studies to use this one as a starting point for their own research, a list of processing decisions and assumptions has been included in Appendix K. These recommendations detail the steps taken to analyze Theia3D data via OpenSim.

REFERENCES

[1] J. J. Knapik, K. L. Reynolds, and E. Harman, "Soldier Load Carriage: Historical, Physiological, Biomechanical, and Medical Aspects," *Mil Med*, vol. 169, no. 1, pp. 45–56, Jan. 2004, doi: 10.7205/MILMED.169.1.45.

[2] L. L. M. Bossi, M. L. H. Jones, A. Kelly, and D. W. Tack, "A Preliminary Investigation of the Effect of Protective Clothing Weight, Bulk and Stiffness on Combat Mobility Course Performance," *Proceedings of the Human Factors and Ergonomics Society Annual Meeting*, vol. 60, no. 1, pp. 702–706, Sep. 2016, doi: 10.1177/1541931213601161.

[3] DOT&E, "Integrated Survivability Assessment-Guidance." Accessed: Dec. 13, 2022. [Online]. Available: https://www.dote.osd.mil/Portals/97/docs/TEMPGuide/Integrated_Survivability_Assessment_Guidance_3.0.pdf

[4] D. Majumdar, M. S. Pal, and D. Majumdar, "Effects of military load carriage on kinematics of gait," *Ergonomics*, vol. 53, no. 6, pp. 782–791, Jun. 2010, doi: 10.1080/00140131003672015.

[5] R. L. Attwells, S. A. Birrell, R. H. Hooper, and N. J. Mansfield, "Influence of carrying heavy loads on soldiers' posture, movements and gait," *Ergonomics*, vol. 49, no. 14, pp. 1527–1537, Nov. 2006, doi: 10.1080/00140130600757237.

[6] J. T. Sturdy, P. H. Sessoms, and A. K. Silverman, "A backpack load sharing model to evaluate lumbar and hip joint contact forces during shoulder borne and hip belt assisted load carriage," *Appl Ergon*, vol. 90, p. 103277, Jan. 2021, doi: 10.1016/j.apergo.2020.103277.

[7] F. Thériault, K. Gabler, and K. Naicker, "Health and Lifestyle Information Survey of Canadian Armed Forces Personnel 2013/2014 – Regular Force Report," Ottawa. Accessed: Oct. 27, 2022. [Online]. Available: https://publications.gc.ca/collections/collection_2017/mdn-dnd/D2-293-2016-eng.pdf

[8] D. Boffey, I. Harat, Y. Gepner, C. L. Frosti, S. Funk, and J. R. Hoffman, "The Physiology and Biomechanics of Load Carriage Performance," *Mil Med*, vol. 184, no. 1–2, pp. e83–e90, Jan. 2019, doi: 10.1093/milmed/usy218.

[9] E. van der Kruk and M. M. Reijne, "Accuracy of human motion capture systems for sport applications; state-of-the-art review," *Eur J Sport Sci*, vol. 18, no. 6, pp. 806–819, Jul. 2018, doi: 10.1080/17461391.2018.1463397.

[10] B. R. Hindle, J. W. L. Keogh, and A. v. Lorimer, "Inertial-Based Human Motion Capture: A Technical Summary of Current Processing Methodologies for Spatiotemporal and Kinematic Measures," *Appl Bionics Biomech*, vol. 2021, pp. 1–14, Mar. 2021, doi: 10.1155/2021/6628320.

[11] R. M. Kanko, "Validation of a Markerless Motion Capture System for Human Movement Analysis. (Master's Thesis)," Master's Thesis, Queen's University, 2020. Accessed: Nov. 11, 2020. [Online]. Available: https://qspace.library.queensu.ca/handle/1974/28019

[12] R. Kanko, G. Strutzenberger, M. Brown, S. Selbie, and K. Deluzio, "Assessment of spatiotemporal gait parameters using a deep learning algorithm-based markerless motion capture system," *ISBS Proceedings Archive*, vol. 38, no. 1, Jul. 2020, doi: 10.31224/osf.io/j4rbg.

[13] R. Kanko, E. Laende, S. Selbie, and K. Deluzio, "Inter-session repeatability of Theia3D markerless motion capture gait kinematics," *bioRxiv*, p. 2020.06.23.155358, Jun. 2020, doi: 10.1101/2020.06.23.155358.

[14] J. B. Davidson, R. B. Graham, S. Beck, R. T. Marler, and S. L. Fischer, "Improving human-in-the-loop simulation to optimize soldier-systems integration," *Appl Ergon*, vol. 90, p. 103267, Jan. 2021, doi: 10.1016/j.apergo.2020.103267.

[15] Y. P. Ivanenko, R. E. Poppele, and F. Lacquaniti, "Five basic muscle activation patterns account for muscle activity during human locomotion," *J Physiol*, vol. 556, no. 1, pp. 267–282, Apr. 2004, doi: 10.1113/jphysiol.2003.057174.

[16] T. K. Uchida and A. Seth, “Conclusion or Illusion: Quantifying Uncertainty in Inverse Analyses From Marker-Based Motion Capture due to Errors in Marker Registration and Model Scaling,” *Front Bioeng Biotechnol*, vol. 10, May 2022, doi: 10.3389/fbioe.2022.874725.

[17] G. Bergmann *et al.*, “Hip contact forces and gait patterns from routine activities,” *J Biomech*, vol. 34, no. 7, pp. 859–871, Jul. 2001, doi: 10.1016/S0021-9290(01)00040-9.

[18] G. K. Lenton *et al.*, “Tibiofemoral joint contact forces increase with load magnitude and walking speed but remain almost unchanged with different types of carried load,” *PLoS One*, vol. 13, no. 11, p. e0206859, Nov. 2018, doi: 10.1371/journal.pone.0206859.

[19] Y. Kim, K. M. Lee, and S. Koo, “Joint moments and contact forces in the foot during walking,” *J Biomech*, vol. 74, pp. 79–85, Jun. 2018, doi: 10.1016/j.jbiomech.2018.04.022.

[20] R. Orr *et al.*, “Soldier Load Carriage, Injuries, Rehabilitation and Physical Conditioning: An International Approach,” *Int J Environ Res Public Health*, vol. 18, no. 8, p. 4010, Apr. 2021, doi: 10.3390/ijerph18084010.

[21] M. P. Mavor, G. B. Ross, A. L. Clouthier, T. Karakolis, and R. B. Graham, “Validation of an IMU Suit for Military-Based Tasks,” *Sensors*, vol. 20, no. 15, p. 4280, Jul. 2020, doi: 10.3390/s20154280.

[22] Maciej Serda *et al.*, “Duty loads carried by the Los Angeles Sheriff’s Department Deputies,” *Journal of Australian Strength and Conditioning*, vol. 26, no. 5, pp. 34–38, 2018, doi: 10.2/JQUERY.MIN.JS.

[23] J. Keeler, “The Effect of Tactical Tasks and Gear on Muscle Activation of SWAT Officers,” *Theses and Dissertations--Kinesiology and Health Promotion*, Jan. 2014, Accessed: Oct. 02, 2022. [Online]. Available: https://uknowledge.uky.edu/khp_etds/19

[24] D. L. Smith, S. J. Petruzzello, M. A. Chludzinski, J. J. Reed, and J. A. Woods, “Effect of strenuous live-fire fire fighting drills on hematological, blood chemistry and psychological measures,” *J Therm Biol*, vol. 26, no. 4–5, pp. 375–379, Sep. 2001, doi: 10.1016/S0306-4565(01)00047-X.

[25] R. M. Orr, R. Pope, J. Coyle, and V. Johnston, "Occupational loads carried by Australian soldiers on military operations," *Journal of Health, Safety and Environment*, vol. 31, no. 1, pp. 451–467, 2015.

[26] R. Orr, "The History of the Soldier's Load," *Australian Army Journal* •, vol. VII, no. 2, p. 67, doi: 10.3316/ielapa.201008831.

[27] J. Knapik, E. Harman, and K. Reynolds, "Load carriage using packs: A review of physiological, biomechanical and medical aspects," *Appl Ergon*, vol. 27, no. 3, pp. 207–216, Jun. 1996, doi: 10.1016/0003-6870(96)00013-0.

[28] C. L. Koerhuis, B. J. Veenstra, J. J. van Dijk, and N. J. Delleman, PhD, "Predicting Marching Capacity While Carrying Extremely Heavy Loads," *Mil Med*, vol. 174, no. 12, pp. 1300–1307, Dec. 2009, doi: 10.7205/MILMED-D-00-7508.

[29] S. D. Blacker, J. L. Fallowfield, J. L. J. Bilzon, and M. E. T. Willems, "Physiological Responses to Load Carriage During Level and Downhill Treadmill Walking," *Medicina Sportiva*, vol. 13, no. 2, pp. 116–124, Mar. 2009, doi: 10.2478/v10036-009-0018-1.

[30] A. V. Pedersen, R. Stokke, and A. Mamen, "Effects of extra load position on energy expenditure in treadmill running," *Eur J Appl Physiol*, vol. 102, no. 1, pp. 27–31, Dec. 2007, doi: 10.1007/S00421-007-0553-1/TABLES/2.

[31] J. S. Coombes and C. Kingswell, "Biomechanical and physiological comparison of conventional webbing and the M83 assault vest.," *Appl Ergon*, vol. 36, no. 1, pp. 49–53, Jan. 2005, doi: 10.1016/j.apergo.2004.09.004.

[32] R. G. Soule, K. B. Pandolf, and R. F. Goldman, "Energy Expenditure of Heavy Load Carriage," *Ergonomics*, vol. 21, no. 5, pp. 373–381, May 1978, doi: 10.1080/00140137808931734.

[33] P. A. Scott and L. Ramabhai, "Load carrying : in situ physiological responses of an infantry platoon," *Ergonomics*, vol. 2000, no. 1, pp. 18–24, 2000.

[34] J. Lyons, A. Allsopp, and J. Bilzon, “Influences of body composition upon the relative metabolic and cardiovascular demands of load-carriage,” *Occup Med (Chic Ill)*, vol. 55, no. 5, pp. 380–384, Aug. 2005, doi: 10.1093/occmed/kqi087.

[35] T. A. Crowder, M. D. Beekley, R. X. Sturdivant, C. A. Johnson, and A. Lumpkin, “Metabolic Effects of Soldier Performance on a Simulated Graded Road March while Wearing Two Functionally Equivalent Military Ensembles,” *Mil Med*, vol. 172, no. 6, pp. 596–602, Jun. 2007, doi: 10.7205/MILMED.172.6.596.

[36] P. W. Richmond, A. W. Potter, and W. R. Santee, “Terrain Factors for Predicting Walking and Load Carriage Energy Costs: Review and Refinement,” *Journal of Sport and Human Performance*, vol. 3, no. 3, Oct. 2015, doi: 10.12922/jshp.v3i3.67.

[37] P. W. Richmond, A. W. Potter, D. P. Looney, and W. R. Santee, “Terrain coefficients for predicting energy costs of walking over snow,” *Appl Ergon*, vol. 74, pp. 48–54, Jan. 2019, doi: 10.1016/j.apergo.2018.08.017.

[38] K. B. Pandolf, M. F. Haisman, and R. F. Goldman, “Metabolic Energy Expenditure and Terrain Coefficients for Walking on Snow,” *Ergonomics*, vol. 19, no. 6, pp. 683–690, Nov. 1976, doi: 10.1080/00140137608931583.

[39] R. G. Soule and R. F. Goldman, “Terrain coefficients for energy cost prediction.,” *J Appl Physiol*, vol. 32, no. 5, pp. 706–708, May 1972, doi: 10.1152/jappl.1972.32.5.706.

[40] S. A. Birrell and R. A. Haslam, “The effect of military load carriage on 3-D lower limb kinematics and spatiotemporal parameters,” *Ergonomics*, vol. 52, no. 10, pp. 1298–1304, Oct. 2009, doi: 10.1080/00140130903003115.

[41] M. Baggaley, M. Esposito, C. Xu, G. Unnikrishnan, J. Reifman, and W. B. Edwards, “Effects of load carriage on biomechanical variables associated with tibial stress fractures in running,” *Gait Posture*, vol. 77, pp. 190–194, Mar. 2020, doi: 10.1016/j.gaitpost.2020.01.009.

[42] S. A. Birrell, R. H. Hooper, and R. A. Haslam, “The effect of military load carriage on ground reaction forces,” *Gait Posture*, vol. 26, no. 4, pp. 611–614, Oct. 2007, doi: 10.1016/J.GAITPOST.2006.12.008.

[43] J. Knapik, K. Reynolds, J. Staab, J. A. Vogel, and B. Jones, “Injuries Associated with Strenuous Road Marching,” *Mil Med*, vol. 157, no. 2, pp. 64–67, Feb. 1992, doi: 10.1093/milmed/157.2.64.

[44] J. J. Knapik and K. Reynolds, “Load Carriage-Related Injury Mechanisms, Risk Factors, and Prevention,” *Studies in Mechanobiology, Tissue Engineering and Biomaterials*, vol. 19, pp. 107–137, 2016, doi: 10.1007/8415_2014_182/COVER.

[45] E. F. D. Canetti, B. Schram, R. M. Orr, J. Knapik, and R. Pope, “Risk factors for development of lower limb osteoarthritis in physically demanding occupations: A systematic review and meta-analysis,” *Appl Ergon*, vol. 86, p. 103097, Jul. 2020, doi: 10.1016/j.apergo.2020.103097.

[46] E. Chassé, M.-A. Laroche, C.-A. Dufour, R. Guimond, and F. Lalonde, “Association Between Musculoskeletal Injuries and the Canadian Armed Forces Physical Employment Standard Proxy in Canadian Military Recruits,” *Mil Med*, vol. 185, no. 7–8, pp. e1140–e1146, Aug. 2020, doi: 10.1093/milmed/usaa011.

[47] L. Mündermann, S. Corazza, and T. P. Andriacchi, “The evolution of methods for the capture of human movement leading to markerless motion capture for biomechanical applications,” *J Neuroeng Rehabil*, vol. 3, no. 1, pp. 1–11, Mar. 2006, doi: 10.1186/1743-0003-3-6/FIGURES/5.

[48] T. K. Uchida and S. L. Delp, *Biomechanics of Movement*. Cambridge, Massachusetts: The MIT Press, 2020.

[49] S. L. Colyer, M. Evans, D. P. Cosker, and A. I. T. Salo, “A Review of the Evolution of Vision-Based Motion Analysis and the Integration of Advanced Computer Vision Methods Towards Developing a Markerless System,” *Sports Med Open*, vol. 4, no. 1, pp. 1–15, Dec. 2018, doi: 10.1186/S40798-018-0139-Y/FIGURES/7.

[50] L. P. Maletsky, J. Sun, and N. A. Morton, "Accuracy of an optical active-marker system to track the relative motion of rigid bodies," *J Biomech*, vol. 40, no. 3, pp. 682–685, Jan. 2007, doi: 10.1016/j.jbiomech.2006.01.017.

[51] R. Hartson and P. Pyla, "Empirical UX Evaluation: UX Goals, Metrics, and Targets," in *The UX Book*, Elsevier, 2019, pp. 453–481. doi: 10.1016/B978-0-12-805342-3.00022-9.

[52] L. A. Hutchinson, M. J. Brown, K. J. Deluzio, and A. R. de Asha, "Self-Selected walking speed increases when individuals are aware of being recorded," *Gait Posture*, vol. 68, pp. 78–80, Feb. 2019, doi: 10.1016/j.gaitpost.2018.11.016.

[53] J. F. Drazan, W. T. Phillips, N. Seethapathi, T. J. Hullfish, and J. R. Baxter, "Moving outside the lab: Markerless motion capture accurately quantifies sagittal plane kinematics during the vertical jump," *J Biomech*, vol. 125, p. 110547, Aug. 2021, doi: 10.1016/j.jbiomech.2021.110547.

[54] H. Tsushima, M. E. Morris, and J. McGinley, "Test-Retest Reliability and Inter-Tester Reliability of Kinematic Data from a Three-Dimensional Gait Analysis System.," *Journal of the Japanese Physical Therapy Association*, vol. 6, no. 1, pp. 9–17, 2003, doi: 10.1298/jjpta.6.9.

[55] U. della Croce, A. Leardini, L. Chiari, and A. Cappozzo, "Human movement analysis using stereophotogrammetry," *Gait Posture*, vol. 21, no. 2, pp. 226–237, Feb. 2005, doi: 10.1016/j.gaitpost.2004.05.003.

[56] B. R. Hando, W. C. Scott, J. F. Bryant, J. N. Tchandja, R. M. Scott, and S. S. Angadi, "Association Between Markerless Motion Capture Screenings and Musculoskeletal Injury Risk for Military Trainees: A Large Cohort and Reliability Study," *Orthop J Sports Med*, vol. 9, no. 10, 2021, doi: 10.1177/23259671211041656/FORMAT/EPUB.

[57] R. Kanko, E. Laende, E. Davis, W. S. Selbie, and K. J. Deluzio, "Concurrent assessment of gait kinematics using marker-based and markerless motion capture," *bioRxiv*, p. 2020.12.10.420075, 2020, [Online]. Available: http://biorxiv.org/content/early/2020/12/11/2020.12.10.420075.abstract

[58] A. Rajagopal, C. L. Dembia, M. S. DeMers, D. D. Delp, J. L. Hicks, and S. L. Delp, "Full-Body Musculoskeletal Model for Muscle-Driven Simulation of Human Gait," *IEEE Trans Biomed Eng*, vol. 63, no. 10, pp. 2068–2079, Oct. 2016, doi: 10.1109/TBME.2016.2586891.

[59] S. Delp, J. Hicks, A. Habib, C. Ong, A. Seth, and T. Uchida, "OpenSim: Project Home," *SimTK*, 2022. https://simtk.org/projects/opensim/ (accessed Nov. 14, 2022).

[60] I. Weygers, M. Kok, M. Konings, H. Hallez, H. de Vroey, and K. Claeys, "Inertial Sensor-Based Lower Limb Joint Kinematics: A Methodological Systematic Review," *Sensors*, vol. 20, no. 3, p. 673, Jan. 2020, doi: 10.3390/s20030673.

[61] OpenSim Documentation, "OpenSense - Kinematics with IMU Data," *SimTK*. https://simtk-confluence.stanford.edu:8443/display/OpenSim/OpenSense+-+Kinematics+with+IMU+Data (accessed Oct. 31, 2022).

[62] S. D. Uhlrich *et al.*, "OpenCap: 3D human movement dynamics from smartphone videos," *bioRxiv*, p. 2022.07.07.499061, Jul. 2022, doi: 10.1101/2022.07.07.499061.

[63] Department of National Defence, "Load Carriage Manual."

[64] R. Merletti, G. Rau, C. Disselhorst-Klug, D. F. Stegeman, and G. M. Hägg, "SENIAM - Recommendations for sensor locations in lower leg or foot muscles." http://www.seniam.org/ (accessed Oct. 25, 2022).

[65] OpenSim Documentation, "Getting Started with Scaling," *SimTK*. https://simtk-confluence.stanford.edu:8443/display/OpenSim/Getting+Started+with+Scaling (accessed Oct. 26, 2022).

[66] OpenSim Documentation, "Getting Started with Inverse Kinematics," *SimTK*. https://simtk-confluence.stanford.edu:8443/display/OpenSim/Getting+Started+with+Inverse+Kinematics (accessed Oct. 26, 2022).

[67] OpenSim Documentation, "Getting Started with RRA," *SimTK*. https://simtk-confluence.stanford.edu:8443/display/OpenSim/Getting+Started+with+RRA (accessed Oct. 26, 2022).

[68] S. R. Hamner, A. Seth, and S. L. Delp, “Muscle contributions to propulsion and support during running,” *J Biomech*, vol. 43, no. 14, pp. 2709–2716, Oct. 2010, doi: 10.1016/j.jbiomech.2010.06.025.

[69] OpenSim Documentation, “Getting Started with Static Optimization,” *SimTK*. https://simtk-confluence.stanford.edu:8443/display/OpenSim/Getting+Started+with+Static+Optimization (accessed Oct. 26, 2022).

[70] OpenSim Documentation, “Joint Reactions Analysis,” *SimTK*. https://simtk-confluence.stanford.edu:8443/display/OpenSim/Joint+Reactions+Analysis (accessed Oct. 26, 2022).

[71] R. Roithner, H. Schwameder, and E. Müller, “Determination of optimal filter parameters for filtering kinematic walking data using butterworth low pass filter,” in *ISBS*, 2000. Accessed: Oct. 06, 2022. [Online]. Available: https://www.researchgate.net/publication/242203849_Determination_of_optimal_filter_parameters_for_filtering_kinematic_walking_data_using_butterworth_low_pass_filter

[72] P. Schober and L. A. Schwarte, “Correlation coefficients: Appropriate use and interpretation,” *Anesth Analg*, vol. 126, no. 5, pp. 1763–1768, May 2018, doi: 10.1213/ANE.0000000000002864.

[73] D. Giavarina, “Understanding Bland Altman analysis,” *Biochem Med (Zagreb)*, vol. 25, no. 2, p. 141, 2015, doi: 10.11613/BM.2015.015.

[74] P. Taffé, “When can the Bland & Altman limits of agreement method be used and when it should not be used,” *J Clin Epidemiol*, vol. 137, pp. 176–181, Sep. 2021, doi: 10.1016/j.jclinepi.2021.04.004.

[75] A. Kallner, “Formulas,” in *Laboratory Statistics*, Elsevier, 2018, pp. 1–140. doi: 10.1016/B978-0-12-814348-3.00001-0.

[76] D. G. E. Robertson, G. E. Caldwell, J. Hamil, G. Kamen, and S. N. Whittlesey, “Methods in Research Biomechanics,” *Human Kinetics*, p. 443, 2013.

[77] Theia3D 2022.2 documentation, "9. Model Reference," *TheiaMarkerless*. https://www.theiamarkerless.ca/docs/model.html (accessed Nov. 21, 2022).

[78] T. N. Brown, M. O'Donovan, L. Hasselquist, B. D. Corner, and J. M. Schiffman, "Body borne loads impact walk-to-run and running biomechanics," *Gait Posture*, vol. 40, no. 1, pp. 237–242, 2014, doi: 10.1016/j.gaitpost.2014.04.001.

[79] "Tutorial: Foot and Ankle Angles - Visual3D Wiki Documentation." https://c-motion.com/v3dwiki/index.php?title=Tutorial:_Foot_and_Ankle_Angles#Virtual_Foot_Method_1_-_Heel_to_Toe (accessed Nov. 22, 2022).

[80] H. Tang, J. Pan, B. Munkasy, K. Duffy, and L. Li, "Comparison of Lower Extremity Joint Moment and Power Estimated by Markerless and Marker-Based Systems during Treadmill Running," *Bioengineering*, vol. 9, no. 10, p. 574, Oct. 2022, doi: 10.3390/bioengineering9100574.

[81] R. Fernandes, P. Armada-da-Silva, A. Pool-Goudaazward, V. Moniz-Pereira, and A. P. Veloso, "Three dimensional multi-segmental trunk kinematics and kinetics during gait: Test-retest reliability and minimal detectable change," *Gait Posture*, vol. 46, pp. 18–25, May 2016, doi: 10.1016/J.GAITPOST.2016.02.007.

[82] J. L. Hicks, T. K. Uchida, A. Seth, A. Rajagopal, and S. L. Delp, "Is My Model Good Enough? Best Practices for Verification and Validation of Musculoskeletal Models and Simulations of Movement," *J Biomech Eng*, vol. 137, no. 2, Feb. 2015, doi: 10.1115/1.4029304/371243.

[83] E. M. Walker, M. Nelson, M. D. Drew, S. M. Krammer, and T. N. Brown, "Tibial compression during sustained walking with body borne load," *J Biomech*, vol. 133, p. 110969, Mar. 2022, doi: 10.1016/J.JBIOMECH.2022.110969.

[84] E. S. Matijevich, L. M. Branscombe, L. R. Scott, and K. E. Zelik, "Ground reaction force metrics are not strongly correlated with tibial bone load when running across speeds and slopes: Implications for science, sport and wearable tech," *PLoS One*, vol. 14, no. 1, p. e0210000, Jan. 2019, doi: 10.1371/journal.pone.0210000.

[85] X. Wang, Y. Ma, B. Y. Hou, and W.-K. Lam, “Influence of Gait Speeds on Contact Forces of Lower Limbs,” *J Healthc Eng*, vol. 2017, pp. 1–6, 2017, doi: 10.1155/2017/6375976.

[86] V. Camomilla, A. Cereatti, A. G. Cutti, S. Fantozzi, R. Stagni, and G. Vannozzi, “Methodological factors affecting joint moments estimation in clinical gait analysis: a systematic review,” *Biomed Eng Online*, vol. 16, no. 1, p. 106, Dec. 2017, doi: 10.1186/s12938-017-0396-x.

Appendix A – Participant anthropometrics and sizing

Table A.1: Participant anthropometrics and sizing

Participant	Sex	Weight (kg)	Height (m)	Helmet size	Tactical boots size	Frag vest size	Tactical vest size	Rucksack size
P01	M	76.2	1.8	L	10	S	M	S
P02	M	69.0	1.8	M	10	S	M	S
P03	M	70.5	1.7	M	9	S	M	S
P04	F	61.5	1.6	M	5	S	M	S
P05	F	57.5	1.7	M	5	S	M	S
P06	F	77.5	1.7	M	9	S	M	S
P07	F	69.5	1.7	M	5	S	M	S
P08	F	78.5	1.7	M	9	S	M	S
P09	F	57.5	1.7	M	5	S	M	S
P10	M	82.0	1.7	M	9	S	M	S
P11	F	74.0	1.8	M	9	S	M	S
P12	M	94.0	1.8	M	10	S	M	S
P13	M	74.5	1.9	M	11	S	M	S
P14	F	70.4	1.6	M	5	S	M	S
P15	M	63.5	1.6	M	9	S	M	S
P16	M	89.0	1.7	M	11	S	M	S

Appendix B – Certificate of ethics approval

20/12/2021

Université d'Ottawa
Bureau d'éthique et d'intégrité de la recherche

University of Ottawa
Office of Research Ethics and Integrity

CERTIFICAT D'APPROBATION ÉTHIQUE | CERTIFICATE OF ETHICS APPROVAL

Numéro du dossier / Ethics File Number	H-06-18-721
Titre du projet / Project Title	A validation of an IMU suit for military-based movements.
Type de projet / Project Type	Recherche de professeur / Professor's research project
Statut du projet / Project Status	Renouvelé / Renewed
Date d'approbation (jj/mm/aaaa) / Approval Date (dd/mm/yyyy)	07/08/2018
Date d'expiration (jj/mm/aaaa) / Expiry Date (dd/mm/yyyy)	06/08/2022

Équipe de recherche / Research Team

Chercheur / Researcher	Affiliation	Role
Ryan GRAHAM	École des sciences de l'activité physique / School of Human Kinetics	Chercheur Principal / Principal Investigator
Isabel COLL	Département de génie mécanique / Department of Mechanical Engineering	Assistant de recherche / Research Assistant
Kristina May GRUEVSKI	École des sciences de l'activité physique / School of Human Kinetics	Collaborateur / Collaborator
Matthew MAVOR	École des sciences de l'activité physique / School of Human Kinetics	Assistant de recherche / Research Assistant
Gwyneth ROSS	École des sciences de l'activité physique / School of Human Kinetics	Assistant de recherche / Research Assistant
Alexandre MIR-OREFICE	University of Ottawa	Étudiant-chercheur / Student-researcher
Allison CLOUTHIER	École des sciences de l'activité physique / School of Human Kinetics	Collaborateur / Collaborator

Conditions spéciales ou commentaires / Special conditions or comments

550, rue Cumberland, pièce 154 Ottawa (Ontario) K1N 6N5 Canada
550 Cumberland Street, Room 154 Ottawa, Ontario K1N 6N5 Canada

613-562-5387 • 613-562-5338 • ethique@uOttawa.ca / ethics@uOttawa.ca
www.recherche.uottawa.ca/deontologie | www.recherche.uottawa.ca/ethics

Université d'Ottawa
Bureau d'éthique et d'intégrité de la recherche

University of Ottawa
Office of Research Ethics and Integrity

Le Comité d'éthique de la recherche (CÉR) de l'Université d'Ottawa, opérant conformément à l'*Énoncé de politique des Trois conseils* (2014) et toutes autres lois et tous règlements applicables, a examiné et approuvé la demande d'éthique du projet de recherche ci-nommé.

L'approbation est valide pour la durée indiquée plus haut et est sujette aux conditions énumérées dans la section intitulée "Conditions Spéciales ou Commentaires". Le formulaire « Renouvellement ou Fermeture de Projet » doit être complété quatre semaines avant la date d'échéance indiquée ci-haut afin de demander un renouvellement de cette approbation éthique ou afin de fermer le dossier.

Toutes modifications apportées au projet doivent être approuvées par le CÉR avant leur mise en place, sauf si le participant doit être retiré en raison d'un danger immédiat ou s'il s'agit d'un changement ayant trait à des éléments administratifs ou logistiques du projet. Les chercheurs doivent aviser le CÉR dans les plus brefs délais de tout changement pouvant augmenter le niveau de risque aux participants ou pouvant affecter considérablement le déroulement du projet, rapporter tout évènement imprévu ou indésirable et soumettre toute nouvelle information pouvant nuire à la conduite du projet ou à la sécurité des participants.

The University of Ottawa Research Ethics Board, which operates in accordance with the *Tri-Council Policy Statement* (2014) and other applicable laws and regulations, has examined and approved the ethics application for the above-named research project.

Ethics approval is valid for the period indicated above and is subject to the conditions listed in the section entitled "Special Conditions or Comments". The "Renewal/Project Closure" form must be completedfour weeks before the above-referenced expiry date to request a renewal of this ethics approval or closure of the file.

Any changes made to the project must be approved by the REB before being implemented, except when necessary to remove participants from immediate endangerment or when the modification(s) only pertain to administrative or logistical components of the project. Investigators must also promptly alert the REB of any changes that increase the risk to participant(s), any changes that considerably affect the conduct of the project, all unanticipated and harmful events that occur, and new information that may negatively affect the conduct of the project or the safety of the participant(s).

Germain ZONGO
Responsable d'éthique en recherche / Protocol Officer
Pour/For **Daniel LAGAREC** Président(e) du/ Chair of the **Comité d'éthique de la recherche en sciences de la santé et sciences / Health Sciences and Sciences Research Ethics Board**

550, rue Cumberland, pièce 154
Ottawa (Ontario) K1N 6N5 Canada

550 Cumberland Street, Room 154
Ottawa, Ontario K1N 6N5 Canada

613-562-5387 • 613-562-5338 • ethique@uOttawa.ca / ethics@uOttawa.ca
www.recherche.uottawa.ca/deontologie | www.recherche.uottawa.ca/ethics

Appendix C – Research consent form

uOttawa

Université d'Ottawa
Faculté des sciences de la santé

École des sciences de l'activité physique

University of Ottawa
Faculty of Health Sciences

School of Human Kinetics

☎ 613-562-5853
613-562-5149

125 University Private
Ottawa ON K1N 6N5 Canada

www.uOttawa.ca

Research Consent Form

Research Project Title: The impact of heavy equipment on a soldier's movement: Application of markerless motion capture for military assessment

Principal Investigators:
Dr. Ryan Graham (Supervisor) **Isabel Coll (MASc Candidate)**

University of Ottawa
Faculty of Health Sciences
Department of Human Kinetics
200 Lees Ave (E020)
Ottawa, ON K1N6N5

COVID-19 Precautions:

For the safety of both yourself and the researchers, precautions have been put in place to try and prevent the spread of COVID-19. Before arriving at the lab, you and the researchers will be screened for COVID-19 symptoms, will certify your vaccination status, and will be asked to use hand sanitizer upon entering and exiting the lab. Both you and the researchers are required to wear a mask at all times during the data collection. All equipment that is touched by either a participant or researcher during the collection will be wiped down with disinfectant before and after the collection and all washable materials will be washed in between each participant starting. There will be a mandatory minimum of one day between data collections.

Background and Purpose of the Study:

Recently, there have been developments in motion capture technology that leverage the power of artificial intelligence to identify movement patterns based on red, green, and blue (RGB) video camera footage, termed markerless motion capture. However, the level of agreement of this technology compared to a gold-standard optical motion capture (OPT) system while wearing military-based equipment is unknown. Therefore, the purpose of this investigation is to assess the validity of a markerless motion capture system (Theia3D, Theia Markerless, Inc., Canada) compared to a gold-standard optical motion capture system (Vantage V5, Vicon, UK) while wearing military equipment.

Description of Study Procedures:

The study consists of a one-day motion analysis procedure of approximately 1.5 hours at the University of Ottawa Human Movement Biomechanics Laboratory (200 Lees Avenue, E020). The study protocol includes a series of 2 movements: walking and running over a 6-meter distance. Both tasks will be performed three times each under four different loading conditions: 6 kg, 23 kg, 39 kg and 43 kg (2 movements x 3 repetitions x 4 configurations = 24 trials). These loading conditions will be accomplished through backpacks and protective equipment similar to what the Canadian Armed Forces wear. There will be a 30 second to 1-minute rest periods after each trial to reduce fatigue.

Upon arrival, you will be outfitted with an OPT suit: reflective marker clusters and individual markers will be placed on your upper and lower limbs, trunk,

pelvis, and head. Before the experimental trials can begin, you will be asked to perform two five-second static reference calibration trials and a functional range of motion trial, which will both be used to create an individualized biomechanical model. After these calibration trials are completed, some markers will be removed and the experimental trials will begin. Simultaneous to the OPT system, 8 RGB-cameras (Vue, Vicon, UK) will capture video data for the markerless motion capture system.

Data Analysis:

The data collected will initially be used for a first-year master's student (Isabel Coll) project assessing the validity of a markerless motion capture system while wearing military equipment. Concurrent validity of the OPT and markerless systems will be assessed using root mean squared errors, intraclass correlation coefficients and Bland-Altman limits of agreement. Data may be used in the future for secondary analyses.

Possible Risks and Discomforts:

There are no significant risks associated with participating in this study. You may experience pain and fatigue due to the nature of the tasks; however, sufficient rest will be given to reduce these effects. The tape used to attach the individual reflective markers may cause minor skin irritation; this is similar to what is experienced with a bandage and typically fades within 2 to 3 days.

Should you experience any major discomfort, please tell us immediately and seek primary care from a medical professional on campus (100 Marie Curie, Ottawa, Tel.: 613-564-3950) or a medical professional of your choosing.

Possible Benefits:

You will not directly benefit from participating in this study. However, the results of this study will greatly add to our knowledge of the validity of different motion capture systems.

Voluntary Participation:

You are not obliged to participate in this study; your participation is voluntary. You may also withdraw from the study at any time with no penalty or coercion. If chosen to withdaw, your data will be destroyed (i.e., it will not be used in the study).

Confidentiality:

All personal information is kept confidential. Information gained from this study will be stored electronically and will need a password to access, which will only be known to Dr. Ryan Graham and the research team (including Isabel Coll). Paper study records are stored in a locked cabinet and will be destroyed after 5 years post publication; electronic records will be deleted and paper records will be shredded. You will not be identified by name in any reports of the completed study. Your anonymity will be strictly maintained – you will not be identified by your name but will be determined by an independent study number.

Compensation:

You will not be compensated for your participation in this study.

Questions about the Study:

You are free to ask questions at any time during the protocol and by contacting the principal investigator by email: Dr. Ryan Graham (ryan.graham@uottawa.ca). The ethical components of this research project has been approved by the University of Ottawa research ethics board. If you have any questions regarding the ethical conduct of this study, you may contact the Protocol Officer for Ethics in Research, University of Ottawa, Tabaret Hall, 550 Cumberland Street, Room 154, Ottawa ON, K1N 6N5. Tel.: (613) 562-5387 Email: ethics@uottawa.ca. There are two copies of the consent form, one of which is yours to keep.

Research Project Title: The impact of heavy equipment on a soldier's movement: Application of markerless motion capture for military assessment

Consent:

I have read this consent form, and I agree to participate in the procedures of this study.

_____
Printed Name of Participant

_____ _____
Signature of Participant Date

Investigator Statement (or Person Explaining the Consent):
I have carefully explained to the research participant the nature of the above research study. To the best of my knowledge, the research participant signing this consent form understands the nature, demands, risks and benefits involved in participating in this study. I acknowledge my responsibility for the care and well-being of the above research participant, to respect the rights and wishes of the research participant, and to conduct the study according to applicable Good Clinical Practice guidelines and regulations.

_____
Name of Investigator/Delegate (printed)

_____ _____
Signature of Investigator/Delegate Date

Informed Consent to have Videos Taken:
I consent to have video foot taken during the protocol. I understand that these videos are being used as part of the analysis and if any of these videos are used in a subsequent presentation or publication, that my face and any other identifiers will be blurred. You cannot participate in the research study without consenting to having video footage taken.

_____ _____
Name Date

_____
Signature

_____ _____
Witness Name Witness Signature

Future Participation:

- ☐ I am interested in being contacted to participate in future research performed by this laboratory (your email information will be saved in a password protected file).

Appendix D – Equipment weight per loading condition

Table D.1: Equipment weight per loading condition

Equipment	Measured weight of equipment (kg)	Condition 1 (Slick)	Condition 2 (Medium)	Condition 3 (Heavy1)	Condition 4 (Heavy2)
Tactical boots 	1.3	X	X	X	X
Helmet 	1.5	X	X	X	X
Mock rifle 	2.0	X	X	X	X
Tactical vest 	8.6		X	X	X
Fragmentation vest 	7.4		X	X	X
Daypack 	13.8			X	
Rucksack 	19.9				X
TOTAL CONDITION WEIGHT (kg)		**4.8**	**20.8**	**34.6**	**40.7**

Appendix E – Experimental marker set

Table E.1: Individual anatomical marker set

#	Anatomical Landmark	Marker Label
1	Xyphoid	XP
2	C7	C7
3	Sternal Notch	SN
4	Acromions	LAC
5		RAC
6	Elbows	LELBL
7		LELBM
8		RELBL
9		RELBM
10	Wrists	LRAD
11		LULN
12		RULN
13		RRAD
14	Hands (top of 3rd finger)	RHND
15		LHND
16	Iliac Crests	RIC
17		LIC
18	ASIS/PSIS	RPSI
19		LPSI
20		LASI
21		RASI
22	Greater Trochanters	RGT
23		LGT
24	Knees	RKNL
25		RKNM
26		LKNL
27		LKNM
28	Ankles	RANL
29		RANM
30		LANL
31		LANM
32	Left Foot	LHEE
33		LM1
34		LM5
35	Right Foot	RHEE
36		RM1
37		RM5

Table E.2: Cluster marker set

#	Cluster Area	Marker Label
1	Left FA Cluster	LFAPA
		LFAPP
		LAFADP
		LFADA
2	Right FA Cluster	RFAPA
		RFAPP
		RFADP
		RFADA
3	Left UA Cluster	LUAPA
		LUAPP
		LUADP
		LUADA
4	Right UA Cluster	RUAPA
		RUAPP
		RUADP
		RUADA
5	Pelvis Cluster	PVUL
		PVLL
		PVLR
		PVUR
6	Left Thigh Cluster	LTHPA
		LTHPP
		LTHDP
		LTHDA
7	Right Thigh Cluster	RTHPA
		RTHPP
		RTHDP
		RTHDA
8	Left Shank Cluster	LSHPA
		LSHPP
		LSHDP
		LSHDA
9	Right Shank Cluster	RSHPA
		RSHPP
		RSHDP
		RSHDA
10	Front Pelvis Cluster	FPVUL
		FPVLL
		FPVLR
		FPVUR

Table E.3: Equipment marker set

#	Equipment	Marker Label
1	Helmet	LFHD
2		RFHD
3		FHD
4	Rifle	Stock
5		Handle
6		Barrel
7	Daypack/ Rucksack	DPUL
8		DPUR
9		DPLR
10		DPLL

Appendix F – List of trials excluded from the analysis and reason

Table F.1: List of trials excluded from the analysis and reason

Trial name	Reason	Motion capture system responsible
P01_c4_run01	Lack of pelvis markers visible	Marker-based
P01_c4_run02	Lack of pelvis markers visible	Marker-based
P01_c4_run03	Lack of pelvis markers visible	Marker-based
P01_c4_walk01	Lack of pelvis markers visible	Marker-based
P01_c4_walk02	Lack of pelvis markers visible	Marker-based
P01_c4_walk03	Lack of pelvis markers visible	Marker-based
P05_c2_walk03	Cluster dangling from participant	Marker-based
P05_c3_walk01	Cluster dangling from participant	Marker-based
P07_c1_walk03	Gap in markerless data	Markerless
P10_c4_walk02	Not a full gait cycle/Trial collection stopped early	-
P10_c2_walk03	Inadequate markerless tracking	Markerless
P10_c2_walk01	SO fails for markerless trial	Markerless
P10_c3_walk01	SO fails for markerless trial	Markerless
P11_c3_run02	SO fails for marker-based trial	Marker-based
P13_c1_walk02	Inadequate markerless tracking	Markerless
P14_c4_run01	Lack of pelvis markers visible	Marker-based
P14_c4_run02	Lack of pelvis markers visible	Marker-based
P14_c4_run03	Lack of pelvis markers visible	Marker-based
P14_c4_walk03	Lack of pelvis markers visible	Marker-based
P15_c4_walk02	Gap in markerless data	Markerless
P15_c3_run01	Lack of pelvis markers visible	Marker-based
P15_c3_run02	Lack of pelvis markers visible	Marker-based
P15_c3_run03	Lack of pelvis markers visible	Marker-based

NB: The trial names follow the convention *Participant_Condition_MovementIteration.* For example, trial "P01_c4_run02" would indicate the first participant's second running trial in the heaviest loading condition (C4).

Appendix G – Results of the initial musculoskeletal analysis with initial angle bias

Here are the initial results of the musculoskeletal analysis. Using these results as a starting point, changes were made leading to the results presented in the thesis. The principal differences between the initial results presented here and the most current results presented in the body of the thesis are that, for the most current results, the marker-based scaling weights were corrected and the markerless data do not consider the computed values of angle bias. Thus, the results presented below compare marker-based results uncorrected for scaling weights as well as markerless results adjusted with the computed values of angle bias.

G1. Kinematics comparison – Static trials

Table G.1 presents values of angle bias for joints of the lower limbs in all four loading conditions as obtained in the initial musculoskeletal analysis.

Table G.1: Angle bias between the marker-based and markerless models averaged over participants for hip, knee, and ankle flexion, from the initial musculoskeletal analysis

		Hip flexion (°)			Knee flexion (°)			Ankle flexion (°)		
Motion capture system		Marker-based	Markerless	Bias	Marker-based	Markerless	Bias	Marker-based	Markerless	Bias
Loading condition	C1	1.02	-1.67	2.69	5.76	0.09	5.67	0.01	5.13	-5.12
	C2	1.92	-1.65	3.57	7.23	0.67	6.56	0.52	4.86	-4.34
	C3	15.57	1.04	14.53	8.01	-1.39	9.40	-0.38	3.73	-4.11
	C4	23.65	0.50	23.16	12.47	-1.61	14.07	0.77	6.27	-5.50

G2. Kinematics comparison – Dynamic trials

Angle biases computed as the difference between marker-based and markerless static poses were applied to the markerless IK results to account for differences between the models. As such, the constant values of angle biases presented in Table G.1 were added to joint angles estimated from the Theia3D software, at all timeframes of the dynamic trials. For reference, the IK results of the initial musculoskeletal analysis before the application of angle biases on the markerless kinematics are included in Appendix I. Results for the walking trials before correcting marker-based scaling weights and with angle bias applied are represented in Figure G.1.

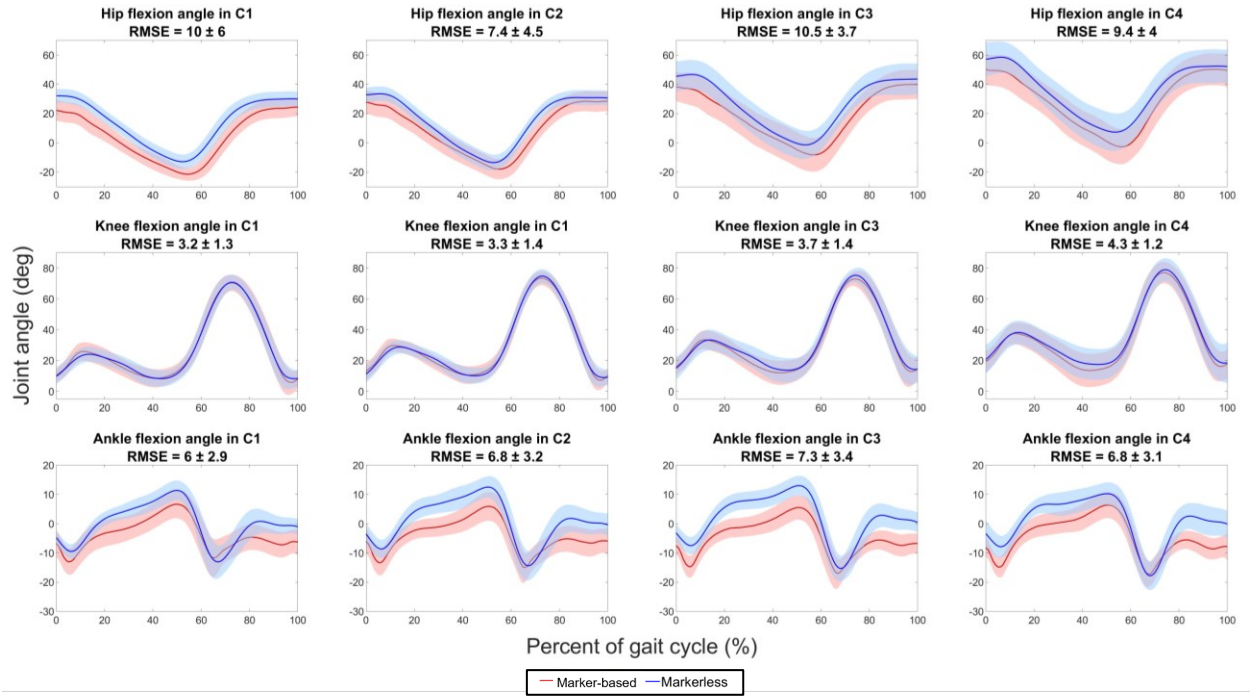

Figure G.1: Plots of lower limb joint angles for a full gait cycle under all loading conditions for walking trials with angle bias applied to the markerless results, from the initial musculoskeletal analysis. RMSEs computed as the difference between both curves through all timeframes.

Looking at RMSE values for all subplots, it seems that markerless data best matches marker-based data for the knee joint and does worst for the hip joint. While the knee flexion RMSE peaks at 4.3° in C4, hip flexion RMSE is higher in C3 with a value of 10.5°. Through loading conditions, RMSEs do not seem considerably affected by the increase of equipment on the participant. For example, when looking at ankle flexion RMSEs, a difference of only 1.3° is observed between minimal and maximal RMSEs of 6° and 7.3° in C1 and C3, respectively.

Similarly, lower limb joint angles for a full gait cycle under all loading conditions for running trials are presented in Figure G.2. Again, knee flexion seems to match the best between the two motion capture systems, with a minimal RMSE value of 3.4° in C2 and a maximal RMSE value of 4.1° in C4. Hip flexion is again the worst joint angle for running trials. Its peak RMSE value of 10.2° in C3 is comparable to the 10.5° observed for walking trials in the same loading condition.

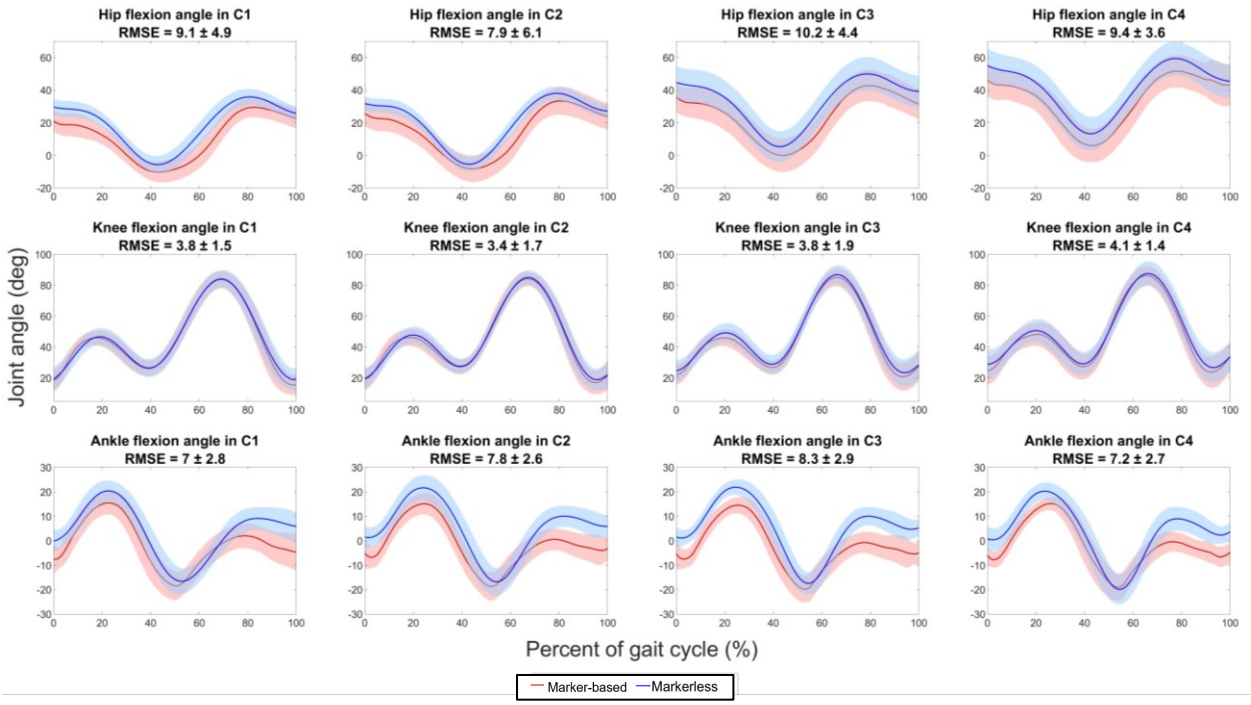

Figure G.2: Plots of lower limb joint angles for a full gait cycle under all loading conditions for running trials with angle bias applied to the markerless results, from the initial musculoskeletal analysis. RMSEs computed as the difference between both curves through all timeframes.

For the hip flexion angle curves, there seems to be an almost constant offset between the two curves for all loading conditions in both walking and running trials. This suggests that the angle bias applied might have been insufficient for the two curves to align. In fact, Appendix I presents results of markerless kinematics during dynamic trials before bias adjustments are performed. When adjusting biases knee flexion RMSEs are reduced from 5.8–12.6° to 3.2–4.3° and ankle flexion RMSEs are lowered from 9.5–12° to 6–8.3°. However, differences in hip flexion RMSEs before and after the bias adjustment seem more complex. Plots in Appendix I indicate that the marker-based motion capture system measures an increase in hip flexion over the entire gait cycle through loading conditions, resulting in the hip flexion curve moving upwards through conditions. However, literature reports that hip flexion does not increase during the entire gait cycle when loads are increased. Rather, hip flexion increases at heel strike and hip extension increases at toe-off, thus increasing hip range of motion (ROM) [4]. While hip flexion RMSEs varied between 7.1° and 17.2° before adjusting for bias, they range between 7.4° and 10.5° afterwards. This would indicate that biases adjustments have not successfully reduced hip flexion RMSEs in all loading conditions. Therefore, there is a need to clarify the values of angle bias between the Theia3D standard markerless model and the OpenSim Rajagopal model.

In addition to RMSEs, the results of joint angles were also compared using Pearson's correlation coefficient. Before computing Pearson's correlation coefficient, a kurtosis test was performed to verify that the difference data was normal. Average kurtosis results of 2.5, 2.7, and 2.9 were found at the hip, knee, and ankle respectively for walking and running trials. These values were deemed sufficiently close to a mesokurtic distribution to assume normality in kinematics differences. Table G.2 displays the correlation coefficient results for the ankle, knee, and hip joint angles of marker-based and markerless data through all loading conditions for walking and running trials. Looking at the values presented in Table G.2, all of them suggest a very strong correlation between the motion capture systems. Knee flexion results show the best correlation with minimal correlation coefficients of 0.992 and 0.991 for walking and running trials, respectively. Hip flexion results also show very strong correlation with minimal correlation coefficients of 0.968 for walking trials and 0.969 for running trials. Only the correlation coefficient for the ankle flexion in loading condition C4 of the walking trials is on the limit between strong and very strong correlation, with a value of 0.899.

Table G.2: Pearson's correlation coefficient for the ankle, knee, and hip joint angles of marker-based and markerless data through all loading conditions for walking and running trials, from the initial musculoskeletal analysis

			Joint		
			Hip	Knee	Ankle
Walking trials	Loading condition	C1	0.985	0.994	0.906
		C2	0.979	0.993	0.932
		C3	0.968	0.992	0.941
		C4	0.980	0.992	0.899
Running trials		C1	0.969	0.993	0.931
		C2	0.973	0.995	0.948
		C3	0.978	0.994	0.955
		C4	0.975	0.991	0.937

Finally, Bland-Altman limits of agreement (LOA) were also computed to quantify the agreement between the motion capture systems. Table G.3 presents means of the Bland-Altman limits of agreement for the ankle, knee, and hip joint angles of marker-based and markerless data through all loading conditions for walking and running trials. All values in Table G.3 are in units of degrees (°), the same unit used to measure the joint angles previously. Results look best at the

knee level with low mean difference between the systems. Walking trials experienced a maximal 1.96° of mean difference for knee flexion in C4, while running trials displayed a maximal mean difference of 1.88° for knee flexion in C3. The largest mean differences were observed for the hip flexion, where maximal values of 9.56° and 8.38° of mean difference were computed for walking trials in C1 and running trials in C3.

Table G.3: Bland-Altman limits of agreement for the ankle, knee, and hip joint angles of marker-based and markerless data through all loading conditions for walking and running trials, from the initial musculoskeletal analysis

			Joint		
			Hip (°)	Knee (°)	Ankle (°)
Walking trials	Loading condition	C1	9.56 ± 5.83	-0.06 ± 4.65	3.74 ± 6.06
		C2	6.03 ± 7.12	0.06 ± 4.72	5.23 ± 6.05
		C3	7.88 ± 8.68	1.35 ± 4.97	6.52 ± 5.92
		C4	7.38 ± 8.14	1.96 ± 5.17	5.12 ± 6.78
Running trials		C1	7.86 ± 7.42	0.62 ± 4.95	4.84 ± 7.98
		C2	6.14 ± 6.98	0.64 ± 4.50	6.42 ± 7.19
		C3	8.38 ± 6.72	1.88 ± 4.41	7.35 ± 6.84
		C4	7.68 ± 6.52	1.72 ± 5.11	5.32 ± 7.95

Table G.4 presents a comparison of average maximum residuals between marker-based and markerless motion capture systems through all loading conditions for walking and running trials. Values of residuals have been normalized as percentage of maximal GRFs. From the results presented in Table G.4, the marker-based motion capture model seems to have lower residual forces for most of the trials. Marker-based average maximum residuals vary between 1.6 and 12.5% of maximal anteroposterior GRFs, 1.5 and 4.2% of maximal vertical GRFs and 7.1 and 30.2% of maximal mediolateral GRFs. However, while markerless average maximum residuals do not differ so much from the marker-based ones in the anteroposterior and vertical directions, they are considerably larger in the mediolateral direction with values between 17.2 and 88.3% of maximal mediolateral GRFs. The highest value of residual force is observed during running trials in loading condition C4 in the *z*-direction for the markerless system.

Table G.4: Comparison of average maximum residuals between marker-based and markerless motion capture systems through all loading conditions for walking and running trials, from the initial musculoskeletal analysis

		Motion capture system	Marker-based	Markerless	Marker-based	Markerless	Marker-based	Markerless
			Anteroposterior residual F_x (% of max. GRF)		Vertical residual F_y (% of max. GRF)		Mediolateral residual F_z (% of max. GRF)	
Walking trials	Loading condition	C1	1.6	2.5	1.5	2.4	9.6	18.1
		C2	2.6	5.8	2.0	2.9	7.1	31.9
		C3	3.8	11.3	3.1	3.0	13.0	58.2
		C4	6.9	18.9	4.2	1.8	14.4	67.6
Running trials		C1	2.9	4.0	1.7	2.3	7.6	17.2
		C2	7.5	9.0	2.0	2.8	11.3	29.6
		C3	11.8	17.7	2.0	2.2	15.8	65.4
		C4	12.5	24.1	2.4	2.0	30.2	88.3

G3. Muscle activation comparison

Figure G.3 presents the results of the muscle activation for the gastrocnemius lateralis and medialis when estimated from marker-based motion capture data (red) and markerless motion capture data (blue) for walking trials. Muscle activation measured by EMG sensors placed on the participants during the trials is also displayed in these plots (green). From, it can be observed that all curves peak around 40–50% of the gait cycle. RMSEs between the muscle activation estimated from the marker-based and markerless data do appear dependent on loading condition. While a minimal gastrocnemius lateralis RMSE value of 0.087 is observed for walking trials in C4, a maximal value of 0.109 is observed for walking trials in C3. The same goes for the gastrocnemius medialis where minimal and maximal values of 0.085 and 0.106 are observed in C4 and C3, respectively.

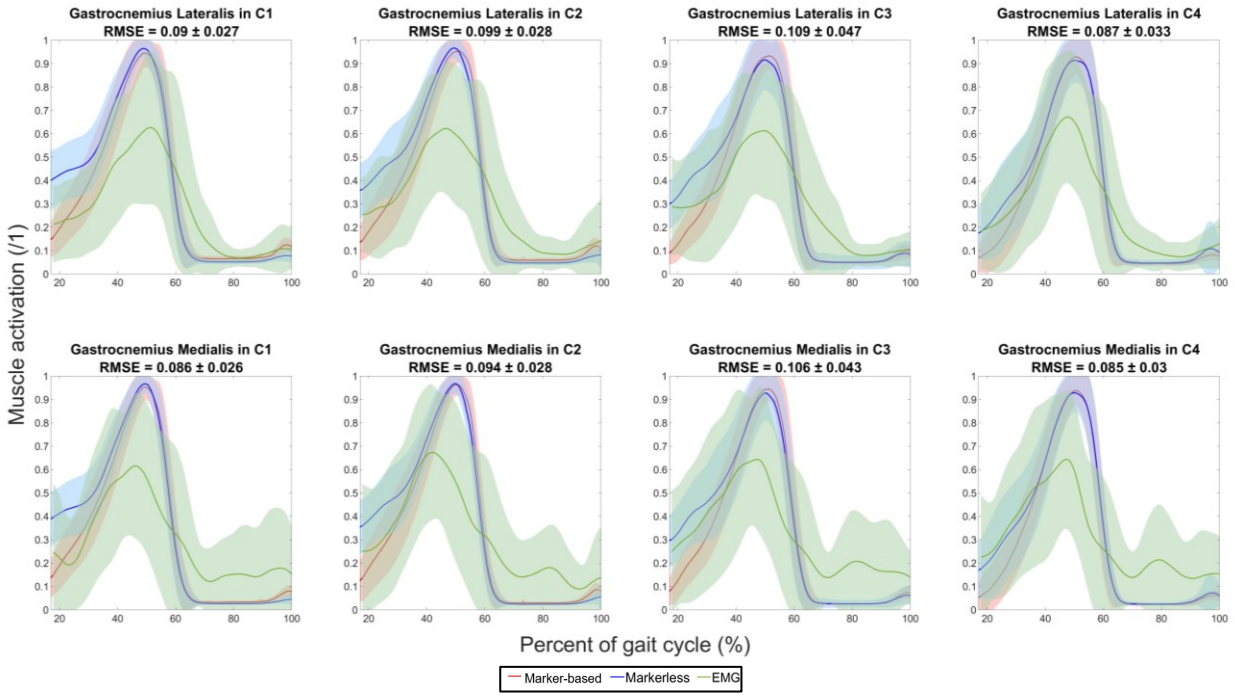

Figure G.3: Plots of gastrocnemius lateralis and medialis muscle activity as measured by EMG sensors and estimated from the marker-based and markerless data through gait under all loading conditions for walking trials, from the initial musculoskeletal analysis. RMSEs computed as the difference between the motion capture curves through all timeframes.

Muscle activation from running trials is also presented in Figure G.4 which presents data from marker-based and markerless motion capture, as well as EMG sensors. Again, all curves appear to peak around 30–40% of gait cycle. Gastrocnemius lateralis RMSE values vary between 0.098 and 0.121. As for gastrocnemius medialis RMSE values, they vary between 0.106 and 0.134.

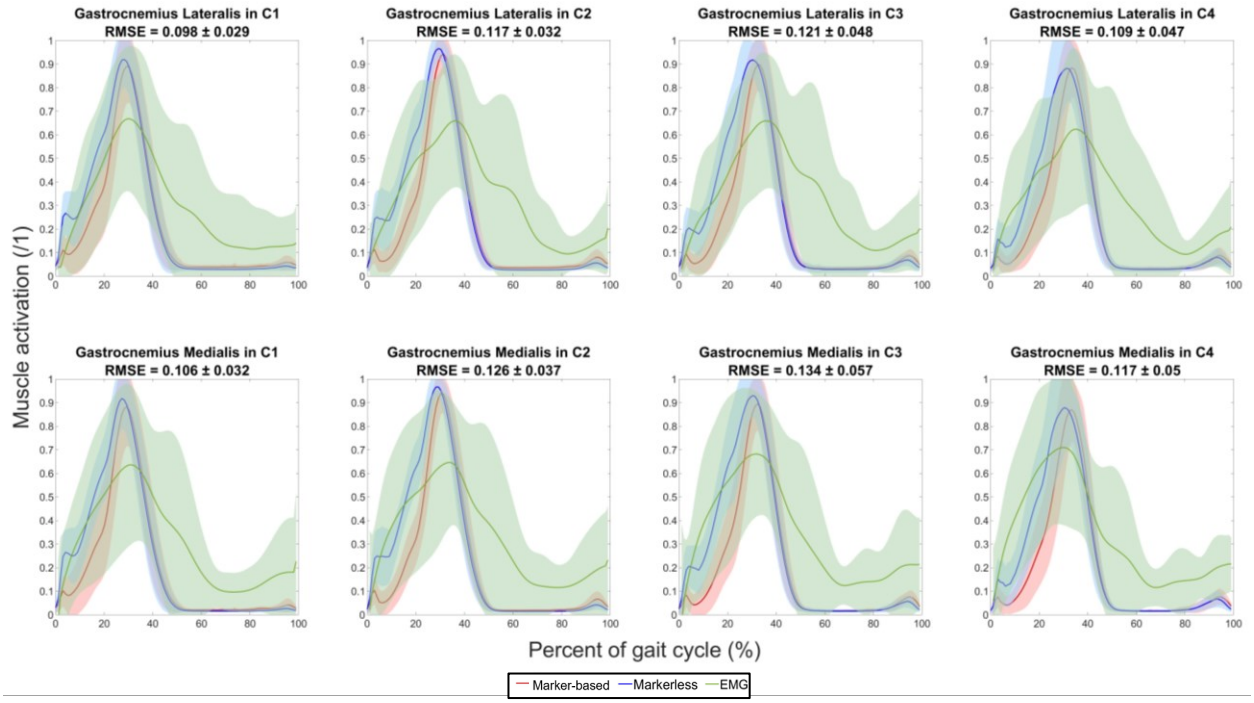

Figure G.4: Plots of gastrocnemius lateralis and medialis muscle activity as measured by EMG sensors and estimated from the marker-based and markerless data through gait under all loading conditions for running trials, from the initial musculoskeletal analysis. RMSEs computed as the difference between the motion capture curves through all timeframes.

G4. Joint loading comparison

Figure G.5 presents a plot of the magnitude of lower limbs' joint reaction forces through gait under all loading conditions for walking trials. Looking at RMSE values, the motion capture systems still seem in best agreement for the knee joint reaction force where RMSEs vary between 0.27 xBW and 0.383 xBW. The ankle reaction force seems to be increasing with increasing load. RMSE values for the ankle joint reaction forces go from 0.446 xBW in C1 up to 0.784 xBW in C4. As for the hip reaction force, RMSE values vary between 0.474 xBW and 0.567 xBW.

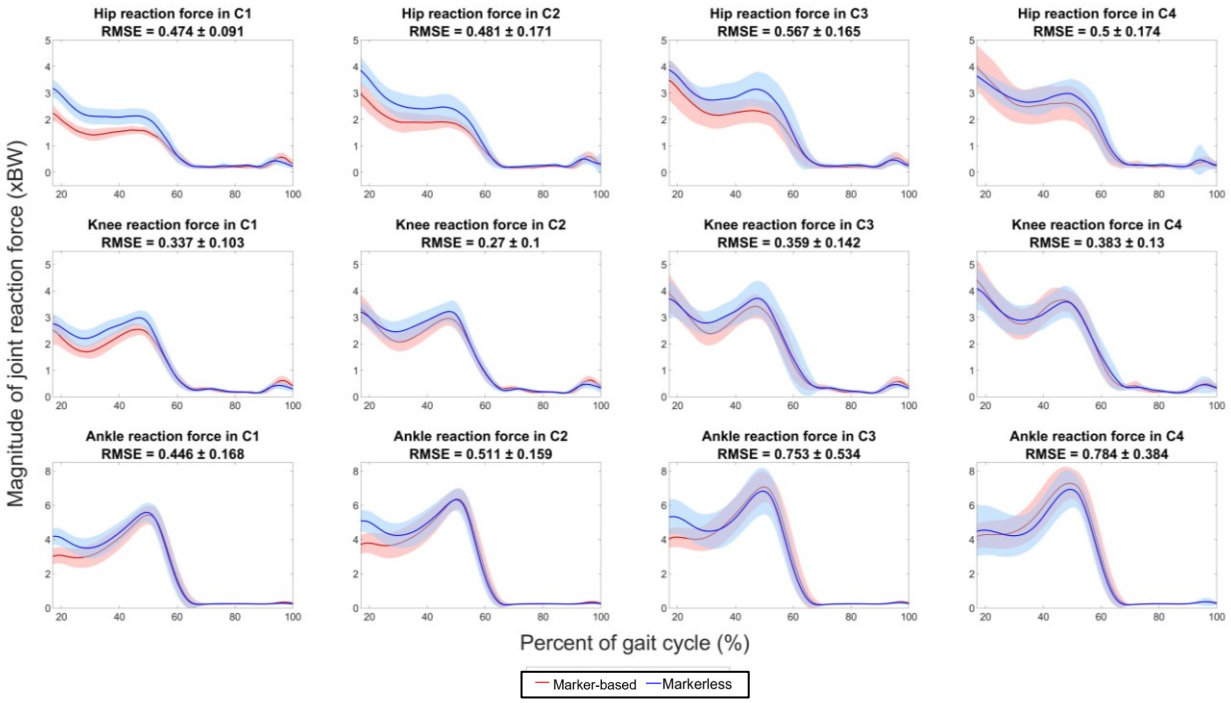

Figure G.5: Plots of lower limb joint reaction forces through gait under all loading conditions for walking trials, from the initial musculoskeletal analysis. RMSEs computed as the difference between both curves through all timeframes.

Figure G.6 presents subplots of lower limbs' joint reaction forces through gait under all loading conditions. Like the results for walking trials, knee joint reaction forces present the best values of RMSE with values between 0.44 xBW and 0.547 xBW. These values of knee reaction force RMSE are larger than the ones found for walking trials. This does not appear to be so much the case for the hip reaction forces where RMSE values between 0.469 xBW and 0.537 xBW are similar to the ones computed for walking trials. The worst values of RMSE are observed at the ankle joint reaction forces where they range between 0.632 xBW and 0.969 xBW.

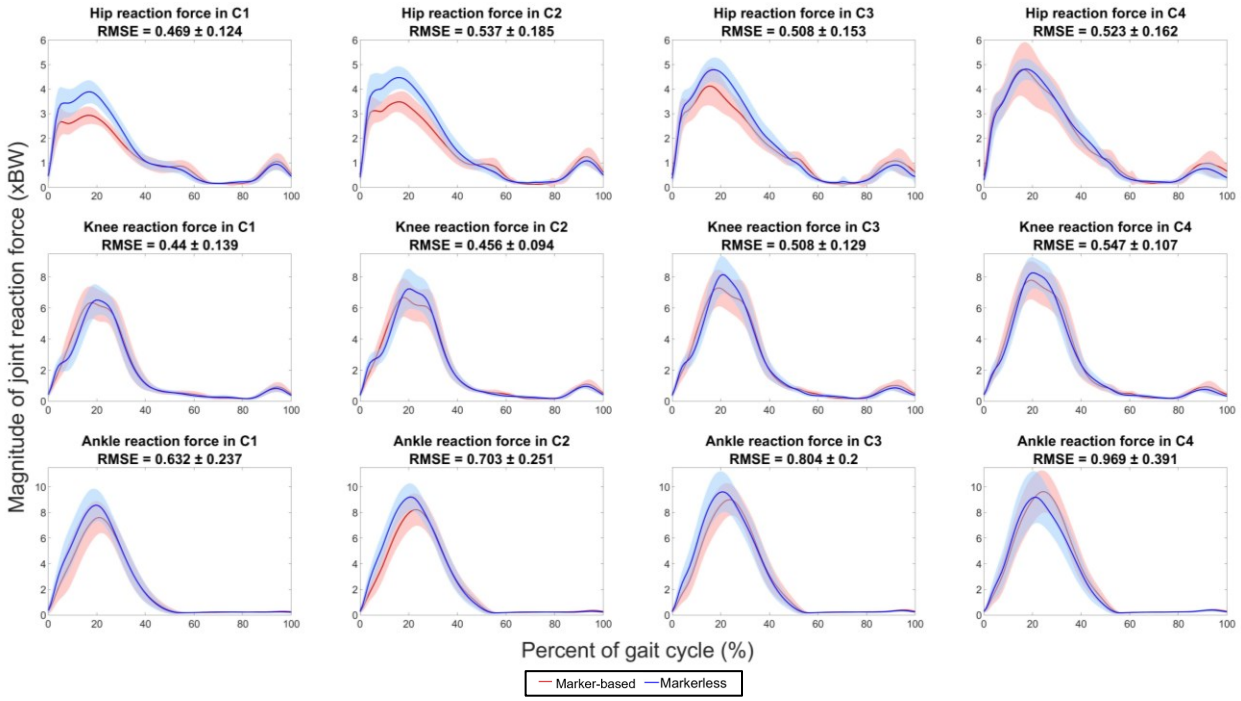

Figure G.6: Plots of lower limb joint reaction forces through gait under all loading conditions for running trials, from the initial musculoskeletal analysis. RMSEs computed as the difference between both curves through all timeframes.

Pearson's correlation coefficient was computed between data from the marker-based and markerless motion capture systems to test their correlation. Average kurtosis results of 2.4, 3.9, and 3.4 were found at the hip, knee, and ankle, respectively for all trials. Table G.5 presents the resulting coefficients for the ankle, knee, and hip joint angles of marker-based and markerless data through all loading conditions for walking and running trials. Again, all of them indicate a very strong correlation between the curves, i.e., values above 0.90.

Table G.5: Pearson's correlation coefficient for the ankle, knee, and hip joint reaction forces of marker-based and markerless data through all loading conditions for walking and running trials, from the initial musculoskeletal analysis

			Joint		
			Hip	Knee	Ankle
Walking trials	Loading condition	C1	0.978	0.984	0.986
		C2	0.982	0.987	0.983
		C3	0.970	0.982	0.980
		C4	0.970	0.978	0.988
Running trials		C1	0.982	0.983	0.991
		C2	0.982	0.984	0.986
		C3	0.977	0.983	0.986
		C4	0.979	0.985	0.986

Table G.6 presents the results of the mean difference with corresponding LOA for the ankle, knee, and hip joint angles of marker-based and markerless data through all loading conditions for walking and running trials. The knee joint reaction forces displayed the lowest mean difference with values ranging between -0.01 xBW and 0.18 xBW for walking trials and between -0.07 xBW and 0 xBW for running trials. LOA were the widest for ankle joint reaction forces with values going up to 1.65 xBW for running trials in C4.

Table G.6: Bland-Altman limits of agreement for the ankle, knee, and hip joint reaction forces of marker-based and markerless data through all loading conditions for walking and running trials, from the initial musculoskeletal analysis

			Joint		
			Hip (xBW)	Knee (xBW)	Ankle (xBW)
Walking trials	Loading condition	C1	0.31 ± 0.72	0.18 ± 0.55	0.18 ± 0.76
		C2	0.31 ± 0.71	0.10 ± 0.47	0.16 ± 0.90
		C3	0.31 ± 0.87	0.12 ± 0.62	0.04 ± 1.23
		C4	0.10 ± 0.81	-0.01 ± 0.67	-0.16 ± 1.18
Running trials		C1	0.22 ± 0.81	-0.07 ± 0.82	0.24 ± 1.08
		C2	0.26 ± 0.92	0.00 ± 0.86	0.26 ± 1.25
		C3	0.16 ± 0.91	0.00 ± 0.96	0.16 ± 1.41
		C4	-0.01 ± 0.90	-0.04 ± 1.02	-0.13 ± 1.65

Appendix H – Participant angle bias per loading condition for the hip, knee, and ankle flexion

Table H.1: Participant angle bias per loading condition for the hip, knee, and ankle flexion

Participant_LoadingCondition	'hip_flexion_r'	'knee_angle_r'	'ankle_angle_r'
P01_c1	-0.38	7.06	-11.32
P01_c2	-0.74	7.22	-10.95
P01_c3	-0.83	6.94	-7.24
P01_c4	5.22	8.52	-11.13
P02_c1	4.63	4.77	-8.12
P02_c2	5.73	5.30	-8.53
P02_c3	9.72	5.90	-5.53
P02_c4	8.58	5.07	-7.50
P03_c1	10.54	4.12	-16.84
P03_c2	4.88	4.77	-14.70
P03_c3	7.97	4.52	-13.54
P03_c4	12.25	6.99	-11.79
P04_c1	-4.27	5.24	-2.10
P04_c2	4.72	8.42	-1.93
P04_c3	12.13	7.66	0.94
P04_c4	15.39	8.09	0.11
P05_c1	2.88	8.67	-4.86
P05_c2	5.16	8.41	-6.07
P05_c3	16.37	8.53	-3.51
P05_c4	13.74	13.36	-2.53
P06_c1	4.57	12.44	-7.09
P06_c2	7.02	7.22	-7.06
P06_c3	15.10	9.98	-5.95
P06_c4	21.72	12.74	-3.79
P07_c1	0.14	6.49	0.90
P07_c2	-1.35	7.23	0.37
P07_c3	9.11	8.73	4.43
P07_c4	10.76	9.61	3.88
P08_c1	-7.44	5.60	-12.06
P08_c2	-11.69	4.44	-6.16
P08_c3	-5.10	3.41	-2.48
P08_c4	-0.49	4.60	-5.51
P09_c1	9.27	13.59	-3.41

P09_c2	6.44	10.64	-5.90
P09_c3	11.96	9.40	-8.09
P09_c4	10.21	9.28	-6.89
P10_c1	-2.08	1.44	-7.33
P10_c2	-2.32	-0.51	-9.81
P10_c3	3.72	3.24	-9.04
P10_c4	7.61	4.51	-6.15
P11_c1	2.06	6.83	-2.76
P11_c2	3.04	7.46	-2.97
P11_c3	6.03	6.57	-2.85
P11_c4	19.51	10.04	-6.29
P12_c1	-2.69	-2.18	-10.46
P12_c2	-2.50	0.13	-7.32
P12_c3	10.30	2.98	-5.20
P12_c4	16.15	7.53	-3.35
P13_c1	-1.32	2.67	-6.36
P13_c2	0.43	3.66	-7.17
P13_c3	4.54	5.80	-1.77
P13_c4	9.06	6.90	-3.93
P14_c1	3.19	3.91	-9.76
P14_c2	6.26	7.39	-2.87
P14_c3	15.41	8.19	-6.67
P14_c4	7.79	14.03	-5.32
P15_c1	1.37	1.37	-15.87
P15_c2	2.94	3.66	-10.43
P15_c3	19.78	10.17	-10.98
P15_c4	37.84	20.83	-7.12
P16_c1	-1.73	-1.85	-15.60
P16_c2	-3.20	2.11	-16.24
P16_c3	4.90	7.09	-11.24
P16_c4	4.85	5.33	-14.10

Appendix I – Plots of lower limb joint angles from the initial musculoskeletal analysis without angle bias applied

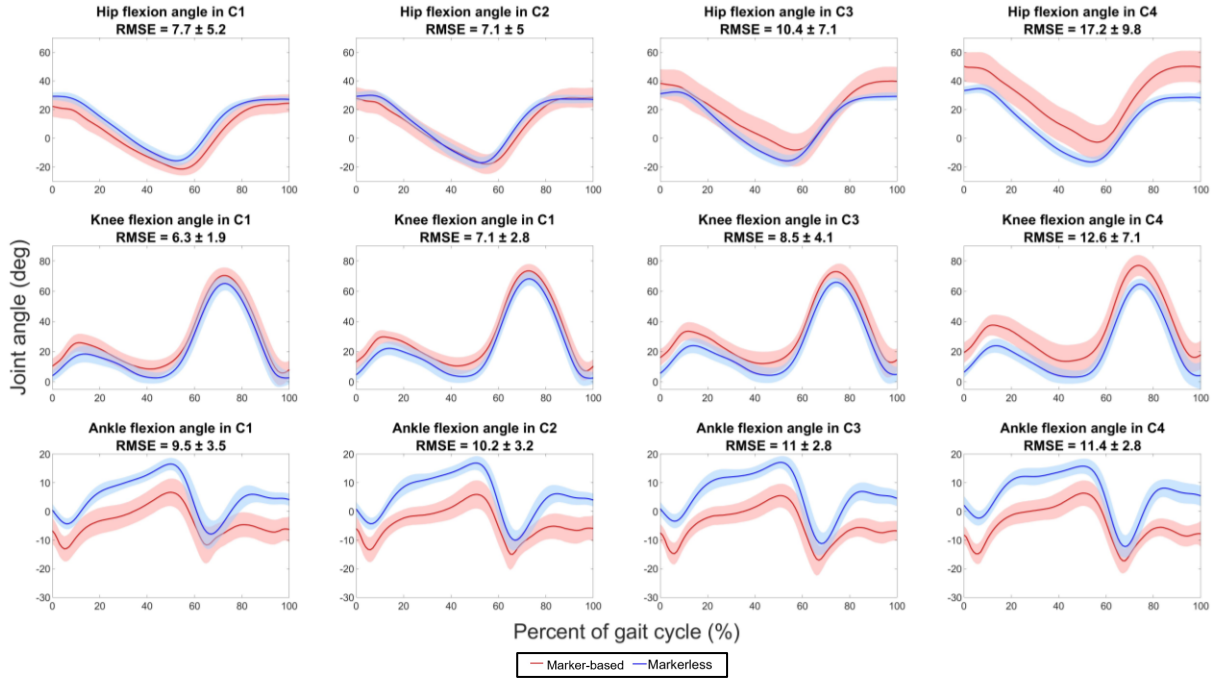

Figure I.1: Plots of lower limb joint angles for a full gait cycle under all loading conditions for walking trials without angle bias applied to the markerless results

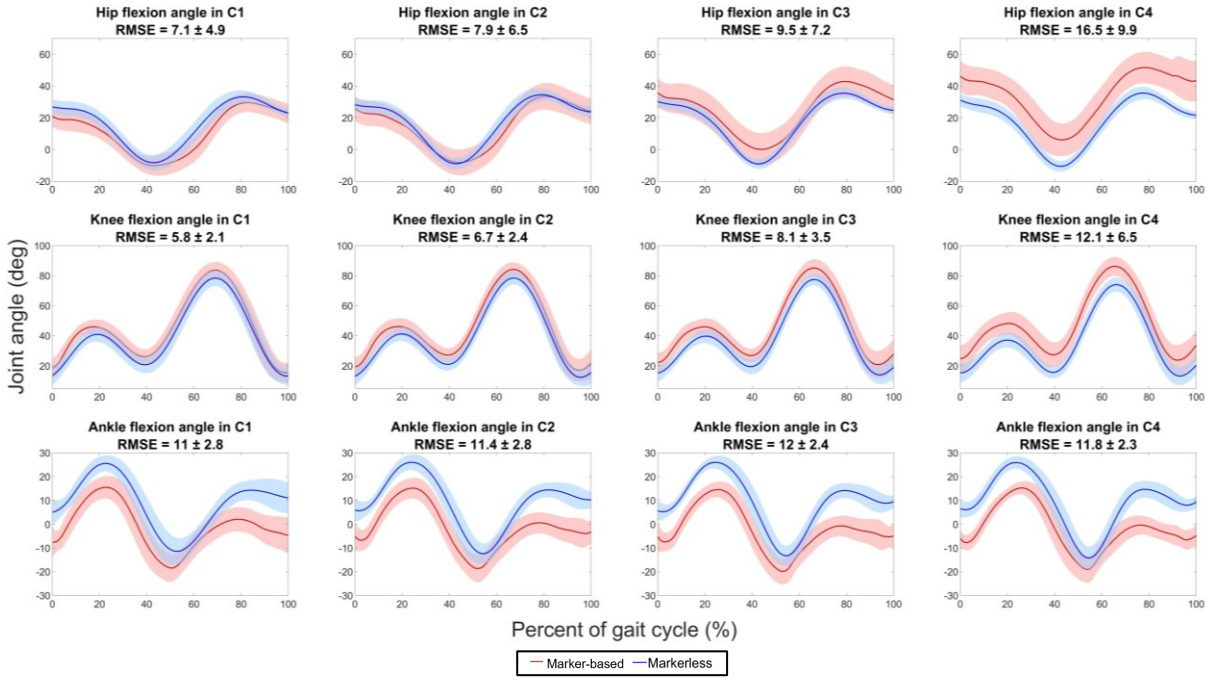

Figure I.2: Plots of lower limb joint angles for a full gait cycle under all loading conditions for running trials without angle bias applied to the markerless results

Appendix J – Plots of lower limb muscle activation

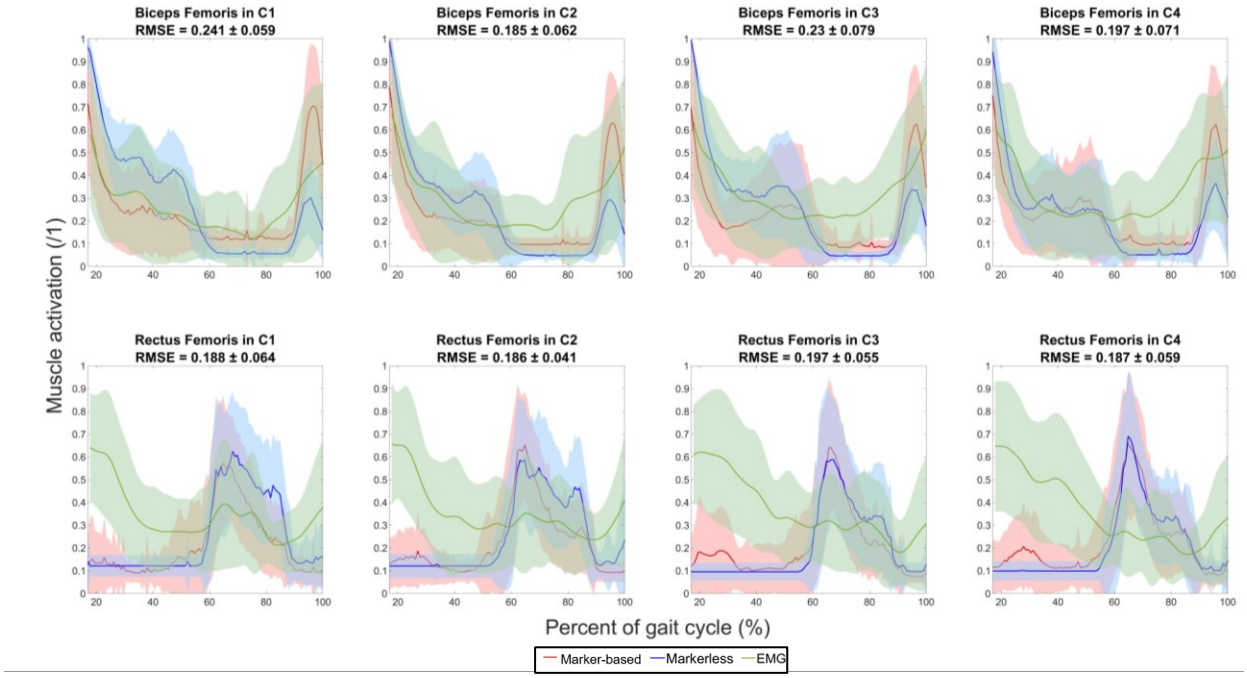

Figure J.1: Plots of biceps and rectus femoris muscle activity as measured by EMG sensors and estimated from the marker-based and markerless data through gait under all loading conditions for walking trials. RMSEs computed as the difference between the motion capture curves through all timeframes.

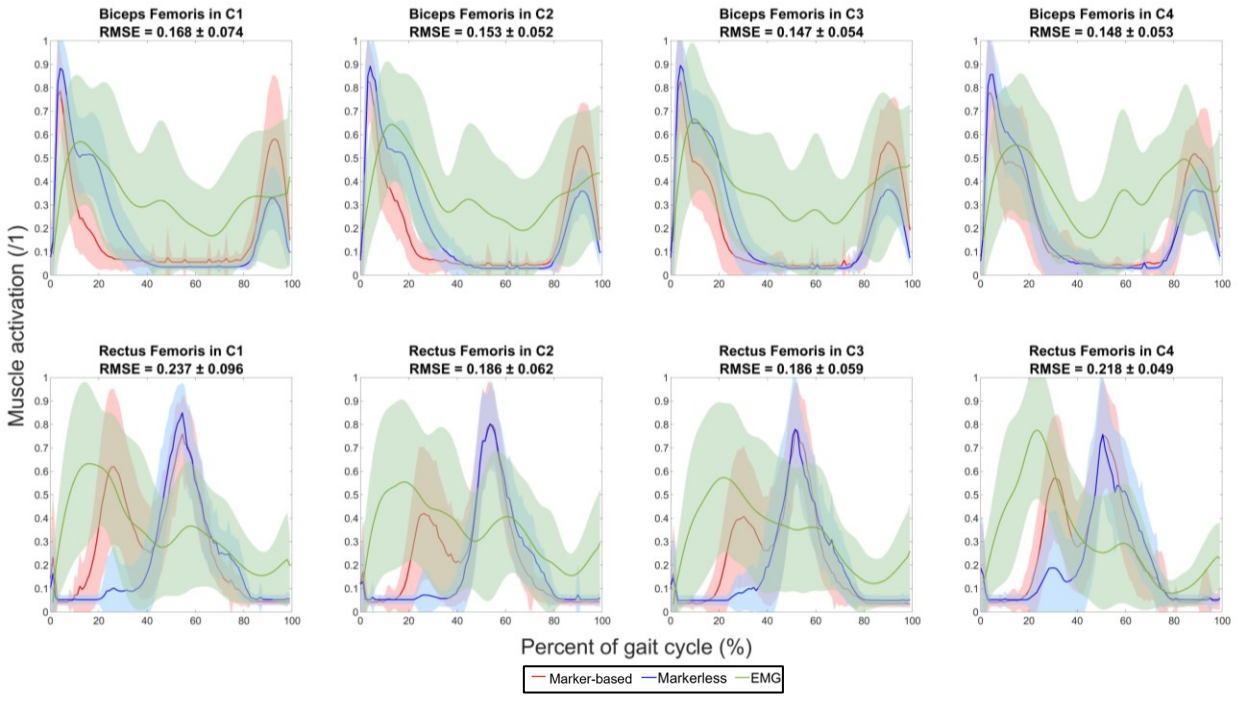

Figure J.2: Plots of biceps and rectus femoris muscle activity as measured by EMG sensors and estimated from the marker-based and markerless data through gait under all loading conditions for running trials. RMSEs computed as the difference between the motion capture curves through all timeframes.

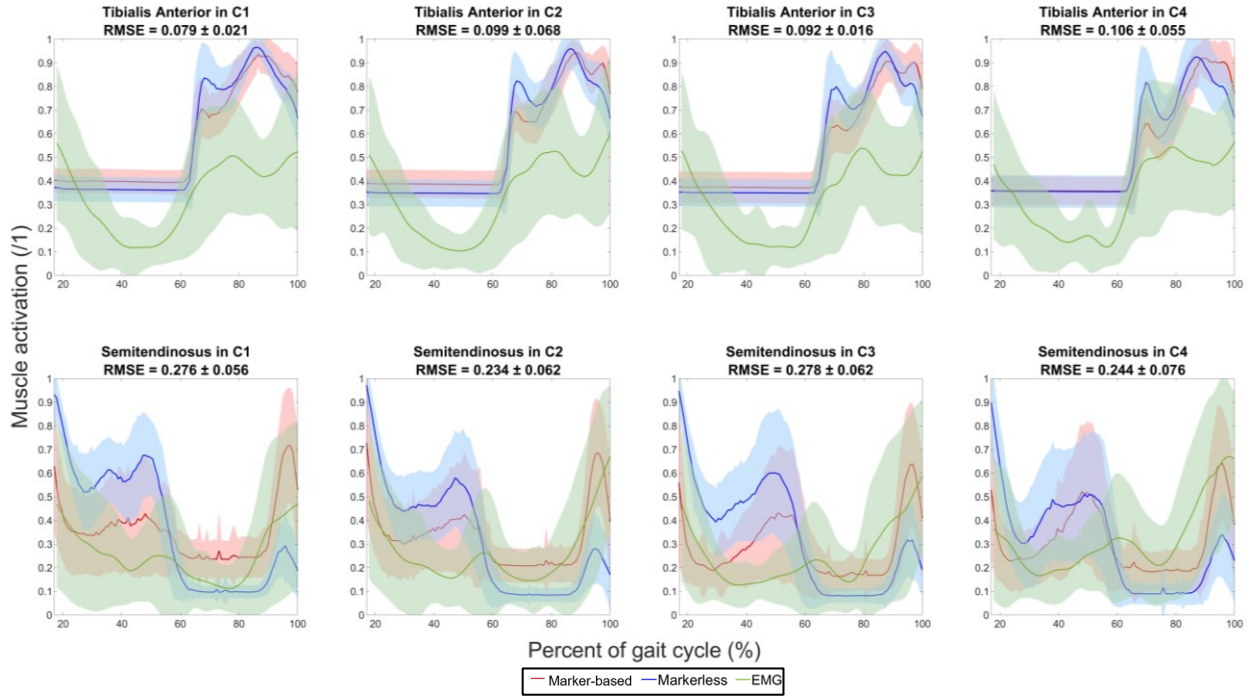

Figure J.3: Plots of tibialis anterior and semitendinosus muscle activity as measured by EMG sensors and estimated from the marker-based and markerless data through gait under all loading conditions for walking trials. RMSEs computed as the difference between the motion capture curves through all timeframes.

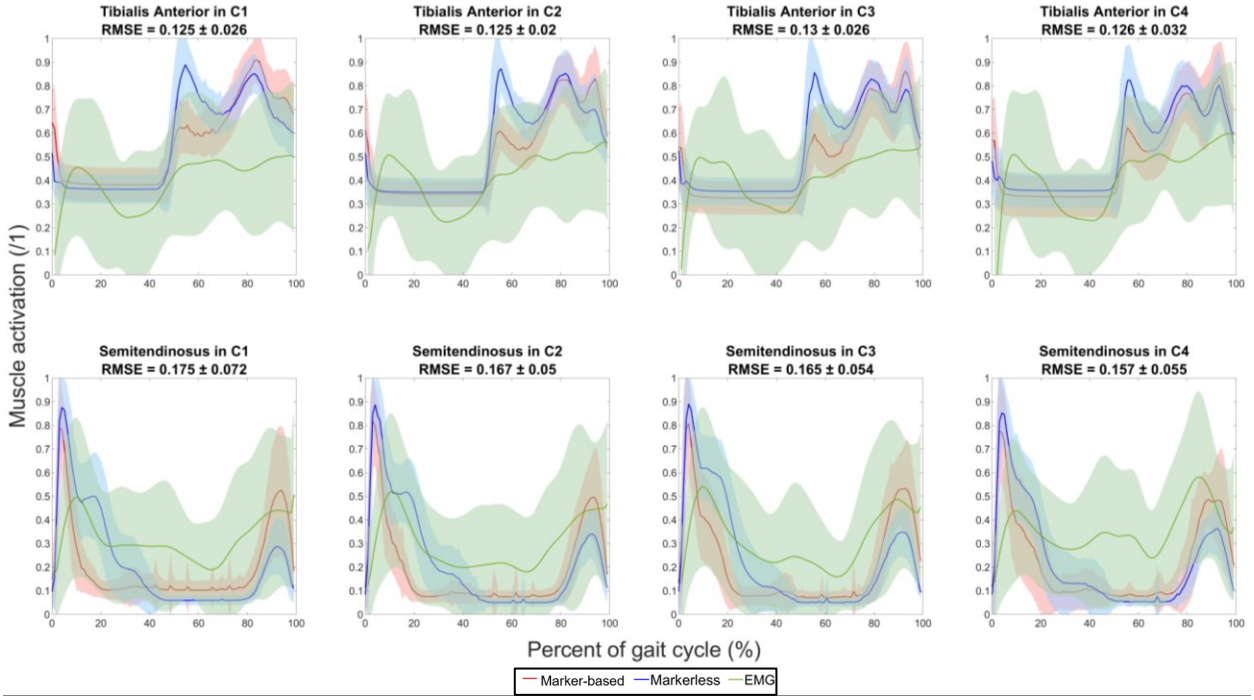

Figure J.4: Plots of tibialis anterior and semitendinosus muscle activity as measured by EMG sensors and estimated from the marker-based and markerless data through gait under all loading conditions for running trials. RMSEs computed as the difference between the motion capture curves through all timeframes.

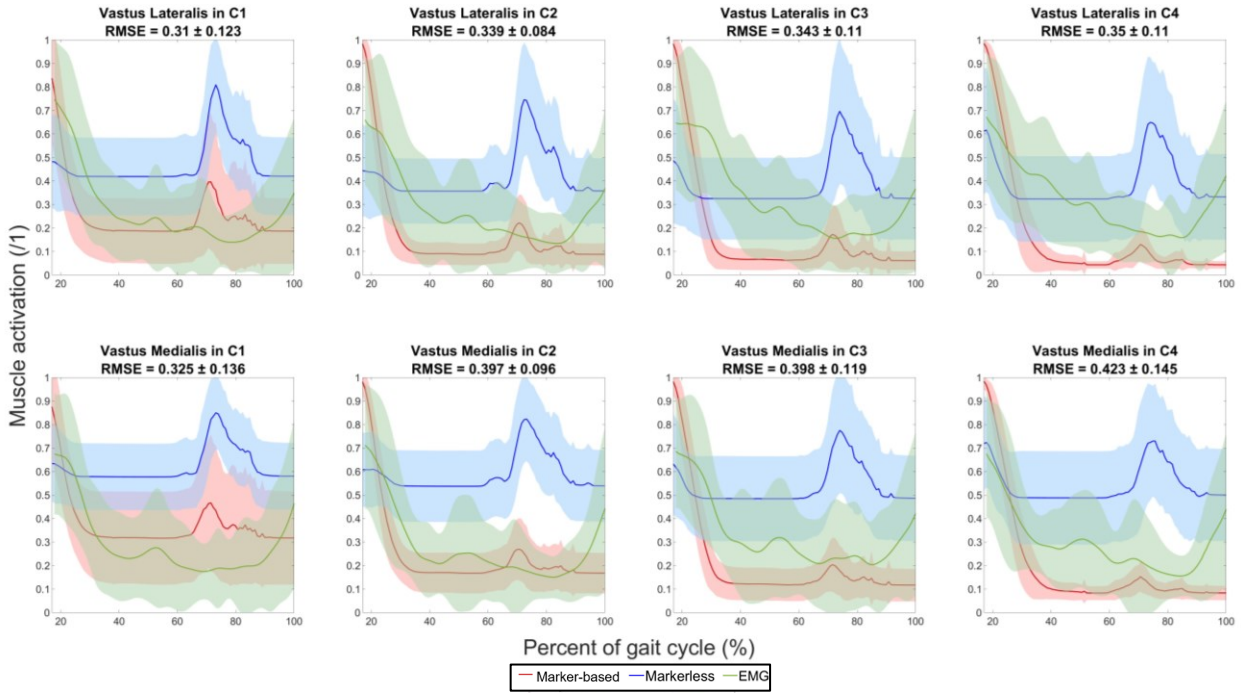

Figure J.5: Plots of vastus lateralis and medialis muscle activity as measured by EMG sensors and estimated from the marker-based and markerless data through gait under all loading conditions for walking trials. RMSEs computed as the difference between the motion capture curves through all timeframes.

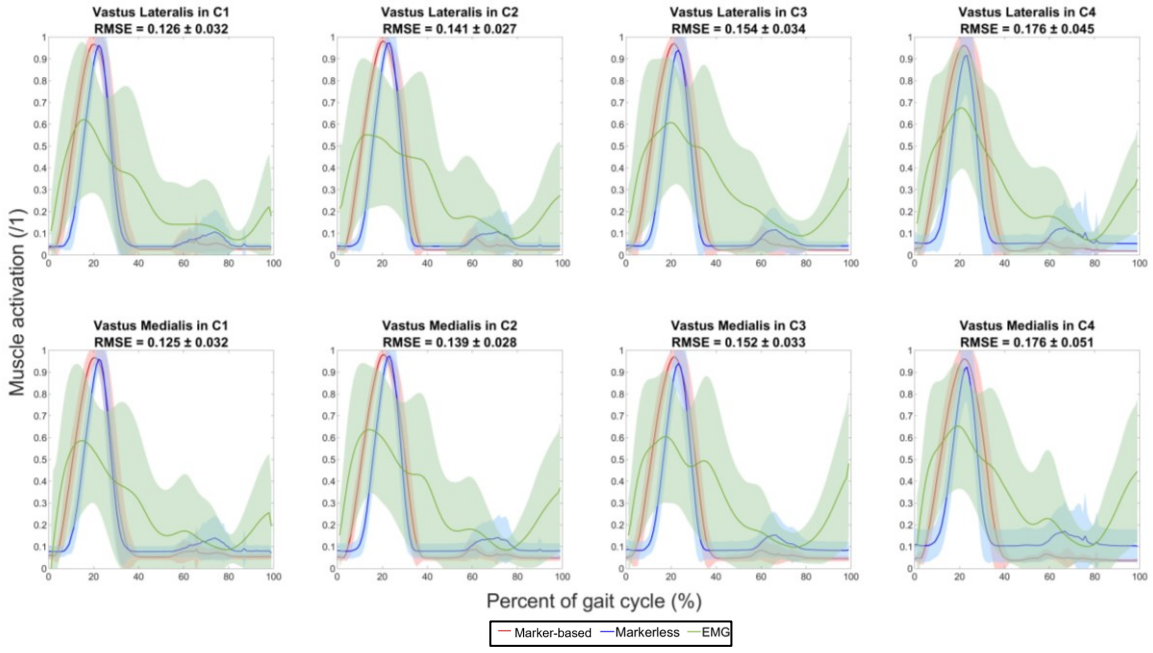

Figure J.6: Plots of vastus lateralis and medialis muscle activity as measured by EMG sensors and estimated from the marker-based and markerless data through gait under all loading conditions for running trials. RMSEs computed as the difference between the motion capture curves through all timeframes.

Appendix K – Summary of recommendations for using Theia3D data in OpenSim

The following includes a list of the decisions taken at each step of the markerless musculoskeletal analysis. It can serve as a starting point for researchers wanting to replicate the study or use Theia3D data in OpenSim analyses. The reader is also referred to Figure 4 and Figure 5 which present an overview of the different steps followed to process and analyze the markerless data.

A. Theia3D via Vicon Nexus

Once all trials in a session have been recorded, the "Theia Batch Interface" allows to process all trials of a specific folder through Theia3D. No specific decisions were taken at this step as Theia3D uses a black box algorithm to estimate biomechanical information from video data. After this step, *.c3d* files with the pose information are created. One of them is filtered and the other one isn't. In these files, the 4x4 pose matrices of all segments from Theia3D's model as well as the coordinates of some anatomical landmarks are included.

B. Visual3D

Information can be extracted from the *.c3d* files created by Theia3D, via Visual3D. It is important to note that the Theia3D Visual3D model has already been applied on these *.c3d* files, and thus there is no need to create or compute a model when opening the file in Visual3D. Files containing the trial's 4x4 pose matrices and joint centre coordinates will be required to run the musculoskeletal analysis in Matlab. In Visual3D, two pipelines were created to export this information in the form of *.mat* (Matlab) files.

1. The first pipeline exports the 4x4 pose matrices for all segments of the Theia3D model through all timeframes of a trial. The pipeline loops through all listed filtered *.c3d* files and uses the "Export_Data_To_Matfile" pipeline to extract information. This data will serve to compute the corresponding joint angles. A sample of that pipeline is included below.

```
For_Each
/ITERATION_PARAMETER_NAME=INDEX
/ITEMS=                                c1_bikerpose+c1_walk01+c1_walk02+c1_walk03+c1_run01+c1_run02+c1_run03+
c2_bikerpose+c2_walk01+c2_walk02+c2_walk03+c2_run01+c2_run02+c2_run03+c3_bikerpose+c3_walk01+c3_walk02+c3_
walk03+c3_run01+c3_run02+c3_run03+c4_bikerpose+c4_walk01+c4_walk02+c4_walk03+c4_run01+c4_run02+c4_run03
;

File_New
;

File_Open
/FILE_NAME=D:\...\P01\22-06-2022\Theia\P01_&::INDEX&_c3d\pose_filt_0.c3d
;

Export_Data_To_Matfile
/SIGNAL_TYPES=ROTATION+ROTATION+ROTATION+ROTATION+ROTATION+ROTATION+ROTATION+ROTATION+ROTATION+ROTATION+RO
TATION+ROTATION+ROTATION+ROTATION+ROTATION+ROTATION
/SIGNAL_FOLDER=ORIGINAL+ORIGINAL+ORIGINAL+ORIGINAL+ORIGINAL+ORIGINAL+ORIGINAL+ORIGINAL+ORIGINAL+ORIGINAL+O
RIGINAL+ORIGINAL+ORIGINAL+ORIGINAL+ORIGINAL+ORIGINAL
/SIGNAL_NAMES=l_foot_4X4+l_larm_4X4+l_shank_4X4+l_thigh_4X4+l_toes_4X4+l_uarm_4X4+pelvis_4X4+pelvis_shifte
d_4X4+r_foot_4X4+r_larm_4X4+r_shank_4X4+r_thigh_4X4+r_toes_4X4+r_uarm_4X4+torso_4X4+worldbody_4X4
/FILE_NAME=D:\Isa_Project\ProcessedFiles_Theia\P01_&::INDEX&_JA.mat
/MATLAB_NAMES=l_foot+l_arm+l_shank+l_thigh+l_toes+l_uarm+pelvis+pelvis_shifted+r_foot+r_larm+r_shank+r_thi
gh+r_toes+r_uarm+torso+worldbody
/USE_NAN_FOR_DATANOTFOUND=TRUE
;

End_For_Each
/ITERATION_PARAMETER_NAME=INDEX
;
```

2. The second pipeline exports the coordinates of anatomical landmarks in the Theia3D model, i.e. the joint centres and the segments' centre of gravity. These coordinates exported through the entire trial will be used in OpenSim as "markers". The second pipeline also loops through all listed filtered *.c3d*. It first makes sure that the thorax depth is properly set. Then, it computes the coordinates of all required landmarks using the "Compute_Model_Based_Data" pipeline. Finally, all information is exported using the "Export_Data_To_Matfile" pipeline. Again, a sample of that pipeline is included below.

```
For_Each
/ITERATION_PARAMETER_NAME=INDEX
/ITEMS=
c1_bikerpose+c1_walk01+c1_walk02+c1_walk03+c1_run01+c1_run02+c1_run03+c2_bikerpose+c2_walk01+c2_walk02+c2_
walk03+c2_run01+c2_run02+c2_run03+c3_bikerpose+c3_walk01+c3_walk02+c3_walk03+c3_run01+c3_run02+c3_run03+c4
_bikerpose+c4_walk01+c4_walk02+c4_walk03+c4_run01+c4_run02+c4_run03
;

File_New
;

File_Open
/FILE_NAME=D:\Isa_Project\Backup_F\P01\22-06-2022\Theia\P01_&::INDEX&_c3d\pose_filt_0.c3d
;

Metric_Explicit
/RESULT_METRIC_NAME=THORAX_DEPTH
/METRIC_VALUE=0.55*DISTANCE(MODEL::ROTATION::R_UARM_2X4,MODEL::ROTATION::L_UARM_4X4)
;

Set_Pipeline_Parameter
/PARAMETER_NAME=DEPTH
```

```
/PARAMETER_VALUE=GLOBAL::METRIC::PROCESSED::THORAX_DEPTH
;

Set_Segment_Properties
/CALIBRATION_FILE=
/SEGMENT_NAME=RTA
/MASS=0.355*Mass
/CG_FROM_PROX_AXIAL=0.5*RTA_Seg_Length
/CG_FROM_PROX_ML=0
/CG_FROM_PROX_AP=0
/INERTIA_XX=0.355*Mass*(3*&::DEPTH&^2+RTA_Seg_Length^2)/12
/INERTIA_YY=0.355*Mass*(3*RTA_Distal_Radius^2+RTA_Seg_Length^2)/12
/INERTIA_ZZ=0.355*Mass*(&::DEPTH&^2+RTA_Distal_radius^2)/4
;

Compute_Model_Based_Data
/RESULT_NAME=LToes_position
/FUNCTION=SEG_DISTAL_JOINT
/SEGMENT=LFT
;

Compute_Model_Based_Data
/RESULT_NAME=LFTCG_position
/FUNCTION=SEG_CGPOSITION
/SEGMENT=LFT
;

Compute_Model_Based_Data
/RESULT_NAME=LAnkle_position
/FUNCTION=SEG_PROXIMAL_JOINT
/SEGMENT=LFT
;

Compute_Model_Based_Data
/RESULT_NAME=LSKCG_position
/FUNCTION=SEG_CGPOSITION
/SEGMENT=LSK
;

Compute_Model_Based_Data
/RESULT_NAME=LKnee_position
/FUNCTION=SEG_PROXIMAL_JOINT
/SEGMENT=LSK
;

Compute_Model_Based_Data
/RESULT_NAME=LTHCG_position
/FUNCTION=SEG_CGPOSITION
/SEGMENT=LTH
;

Compute_Model_Based_Data
/RESULT_NAME=LHip_position
/FUNCTION=SEG_PROXIMAL_JOINT
/SEGMENT=LTH
;

Compute_Model_Based_Data
/RESULT_NAME=PVCG_position
/FUNCTION=SEG_CGPOSITION
/SEGMENT=RPV
;

Compute_Model_Based_Data
/RESULT_NAME=Trunk_position
/FUNCTION=SEG_PROXIMAL_JOINT
/SEGMENT=RPV
;
```

```
Compute_Model_Based_Data
/RESULT_NAME=TKCG_position
/FUNCTION=SEG_CGPOSITION
/SEGMENT=RTA
;

Compute_Model_Based_Data
/RESULT_NAME=Neck_position
/FUNCTION=SEG_DISTAL_JOINT
/SEGMENT=RTA
;

Compute_Model_Based_Data
/RESULT_NAME=RToes_position
/FUNCTION=SEG_DISTAL_JOINT
/SEGMENT=RFT
;

Compute_Model_Based_Data
/RESULT_NAME=RFTCG_position
/FUNCTION=SEG_CGPOSITION
/SEGMENT=RFT
;

Compute_Model_Based_Data
/RESULT_NAME=RAnkle_position
/FUNCTION=SEG_PROXIMAL_JOINT
/SEGMENT=RFT
;

Compute_Model_Based_Data
/RESULT_NAME=RSKCG_position
/FUNCTION=SEG_CGPOSITION
/SEGMENT=RSK
;

Compute_Model_Based_Data
/RESULT_NAME=RKnee_position
/FUNCTION=SEG_PROXIMAL_JOINT
/SEGMENT=RSK
;

Compute_Model_Based_Data
/RESULT_NAME=RTHCG_position
/FUNCTION=SEG_CGPOSITION
/SEGMENT=RTH
;

Compute_Model_Based_Data
/RESULT_NAME=RHip_position
/FUNCTION=SEG_PROXIMAL_JOINT
/SEGMENT=RTH
;

Compute_Model_Based_Data
/RESULT_NAME=LFingers_position
/FUNCTION=SEG_DISTAL_JOINT
/SEGMENT=LHA
;

Compute_Model_Based_Data
/RESULT_NAME=LHDCG_position
/FUNCTION=SEG_CGPOSITION
/SEGMENT=LHA
;

Compute_Model_Based_Data
/RESULT_NAME=LWrist_position
/FUNCTION=SEG_PROXIMAL_JOINT
```

```
/SEGMENT=LHA
;

Compute_Model_Based_Data
/RESULT_NAME=LFACG_position
/FUNCTION=SEG_CGPOSITION
/SEGMENT=LFA
;

Compute_Model_Based_Data
/RESULT_NAME=LElbow_position
/FUNCTION=SEG_PROXIMAL_JOINT
/SEGMENT=LFA
;

Compute_Model_Based_Data
/RESULT_NAME=LUACG_position
/FUNCTION=SEG_CGPOSITION
/SEGMENT=LAR
;

Compute_Model_Based_Data
/RESULT_NAME=LShoulder_position
/FUNCTION=SEG_PROXIMAL_JOINT
/SEGMENT=LAR
;

Compute_Model_Based_Data
/RESULT_NAME=RFingers_position
/FUNCTION=SEG_DISTAL_JOINT
/SEGMENT=RHA
;

Compute_Model_Based_Data
/RESULT_NAME=RHDCG_position
/FUNCTION=SEG_CGPOSITION
/SEGMENT=RHA
;

Compute_Model_Based_Data
/RESULT_NAME=RWrist_position
/FUNCTION=SEG_PROXIMAL_JOINT
/SEGMENT=RHA
;

Compute_Model_Based_Data
/RESULT_NAME=RFACG_position
/FUNCTION=SEG_CGPOSITION
/SEGMENT=RFA
;

Compute_Model_Based_Data
/RESULT_NAME=RElbow_position
/FUNCTION=SEG_PROXIMAL_JOINT
/SEGMENT=RFA
;

Compute_Model_Based_Data
/RESULT_NAME=RUACG_position
/FUNCTION=SEG_CGPOSITION
/SEGMENT=RAR
;

Compute_Model_Based_Data
/RESULT_NAME=RShoulder_position
/FUNCTION=SEG_PROXIMAL_JOINT
/SEGMENT=RAR
;
```

```
Export_Data_To_Matfile
/SIGNAL_TYPES=LINK_MODEL_BASED+LINK_MODEL_BASED+LINK_MODEL_BASED+LINK_MODEL_BASED+LINK_MODEL_BASED+LINK_MO
DEL_BASED+LINK_MODEL_BASED+LINK_MODEL_BASED+LINK_MODEL_BASED+LINK_MODEL_BASED+LINK_MODEL_BASED+LINK_MODEL_
BASED+LINK_MODEL_BASED+LINK_MODEL_BASED+LINK_MODEL_BASED+LINK_MODEL_BASED+LINK_MODEL_BASED+LINK_MODEL_BASE
D+LINK_MODEL_BASED+LINK_MODEL_BASED+LINK_MODEL_BASED+LINK_MODEL_BASED+LINK_MODEL_BASED+LINK_MODEL_BASED+LI
NK_MODEL_BASED+LINK_MODEL_BASED+LINK_MODEL_BASED+LINK_MODEL_BASED+LINK_MODEL_BASED+LINK_MODEL_BASED+LINK_M
ODEL_BASED+LINK_MODEL_BASED
/SIGNAL_FOLDER=ORIGINAL+ORIGINAL+ORIGINAL+ORIGINAL+ORIGINAL+ORIGINAL+ORIGINAL+ORIGINAL+ORIGINAL+ORIGINAL+O
RIGINAL+ORIGINAL+ORIGINAL+ORIGINAL+ORIGINAL+ORIGINAL+ORIGINAL+ORIGINAL+ORIGINAL+ORIGINAL+ORIGINAL+ORIGINAL
+ORIGINAL+ORIGINAL+ORIGINAL+ORIGINAL+ORIGINAL+ORIGINAL+ORIGINAL+ORIGINAL+ORIGINAL+ORIGINAL
/SIGNAL_NAMES=LToes_position+LFTCG_position+LAnkle_position+LSKCG_position+LKnee_position+LTHCG_position+L
Hip_position+LFingers_position+LHDCG_position+LWrist_position+LFACG_position+LElbow_position+LUACG_positio
n+LShoulder_position+RToes_position+RFTCG_position+RAnkle_position+RSKCG_position+RKnee_position+RTHCG_pos
ition+RHip_position+RFingers_position+RHDCG_position+RWrist_position+RFACG_position+RElbow_position+RUACG_
position+RShoulder_position+Neck_position+TKCG_position+Trunk_position+PVCG_position
/FILE_NAME=D:\Isa_Project\ProcessedFiles_Theia\P01_&::INDEX&_JC.mat
/MATLAB_NAMES=LToes_position+LFTCG_position+LAnkle_position+LSKCG_position+LKnee_position+LTHCG_position+L
Hip_position+LFingers_position+LHDCG_position+LWrist_position+LFACG_position+LElbow_position+LUACG_positio
n+LShoulder_position+RToes_position+RFTCG_position+RAnkle_position+RSKCG_position+RKnee_position+RTHCG_pos
ition+RHip_position+RFingers_position+RHDCG_position+RWrist_position+RFACG_position+RElbow_position+RUACG_
position+RShoulder_position+Neck_position+TKCG_position+Trunk_position+PVCG_position
/USE_NAN_FOR_DATANOTFOUND=TRUE
;

End_For_Each
/ITERATION_PARAMETER_NAME=INDEX
;
```

C. Matlab

Matlab was used to properly format the information exported from Visual3D. The first script used served to extract joint angles from the 4x4 pose matrices. To do so, the joint coordinate definitions detailed in Table K.1 were used. The output of that script was in the form of a *.mot* file containing the joint angles off coordinates from the Rajagopal OpenSim model.

Table K.1: Methods used for the computation of OpenSim joint angles from Theia3D pose matrices

JOINT	COORDINATE	METHOD
PELVIS	Translation (x, y, z)	Pelvis translation vector
	Tilt	○ Rotate the pelvis matrix -90° around *z* ○ Resulting first XYZ Euler angle
	List	○ Rotate the pelvis matrix -90° around *z* ○ Resulting second XYZ Euler angle
	Rotation	○ Rotate the pelvis matrix -90° around *z* ○ Resulting third XYZ Euler angle
HIP	Flexion	First XYZ Euler angle between the pelvis and thigh
	Adduction	Second XYZ Euler angle between the pelvis and thigh
	Rotation	Third XYZ Euler angle between the pelvis and thigh
KNEE	Flexion	First XYZ Euler angle between the shank and foot
ANKLE	Flexion	First XYZ Euler angle between the pelvis and thigh
SUBTALAR	Inversion	Not evaluated/Value of 0
METATARSO-PHALANGEAL (MTP)	Flexion	Not evaluated/Value of 0
LUMBAR	Extension	First XYZ Euler angle between the pelvis and torso
	Bending	Second XYZ Euler angle between the pelvis and torso
	Rotation	Third XYZ Euler angle between the pelvis and torso
ARM	Flexion	First XYZ Euler angle between the torso and upper arm
	Adduction	Second XYZ Euler angle between the torso and upper arm
	Rotation	Third XYZ Euler angle between the torso and upper arm
ELBOW	Flexion	First XYZ Euler angle between the upper arm and lower arm
	Pronation-Supination	Third XYZ Euler angle between the upper arm and lower arm
WRIST	Flexion	Not evaluated/Value of 0
	Deviation	Not evaluated/Value of 0

Then, the next step was to convert the landmark coordinates into *.trc* files which could then be used as input in OpenSim. Finally, the last step was to rotate the coordinates into the standard coordinate system also used for the marker-based data.

D. OpenSim

OpenSim was used to run the musculoskeletal analysis. To manage the 768 dynamic trials to be analyzed, OpenSim's Matlab Scripting Environment was used. Table K.2 presents a list of the decisions taken at each step of that analysis.

Table K.2: List of settings used for the scaling step in OpenSim

MENU	SETTING	VALUE
SUBJECT DATA	Marker set (Marker name, parent frame, location)	o RShoulder, torso, (0.01660; 0.38400; 0.15500) o LShoulder, torso, (0.01660; 0.38400; -0.15500) o RElbow, humerus_r, (0.00846; -0.29229; -0.00050) o LElbow, humerus_l, (0.00846; -0.29200; -0.00050) o RKnee, femur_r, (0; -0.40000; -0.00300) o RFTCG, calcn_r, (0.09880; 0.07000; -0.00028) o RAnkle, calcn_r, (0.04000l 0.07000; -0.00500) o RToes, calcn_r, (0.18000; 0.06500; -0.02500) o LKnee, femur_l, (0; -0.40000; -0.00300) o LFTCG, calcn_l, (0.09880; 0.07000; -0.00028) o LAnkle, calcn_l, (0.04000; 0.07000; -0.00500) o LToes, calcn_l, (0.18000; 0.06500; 0.02500) o RUACG, humerus_r, (-0.00230; -0.16400, -0.00140) o RFACG, radius_r, (0.00860; -0.10960; -0.01200) o LUACG, humerus_l, (-0.00230; -0.16400; -0.00140) o LFACG, radius_l, (0.00860; -0.10960; -0.01200) o Trunk, torso, (0.04470; -0.01050; -0.00130) o PVCG, pelvis, (-0.06351; 0.03126; -0.00130) o RTHCG, femur_r, (0.00080; -0.17000; 0.00030) o RSKCG, tibia_r, (-0.00280; -0.18600; -0.00100) o LTHCG, femur_l, (0.00080; -0.17000; 0.00030) o LSKCG, tibia_l, (-0.00280; -0.18600; -0.00100) o RFingers, hand_r, (0.00570; -0.10600; -0.00400) o LFingers, hand_l, (0.00570; -0.10600; -0.00400) o RWrist, radius_r, (-0.01000; -0.24300; 0.01060) o LWrist, radius_l, (-0.01000; -0.24300; -0.012200) o Neck, torso, (0.01523; 0.42716; -0.00316) o LHip, pelvis, (-0.05500; -0.07300; -0.09000) o RHip, pelvis, (-0.05500; -0.07300; -0.09000)

SCALE MODEL	Preserve mass distribution during scale	True
ADJUST MODEL MARKERS	Marker data for measurements	*.trc* file containing the coordinates of anatomical landmarks from the marker set
	Marker data for static pose	*.trc* file containing the coordinates of anatomical landmarks from the marker set
	Coordinate data for static pose	*.mot* file containing the joint angles as estimated from Theia3D
SCALE FACTORS	Applied scale factors	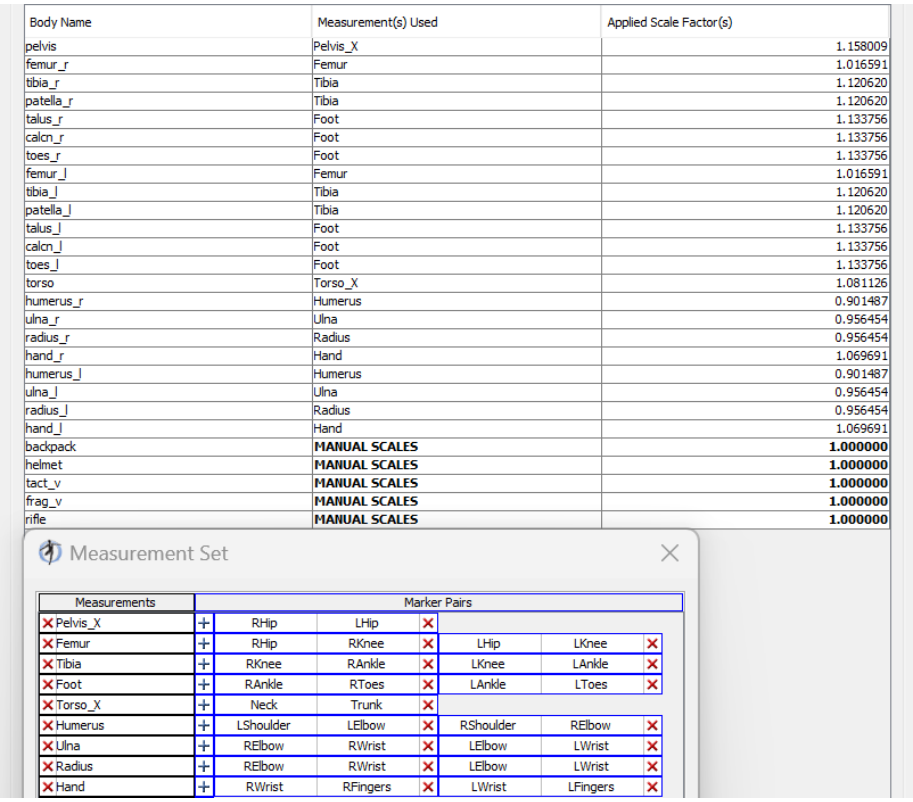
STATIC POSE WEIGHTS	Marker weight	A weight of 1 is applied on all markers.
	Coordinate weight	A weight of 1 is applied on all coordinates. Locked coordinates include subtalar_angle_r, mtp_angle_r, subtalar_angle_l, mtp_angle_l, pro_sup_r, wrist_dev_r, pro_sup_l, and wrist_dev_l.

Figure K.1: Markerless scaling factors in OpenSim

Table K.3 presents a list of the settings used for the inverse kinematics (IK) step in OpenSim.

Table K.3: List of settings used for the inverse kinematics step in OpenSim

MENU	SETTING	VALUE
IK TRIAL	Marker data for trial	*.trc* file containing the coordinates of anatomical landmarks from the marker set
	Coordinate data for trial	*.mot* file containing the joint angles as estimated from Theia3D
WEIGHTS	Marker weight	A weight of 1 is applied on all markers.
	Coordinate weight	A weight of 1 is applied on all coordinates. Locked coordinates include subtalar_angle_r, mtp_angle_r, subtalar_angle_l, mtp_angle_l, pro_sup_r, wrist_dev_r, pro_sup_l, and wrist_dev_l.

Two mass iterations were performed on the loaded models during the residual reduction algorithm (RRA) step. For each RRA iteration, the mass adjustments were applied to the loaded model's segments using the Scale tool without marker movement. Table K.4 presents the settings used at this step of the musculoskeletal analysis.

Table K.4: List of settings used for the residual reduction algorithm step in OpenSim

MENU	SETTING	VALUE
INPUT	Desired kinematics	Kinematics resulting from the IK analysis (*_ik.mot*)
	Filter kinematics	Kinematics were filtered at a low-pass cutoff frequency of 6 Hz.
	Tracking tasks	○ pelvis_tilt, weight = 200 ○ pelvis_list, weight = 200 ○ pelvis_rotation, weight = 10 ○ pelvis_tx, weight = 1 ○ pelvis_ty, weight = 1 ○ pelvis_tz, weight = 1 ○ hip_flexion_r/l, weight = 20 ○ hip_adduction_r/l, weight = 10 ○ hip_rotation_r/l, weight = 10 ○ knee_angle_r/l, weight = 5 ○ ankle_angle_r/l, weight = 2 ○ lumbar_extension, weight = 10 ○ lumbar_bending, weight = 50 ○ lumbar_rotation, weight = 5 ○ arm_flex_r/l, weight = 0.1 ○ arm_add_r/l, weight = 0.1 ○ arm_rot_r/l, weight = 0.1 ○ elbow_flex_r/l, weight = 0.1 ○ pro_sup_r/l, weight = 0.1
REDUCE RESIDUALS	Adjust model	1. For the first iteration of RRA, the "loaded" model is adjusted. 2. For the second iteration of RRA, the adjusted model from the first iteration is readjusted.
	Body COM to adjust	Torso
ACTUATORS	Additional force set files	○ FX, optimal_force = 5 ○ FY, optimal_force = 5 ○ FZ, optimal_force = 5 ○ MX, optimal_force = 2 ○ MY, optimal_force = 2 ○ MZ, optimal_force = 2 ○ hip_flexion_r/l, optimal_force = 300 ○ hip_adduction_r/l, optimal_force = 200 ○ hip_rotation_r/l, optimal_force = 100 ○ knee_angle_r/l, optimal_force = 300

		○ ankle_angle_r/l, optimal_force = 300 ○ lumbar_extension, optimal_force = 200 ○ lumbar_bending, optimal_force = 200 ○ lumbar_rotation, optimal_force = 200 ○ arm_flex_r/l, optimal_force = 500 ○ arm_add_r/l, optimal_force = 500 ○ arm_rot_r/l, optimal_force = 500 ○ elbow_flex_r/l, optimal_force = 500 ○ pro_sup_r/l, optimal_force = 500
EXTERNAL LOADS	Replace model's force set	True
	External loads specification file	Ground reaction force data measured by both in-ground force plates (one force plate per footstep)
INTEGRATOR SETTING	Maximum number of steps	20000
	Maximum step size	1
	Minimum step size	0.00000001
	Integrator error tolerance	0.00001

Table K.5 presents a list of the settings used for the static optimization step (SO) in OpenSim.

Table K.5: List of settings used for the static optimization step in OpenSim

MENU	SETTING	VALUE
INPUT	Motion from file	Adjusted kinematics from the second iteration of RRA (*_Kinematics_q.sto*)
	Filter coordinates	False
OBJECTIVE FUNCTION	Sum of (muscle activation)^	2.0
	Use muscle force-length-velocity relation:	True
STEP INTERVAL	Analyze every	10 steps
ACTUATORS	Additional force set files	o FX, optimal_force = 100 o FY, optimal_force = 200 o FZ, optimal_force = 100 o MX, optimal_force = 80 o MY, optimal_force = 80 o MZ, optimal_force = 80 o hip_flexion_r/l, optimal_force = 100 o hip_adduction_r/l, optimal_force = 100 o hip_rotation_r/l, optimal_force = 100 o knee_angle_r/l, optimal_force = 100 o ankle_angle_r/l, optimal_force = 100 o lumbar_extension, optimal_force = 100 o lumbar_bending, optimal_force = 100 o lumbar_rotation, optimal_force = 100
	Append to model's force set	True
EXTERNAL LOADS	External loads specification file	Ground reaction force data measured by both in-ground force plates (one force plate per footstep)

Table K.6 presents a list of the settings used for the joint reaction analysis (JRA) in OpenSim, using the Analyze Tool.

Table K.6: List of settings used for the joint reaction analysis in OpenSim

MENU	SETTING	VALUE
INPUT	Controls	False
	Motion from file	Adjusted kinematics from the second iteration of RRA (*_Kinematics_q.sto*)
	Filter coordinates	False
	Solve for equilibrium for actuator states	False
ANALYSIS SET	Active analyses	JointReaction
ACTUATORS	Additional force set files	o FX, optimal_force = 100 o FY, optimal_force = 200 o FZ, optimal_force = 100 o MX, optimal_force = 80 o MY, optimal_force = 80 o MZ, optimal_force = 80 o hip_flexion_r/l, optimal_force = 100 o hip_adduction_r/l, optimal_force = 100 o hip_rotation_r/l, optimal_force = 100 o knee_angle_r/l, optimal_force = 100 o ankle_angle_r/l, optimal_force = 100 o lumbar_extension, optimal_force = 100 o lumbar_bending, optimal_force = 100 o lumbar_rotation, optimal_force = 100
	Append to model's force set	True
PROPERTIES	step_interval	1
	forces_file	Forces computed from SO (*_StaticOptimization_force.sto*)
	joint_names	(walker_knee_r, walker_knee_l, ankle_r, ankle_l, hip_r, hip_l)
	apply_on_bodies	(child, child, child, child, child, child)
	express_in_frame	(ground, ground, ground, ground, ground, ground)